Norwegian University of Life Sciences
Faculty of Environmental Science and Technology
Department of Ecology
and Natural Resource Management

Philosophiae Doctor (PhD)
Thesis 2015:12

Estimation of biomass in tropical rainforest using airborne laser scanning

Estimering av biomasse i tropisk regnskog ved bruk av flybåren laserskanning

Endre Hofstad Hansen

Estimation of biomass in tropical rainforest using airborne laser scanning

Estimering av biomasse i tropisk regnskog ved bruk av flybåren laserskanning

Philosophiae Doctor (PhD) Thesis

Endre Hofstad Hansen

Department of Ecology and Nature Management
Faculty of Environmental Sciences and Technology
Norwegian University of Life Sciences

Ås 2015

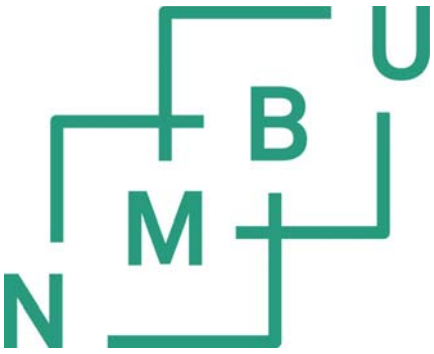

Thesis number 2015:12
ISSN 1894-6402
ISBN 978-82-575-1269-9

PhD supervisors

Professor Terje Gobakken
Department of Ecology and Natural Resource Management
Norwegian University of Life Sciences
P.O. Box 5003, NO – 1432 Ås, Norway

Professor Erik Næsset
Department of Ecology and Natural Resource Management
Norwegian University of Life Sciences
P.O. Box 5003, NO – 1432 Ås, Norway

Dr. Ole Martin Bollandsås
Department of Ecology and Natural Resource Management
Norwegian University of Life Sciences
P.O. Box 5003, NO – 1432 Ås, Norway

Evaluation committee

Dr. Pete Watt
Indufor Asia Pacific Ltd.
P.O. Box 105 039, Auckland City 1143, New Zealand

Professor Timo Tokola
School of Forest Sciences
University of Eastern Finland
P.O. Box 111, FI – 80101 Joensuu, Finland

Associate Professor Katrine Eldegard
Department of Ecology and Natural Resource Management
Norwegian University of Life Sciences
P.O. Box 5003, NO – 1432 Ås, Norway

Preface

The present thesis, together with a program of formal courses, a trial lecture and a public defence, completes my doctoral work. The work began in June 2011 with planning of the field inventory which was carried out in Amani nature reserve in Tanga region, Tanzania. After a short training of the field crew, field inventory commenced in August 2011. I stayed with the field crew until October. From then on the inventory was led by Mr. Nuru Hussein, for which I am truly grateful.

Analysis and writing of the scientific papers and synopsis was carried out at the Department of Ecology and Natural Resource Management, Norwegian University of Life Sciences (NMBU), during the period from October 2011 to February 2015. Courses in research ethics and philosophy of science, statistics, and remote sensing were completed at NMBU, Swedish University of Agricultural Sciences and University of Eastern Finland.

I am grateful to my supervisors, Professors Terje Gobakken and Erik Næsset, and researcher Ole Martin Bollandsås for all critique, guidance, and support. I am also indebted to all members of the “Skogrover” research group for fruitful discussions and socializing. Thanks to all my co-authors outside the research group: Eliakimu Zahabu, Sokoine Agricultural University, Svein Solberg, Norwegian Forest and Landscape Institute and Annika Kangas, NMBU & Natural Resources Institute Finland. Further, I wish to thank Hugh Riley for revising the language in parts of the thesis. A special thanks to Ernest Mauya for the close collaboration and to Roar Økseter for sharing the office with me for the entire work-period. The work was made possible by the funding by the Royal Norwegian Embassy in Tanzania as part of the Norwegian International Climate and Forest Initiative. I appreciate the financial support for such an important field. Further, I would like to thank my family, Guri & Einar, Yngve & Jessica, Lars & Ann-Mari, Torgunn, Ole, and Tormod. Lastly, a loving thanks to Ingvild and Tora for brightening up my days.

Endre Hofstad Hansen
Ås, April 2015

Contents

Abstract

Forest inventories based on field sample surveys, supported by auxiliary remotely sensed data, have the potential to provide transparent and confident estimates of forest carbon stocks required in climate change mitigation schemes such as the REDD+ mechanism. Three-dimensional (3D) information about the density and height of the vegetation, obtained from remotely sensed data, is particularly useful for providing accurate estimates of forest biomass. Most of the research on biomass estimation supported by 3D remotely sensed data has been carried out in boreal and sub-boreal coniferous forests with relatively low biomass quantities and open forest structure. The studies comprising the present thesis were conducted in a dense tropical forest with challenging topography.

In the present thesis two different techniques of collecting remotely sensed 3D data were used: airborne laser scanner (ALS) and spaceborne interferometric synthetic aperture radio detection and ranging (InSAR). While the main focus was on the use of ALS, the high quality digital terrain model (DTM) derived from the ALS data also facilitated the comparison of InSAR data as auxiliary information in biomass estimation.

The analyses and results presented in Paper I of modelling aboveground biomass using ALS data resulted in root mean square errors (RMSE) of about 33% of a mean value of 462 $Mg \cdot ha^{-1}$. Use of texture variables derived from a canopy surface model constructed from ALS data did not result in improved models. Analyses showed that (1) variables derived from ALS-echoes in the lower parts of the canopy and (2) canopy density variables explained more of the aboveground biomass density than variables representing the height of the canopy.

Paper II investigated the potential of using cheaper, low-pulse density ALS data. Effects of reduced pulse density on (1) the digital terrain model (DTM), and (2) explanatory variables derived from ALS data were assessed. Random variation in DTMs and ALS variables increased with reduced pulse density. A reliability ratio, quantifying replication effects in the ALS-variables, indicated that most of the common ALS variables assessed were reliable at pulse densities >0.5 $pulses \cdot m^{-2}$, and at a plot size of 0.07 ha. The plot size of 0.07 ha corresponds to the plot size used in the national forest inventory of Tanzania.

The field plot size is of importance for the precision of carbon stock estimates, and better information of the relationship between plot size and precision can be useful in designing future inventories. The effect of plot size on the precision of biomass estimates assisted by remotely sensed data was therefore assessed in Paper III. Precision estimates of forest biomass estimates developed from 30 concentric field plots with sizes of 700, 900,…, 1900 m^2, were assessed in

a model-based inference framework. Findings indicated that larger field plots were relatively more efficient for inventories supported by ALS and InSAR data compared to a pure field-based survey. Further, a simulation showed that a pure field-based survey would have to comprise 3.5–6.0 times as many observations for the plot sizes of 700–1900 m^2 to achieve the same precision as an inventory supported by ALS data.

Sammendrag

Fjernmålte data brukt sammen med feltobservasjoner, kan potensielt gi grunnlag for troverdige estimat av karbonet som er lagret i skogens biomasse. Informasjon om lagret biomasse er nødvendig for arbeidet med å motvirke klimaendringer. REDD+ er system hvor denne kunnskapen er avgjørende. Fjernmålt 3D-informasjon om skogens høyde og tetthet er særlig nyttig fordi den gir nøyaktige estimat på skogens biomasse. Tidligere forskning på bruk av fjernmålt 3D-data til biomasseestimering har hovedsakelig blitt gjort i boreal og sub-boreal barskog med relativt lav biomasse og åpen skogstruktur. Studiene i denne avhandlingen ble utført i tett tropisk skog med utfordrende terrengforhold.

To ulike metoder for fjernmåling av 3D-data ble benyttet: flybåren laserskanning (ALS) og satellittbåren interferometrisk syntetisk apertur-radar (InSAR). Hovedfokuset for avhandlingen var på bruk av ALS. I tillegg ga en digital terrengmodell av høy kvalitet, produsert med ALS-dataene, muligheter for en sammenligning med bruk av InSAR-data til biomasseestimering. Analysene beskrevet i Paper I viste at modellering av biomasse over bakkenivå ved hjelp av ALS-data ga en standardfeil (RMSE) på ca. 33 % av et gjennomsnitt på 462 $Mg \cdot ha^{-1}$. Bruk av teksturvariabler utledet fra en modell av vegetasjonens overflate konstruert fra ALS-data ga ikke forbedret resultat. Analysene viste videre at (1) variabler utledet fra laser-ekko i lavere deler av vegetasjonen og (2) tetthetsvariabler fra vegetasjonen forklarte biomassetettheten bedre enn variabler som beskrev vegetasjonens høyde.

I Paper II ble muligheten for bruk av billigere ALS-data med lav pulstetthet undersøkt. Effekten av lav pulstetthet på (1) den digitale terrengmodellen, og (2) variabler utledet fra ALS-data ble analysert. Tilfeldig variasjon i digitale terrengmodeller og ALS-variabler økte med redusert pulstetthet. En ratio for pålitelighet, som kvantifiserer replikasjonseffekter i ALS-variablene, viste at mesteparten av de undersøkte variablene var pålitelige ved pulstettheter >0.5 $pulser \cdot m^{-2}$, ved bruk av en feltmålte flater på 0,07 ha. Denne størrelsen på feltflatene tilsvarer den som brukes i Tanzanias nasjonale landsskogtaksering.

Størrelsen på feltflatene er viktig for presisjonen i biomasseestimater. Bedre informasjon om forholdet mellom størrelse på feltflatene og presisjon er nyttig i planleggingen av framtidige skogtakseringer. Presisjonsestimater av skogens estimerte biomasse ble derfor beregnet for 30 konsentriske feltflater med størrelse på 700, 900,…, 1900 m^2. Disse estimatene ble analysert i en modell-basert statistisk metode. Resultatene indikerte at større feltflater relativt sett var mer effektive for taksering understøttet av ALS- og InSAR-data, sammenlignet med en ren feltflatetakst. Videre ble det i en simulering vist at en ren feltflatetakst ville måtte

inneholde 3,5–6,0 ganger så mange observasjoner for henholdsvis flatestørrelser fra 700–1900 m^2 for å oppnå samme presisjon som en takst understøttet av ALS-data.

List of appended papers

I. Hansen, E.H., Gobakken, T., Bollandsås, O.M., Zahabu, E. and Næsset, E. 2015. Modeling aboveground biomass in dense tropical submontane rainforest using airborne laser scanner data. *Remote Sensing*, 7(1): 788–807.

II. Hansen, E.H., Gobakken, T. and Næsset, E. 2015. Effects of pulse density on digital terrain models and canopy metrics using airborne laser scanner in a tropical rainforest. S*ubmitted*.

III. Hansen, E.H., Gobakken, T., Solberg, S., Kangas, A., Ene, L., Mauya, E. and Næsset, E. (2015). Impact of field plot size on the relative efficiency of biomass estimation in a Tanzanian rainforest using airborne laser scanner and interferometric synthetic aperture radar as auxiliary data. *Submitted*.

SYNOPSIS

1 Introduction

The climate is changing! The report from the fifth assessment of the Intergovernmental Panel on Climate Change (IPCC) is conclusive. We are experiencing increased global temperatures because of our emissions of greenhouse gases (IPCC, 2014). With the rise in temperatures we observe changes in habitats for all forms of life on earth that have not been seen in millennia. The extent of Arctic sea-ice is decreasing, glaciers are retracting, and the great ice sheets of Greenland and Antarctica are losing mass. Rainfall patterns are changing across the globe, leaving some areas wetter and some drier than normal. Extreme weather events are more frequent and intense. The salinity of the oceans is changing, some becoming saltier and some less salty. Furthermore, the oceans are becoming more acidic. All of these changes have severe implications for life forms adapted to specific climatic and environmental conditions.

1.1 Global reduction of greenhouse gases

Reduction of greenhouse gases has been a focus area in international environmental work since the late 1980s with the establishment of the IPCC in 1988 and the United Nations Framework Convention on Climate Change (UNFCCC) treaty in 1992. Since then IPCC have compiled scientific evidence about climate change, and specific treaties (called “protocols”), which set limits on greenhouse gas emissions, have been agreed upon by signatories of the UNFCCC treaty.

The main greenhouse gas in terms of emissions and global temperature change is carbon dioxide (CO_2), and CO_2 has contributed to more than 80% of the total temperature increase due to greenhouse gases in the last 15 years (Myhre et al., 2013). Further, a near-linear relationship has been found between total emissions of CO_2 and global temperature change (Matthews et al., 2009). Yearly emissions of CO_2 have increased rapidly since the beginning of the industrial revolution and are estimated to a total of 555 ± 85 petagrammes of carbon (PgC) in the period of 1750–2011 (Ciais et al., 2013). For 2013 Friedlingstein et al. (2014) reported a global estimated total of 10.75 ± 0.71 PgC, with a projected increase of 2.3% in 2014.

1.2 The role of forests in the global carbon cycle

Vegetation, especially trees, removes carbon from the atmosphere and stores it as biomass. If the forest is cleared, or becomes degraded, the carbon is released back to the atmosphere. Human- induced deforestation and forest degradation is often referred to as land use change and the total estimated emissions from land use change in the period 1750–2011 is estimated to 180 ± 80 PgC (Ciais et al., 2013). Although the proportion of emissions stemming from land use change has decreasing trend (Ciais et al., 2013), land use change is still a significant source of carbon emissions with an estimated total of 0.87 ± 0.49 PgC for 2013 (Friedlingstein et al., 2014).

Tropical forests, found on land between latitudes of 23.44°N and 23.44°S, cover around 18 million km^2 (FAO, 2011) and are estimated to store 271 ± 16 PgC (Grace et al., 2014). These forests are under great pressure for conversion to agricultural land (Houghton, 2012) and Grace et al. (2014) report a total carbon loss of 2.01 ± 1.1 PgC yr^{-1} from deforestation, harvesting and peat fires. However, the growth in forests and woodlands is reported to sequester 1.85 ± 0.09 PgC yr^{-1} resulting in a net loss of 0.16 ± 1.1 PgC yr^{-1} from tropical forests. Thus, these forests represent a substantial potential carbon sink, approaching 2 PgC yr^{-1} or up to 20% of the global carbon emissions.

With the prospect of a quick and cheap solution for mitigating carbon emissions, tropical forests have received a lot of attention and have resulted in the policy and economic incentive mechanism known as the REDD+ mechanism. REDD+ (reducing emissions from deforestation and forest degradation, conservation and enhancement of forest carbon stocks and sustainable management of forests in developing countries), described in the 16th session of the Conference of Parties to the United Nations Framework Convention on Climate Change, gives developing countries the opportunity to monetize from the reduction of emissions from deforestation and forest degradation, and enhancement of forest carbon stocks (UNFCCC, 2011).

Accessing carbon finances through REDD+ will require, among other factors, measurement of carbon stock changes in forests (UNFCCC, 2010). Furthermore, a mechanism for commercial trading of forest carbon credits earned through enhancement of forest carbon stocks, conservation of forests or sustainable forest management require trustworthy systems for verification of carbon offsets. In addition, application of the principle of conservatism, which takes into account the uncertainty of estimates to minimize the risk of overestimating emission reductions (UNFCCC, 2006; Grassi et al., 2008), and lack of accurate biomass estimates may result in loss of carbon credits for the project developer (Gibbs et al., 2007).

Establishing a robust and transparent system for measuring, reporting and verification (MRV) of biomass is therefore a requirement for the successful implementation of a REDD+ regime (Plugge et al., 2011).

1.3 Forest inventories supported by remotely sensed data

Forest inventories have the potential to provide transparent and confident estimates of aboveground biomass, hereafter simply referred to as biomass. Forest inventories are usually designed as sample surveys, with observations on the ground collected from field plots, supported by one or several sources of remotely sensed data. Remotely sensed data, in the form of aerial images, has been an important forest inventory tool since the 1940s (FAO, 1948), and the availability of optical satellite images in the 1970s has resulted in global forest cover statistics (Boyd & Danson, 2005). While high cost has prevented the use of aerial images, the use of low-cost optical satellite images has been hampered by low spatial resolution and persistent cloud cover in tropical areas. Furthermore, both aerial and satellite optical images have traditionally only provided two-dimensional information, although recent developments have resulted in three-dimensional (3D) data from aerial and satellite images with the use of digital photogrammetry and image matching (e.g. Næsset, 2002; Bohlin et al., 2012; Persson et al., 2013; Gobakken et al., 2014).

The use of LiDAR (light detection and ranging) sensors, most commonly mounted on a small aircraft and with a scanning capability, known as airborne laser scanning (ALS), has proved to be both effective and accurate for determining biomass in different forest types (Zolkos et al., 2013; Fassnacht et al., 2014). There has been a strong focus on research of ALS during the past two decades, and ALS is now used as an integral part of operational forest management inventories in several countries (McRoberts et al., 2010; Næsset, 2014). Most of the published studies on ALS to estimate biomass have been carried out in boreal and sub-boreal coniferous forests with relatively low biomass and open forest structure. However, in the last five years, use of ALS for biomass estimation has been demonstrated in tropical forests in South America (Asner et al., 2010; Clark et al., 2011; Vincent et al., 2012; Andersen et al., 2013; Asner et al., 2014), Asia (Hou et al., 2011; Jubanski et al., 2012; Ioki et al., 2014) and Africa (Asner et al., 2012; Laurin et al., 2014). The maximum biomass densities in these studies were about 500 metric tonnes of biomass per hectare ($Mg \cdot ha^{-1}$), while biomass densities in tropical rainforests can reach levels beyond 500 $Mg \cdot ha^{-1}$ (Keith et al., 2009).

1.4 Sources of three-dimensional remotely sensed data

Satellite-mounted optical sensors have been used for estimation of global forest cover since the launch of the first Landsat satellite in 1972. More importantly, with data spanning over three decades, these optical sensors provide estimates of global forest cover change (Hansen et al., 2013). For biomass estimation however, the usefulness of the two-dimensional information from satellite images is limited because it lacks information about vegetation height, has limited resolution, and is often obstructed by cloud cover.

ALS systems solve these challenges by emitting a short pulse of laser light and measuring the time between the emission and the reflectance (echoes) detected by the LiDAR sensor. By emitting thousands of pulses per second and recording several echoes per pulse in a scanning motion, the ALS system effectively creates a 3D cloud of echoes. By recording the position and orientation of the sensor at the time of emitting each pulse, using a GPS (global positioning system) receiver and an inertial navigation system unit, each echo is positioned in the 3D space (x, y, and z positions). To derive information about the vegetation, a digital terrain model (DTM) is constructed by classifying echoes as ground echoes. Following the construction of the DTM, the elevation of all echoes in relation to the DTM is computed. Echoes above a certain threshold above the DTM are regarded as vegetation echoes.

Although the best results for biomass estimation have been obtained using ALS, its cost is high compared to using satellite-based sensors. While satellite based optical imagery is frequently obstructed by persistent cloud cover in the tropics, use of active synthetic aperture radio detection and ranging (SAR) sensors penetrate clouds and produce backscatter images that can be used for the prediction of forest biomass. In high biomass conditions however, radar backscatter data has so far not been able to provide data for reliable estimation and has been shown to saturate at biomass levels of between 200–250 $Mg \cdot ha^{-1}$ (Mitchard et al., 2009; Le Toan et al., 2011). Promising results have nevertheless been published for biomass values up to 450 $Mg \cdot ha^{-1}$ (Minh et al., 2014). At present, SAR technologies exist that can produce 3D data using four different techniques: clinometry, stereoscopy, interferometry and polarimetry (Toutin & Gray, 2000). In addition, optical satellite images can produce 3D data by repeat-pass-acquisition and image matching techniques. New applications are being developed continuously and a thorough overview is beyond the scope of this thesis. A shared property of these techniques is that, in order to provide information at a level similar to that of ALS, they require a high quality DTM. At present, the only technology able to provide this DTM quality is ALS, and it is therefore a prerequisite for the other sensors and techniques.

1.5 The area-based method for forest inventories using remotely sensed data

The most common method for utilizing remotely sensed auxiliary information for forest inventory purposes is known as the area-based method. This method, first outlined in Næsset (1997a; 1997b), is based on modelling the relationship between attributes of interest that have been measured or calculated from measurements on field plots, with explanatory variables derived from remotely sensed data from the corresponding field plot area. To apply the model on the area of interest, the remotely sensed data are tessellated into units, usually of the same size as the size of the field plots, and the explanatory variables are derived for each unit. The model is then applied to predict the response variable on each unit.

The alternative method to the area-based one is known as the individual-tree-crown method. As the name suggests, it is based on modelling the attributes of interest on a single tree basis. Identification of individual trees is affected by stand density and spatial pattern, which causes problems related to interlaced tree crowns and trees below the dominant canopy (Vauhkonen et al., 2014). In the tropical rainforest where tree crowns overlap, forming a closed canopy-cover, the separation of individual tree crowns is regarded as a difficult task with presently available technologies.

1.6 Improving the accuracy of biomass estimates

As described in section 1.2 accurate biomass estimates are a requirement for the REDD+ mechanism to function. Increased accuracy would also potentially lead to added carbon credits for the project developer (Gibbs et al., 2007). Accuracy is defined as the sum of trueness and precision (ISO, 2012). Accuracy of an estimation is often expressed by the mean square error (Gregoire & Valentine, 2008, p. 28), or the root mean square error (RMSE), (Equation 4) of the mean estimate as used in this thesis. Thus, accuracy incorporates both trueness, expressed herein by the mean difference (MD), and precision, expressed as standard error of estimation (SE), i.e., the square root of the estimation variance, or standard deviation of a sample (SD). Trueness can only be calculated when the true value is actually known. The simplest way of increasing the precision of biomass estimates is by increasing the sample size. In a design-based framework (see section 3.3.3), the variance of the estimation under simple random sampling is proportional to the square root of the sample size minus the number of explanatory variables minus one (Stoltzenberg, 2009, p. 181). Thus, all else being equal, doubling the number of observations would halve the variance of the estimation. Another option is to use remotely sensed auxiliary information related to the observed biomass. Depending on the correlation

between the biomass and explanatory variables derived from the remotely sensed data, the precision is improved using the auxiliary information from the data.

In boreal forests, where the correlation between ALS-derived variables and forest parameters is high, use of ALS data has been found to reduce the need for field observations by a factor of 3–9 (Næsset et al., 2011; Ene et al., 2013), without reducing the estimated precision. In high-cost countries, such as Norway, use of ALS in forest inventories thus becomes cost-efficient. In Tanzania, where the cost of field labour is low, using additional field plots would probably be the most cost-efficient way of increasing the precision of the estimated biomass. However, the remote and inaccessible nature of forest areas in tropical developing countries means that remotely sensed data can nevertheless be invaluable in providing precise biomass estimates (McRoberts et al., 2013b; McRoberts et al., 2014b).

1.7 Effects of field plot size on the accuracy of biomass estimates

The size of the field plot is a property of great importance for accuracy when estimating biomass by means of remotely sensed data. Studies of modelling the relationship between forest biomass and ALS-derived variables in tropical areas have utilized field plots sizes in the range of 0.1–1.0 ha. Larger plots inevitably increase the accuracy of the biomass estimates due to spatial averaging (Zolkos et al., 2013), as larger field plot sizes reduce the between-plot variance (cf. Gobakken & Næsset, 2009; Mascaro et al., 2011; Magnussen et al., 2012). In addition, larger plots have smaller ratios of the border zone to total plot area than do smaller plots, a zone which is subject to boundary effects (Mascaro et al., 2011; McRoberts et al., 2014a). This implies that the relative influences of the boundary effects are smaller for larger plots, regardless of plot shape. Negative consequences of GPS positioning errors are also smaller for large plots (Gobakken & Næsset, 2009). Likewise, the boundary effects will be more pronounced in forests with large tree crowns and on rectangular or quadratic plots, compared to circular plots with the smallest possible circumference-to-area ratio. Even though larger field plots, e.g. plots larger than 0.25 ha, result in models with better performance, their practical application is limited due to the difficulty of establishing them. This is especially challenging in rugged and steep terrain, and in areas with very dense vegetation. Reducing the field plot size to a more practical and manageable size will, however, reduce the precision of biomass estimates.

1.8 Research objectives

The overall objective of this thesis was to investigate the potential of using ALS as an auxiliary data-source in sample surveys of biomass in a tropical forest with a wide range in biomass densities in rugged and steep terrain. During initial work on the first study it became clear that negative boundary effects were strongly influencing the results. This led to a focus on examining the effects of plot size on the precision of biomass estimates in subsequent studies. Because the ALS data provided a high quality DTM, a comparison of ALS to interferometric SAR, in terms of sampling error, was performed. Specific objectives for the studies were:

I. To model biomass using conventional height and density variables derived from ALS data, and to explore the use of texture variables derived form an ALS canopy surface model.
II. To assess the effects of reduced pulse density on the derived DTM, and on the ALS-derived explanatory variables at spatial units ranging from 0.07 to 0.28 ha in size.
III. To assess, in a model-based inference framework, the impact of plot size on the relative efficiency of ALS and interferometric SAR data compared to models with terrain elevation as the only explanatory variable.

2 Materials

2.1 Study area

The study area, Amani nature reserve (ANR , Figures 1–3, S 5°08', E 38°37', 200–1200 m above sea level), covers around 85 km^2 of tropical sub-montane rainforest and is located in the East Usambara mountains in eastern Tanzania, part of the Eastern Arc mountains. The Eastern Arc mountains region is a global biodiversity hotspot area (Myers et al., 2000) and its unique forest ecosystem, stretching from Udzungwa in Tanzania in the south to Taita Hills in Kenya in the north, contains many endemic species of both animals and plants. Within this mountain system, the East Usambara mountains have been identified as one of three top priority areas for forest conservation (Burgess et al., 2007). Rain falls throughout the year, with two wet seasons, April–May and October–November, and the forest in ANR receives around 2000 mm rainfall per year. Daily mean temperatures vary from about 16 to 25 °C. ANR was gazetted in 1997, comprising of six former forest reserves, Amani-East, Amani-West, Amani-Sigi, Kwamsambia, Kwamkoro and Mnyusi Scarp. In addition, forest land from the neighbouring tea estate, sisal estate and local village was included in the ANR. The area also includes the Amani botanical gardens, established in 1902 under German colonial rule, which has contained over 500 indigenous and non-native tree species (Dawson et al., 2008). Very few of the non-native species have spread successfully from the area in which they were planted, but one species in particular, *Maesopsis eminii*, is found throughout the entire ANR and is the most common species in the reserve. *M. eminii* originated from the lake region in eastern Congo and is a typical light-demanding, pioneer species. It thrives in disturbed areas, but is not able to germinate under thick canopy (Newmark, 2002) and is thus not found in the less disturbed areas of the ANR. In an inventory carried out in 1986/87, about half of the ANR was classified as either logged or covered with *M. eminii* as a result of logging (Hamilton & Bensted-Smith, 1989). Logging was stopped in the late 1980s and most of the ANR is now covered by closed forest.

2.2 Field data

Two different sets of field data were used in the studies. The first field data set (FD1), used in Papers I and II, was originally established by a non-governmental conservation and development organization, Frontier Tanzania, during 1999–2000 (Frontier Tanzania, 2001). Rectangular shaped plots of 50 × 20 m were established on a 450 × 900 m grid covering the ANR (Figure 2). The horizontal area of the plots varies from 0.0639–0.1239 ha because the

plots were laid out along the terrain slope, without any slope correction. All trees with ≥10 cm diameter at breast height (DBH) were callipered, marked and species identified. During two campaigns in 2008 and 2009/2010, 143 of these plots were revisited and all trees re-measured (Mpanda et al., 2011; Mgumia, 2014). Trees that had grown larger than 10 cm in DBH since the first survey were included, and dead or missing trees excluded. All of the initial 173 plot locations were visited again between August 2011 and April 2012 and plots that were not re-measured during the 2008–2010 period were re-measured at this time. All plots were identified in the field by local personnel who had performed their establishment and previous re-measurement. Plots which were not positively identified in the field were re-established and all the trees with a DBH ≥10 cm registered. This was also done for plots with an apparent change in structure (due to landslide or human activity), or trees were added or removed in cases where there was a clear error in the earlier records. Of the 173 plots, 15 plots had one or more corners with missing coordinates after completion of the field work, due to reception of too few satellites during data recording from positioning satellites. One plot was also discarded because one of the processed corner coordinates had a reported error of >10 m (See 2.2.3 for further details about the positioning of the field plots). Furthermore, four plots were found to be outside the study area. The DBH data from the remaining 153 plots contained measurements from four different years; 2008 (19 plots), 2009/2010 (91 plots) and 2011/2012 (43 plots).

In FD1, ten trees per plot were selected for height measurement. The trees were systematically selected by choosing the closest tree to each corner; one tree in the middle of each short end of the plot; and two trees along the sides, 15 m from each corner. Tree height (H) was measured using a Vertex IV hypsometer (Figure 5) and trees with damage were noted. For plots with low stocking, in which the same tree could be selected more than once, less than ten heights were measured. A total of 1497 trees were measured during the fieldwork in 2011 and 2012.

The second field data set (FD2, Figure 3), used in Paper III, consisted of data from 30 circular field plots collected during November 2011 in pre-determined locations with the aim of capturing as much variation in biomass as possible by distributing them in different altitudinal zones. All trees with ≥5 cm diameter at breast height (DBH) were callipered, marked and species identified. The horizontal distance from the plot centre to the front of each tree was measured using a Vertex IV hypsometer. Since the distance was measured to the front of the trees, half of the tree DBH was added during data processing to get the total horizontal distance of the trees from the plot centre. The plot size was determined by the reach of the Vertex, and under the most challenging conditions in ANR, distance measurement started to fail at 25 m.

Thus, in order to contain 30 observations, the maximum plot size was 0.19 ha. The heights of three trees per plot (largest, medium and smallest) were measured using the Vertex hypsometer.

The representativeness of the plots in FD2 was evaluated in Mauya et al. (2015) by comparing the properties of FD2 to FD1. Based on this evaluation Mauya et al. (2015) concluded that, although being sampled in an opportunistic manner, the distribution in different altitudinal zones resulted in a sample which closely resembled properties of the systematic sample.

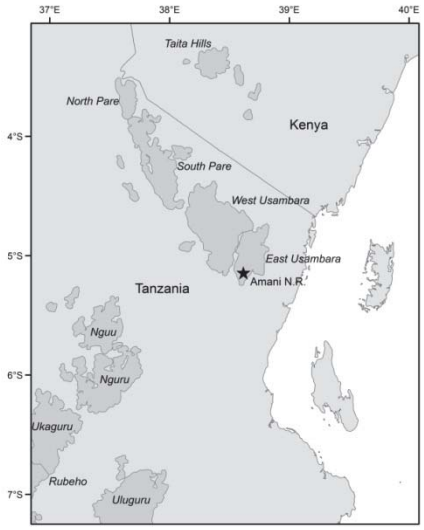

Figure 1. Study area (star) situated in the Eastern Arc Mountains (dark grey areas).

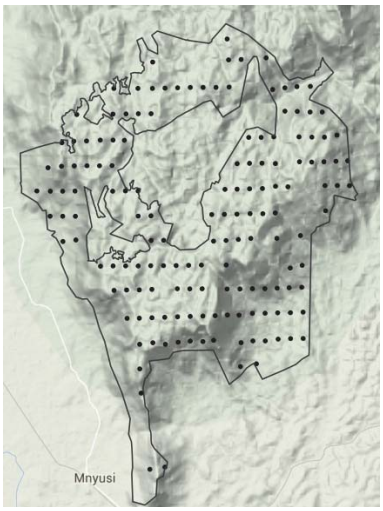

Figure 2. Plot locations for FD1 in Amani nature reserve.

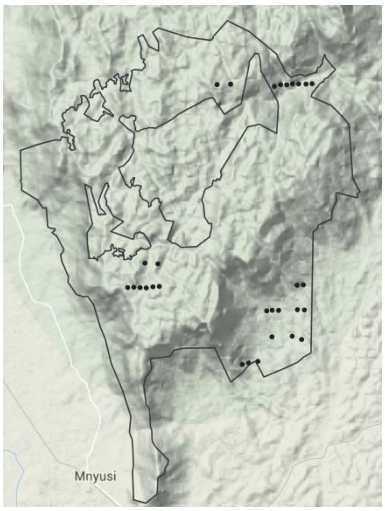

Figure 3. Plot locations for FD2 in Amani nature reserve.

2.2.1 Height-diameter models

Single tree predictions of biomass with both DBH and H as independent variables in the allometric models, give more reliable and lower biomass levels than those without height information (Henry et al., 2010; Marshall et al., 2012). Non-linear height-diameter (H-D) models were developed for both FD1 and FD2, with plot as a random effect. Using the trees measured for height, H-D models were fitted using the "fithd" function in the package "lmfor" (Mehtatalo, 2012) in R software (R Development Core Team, 2013) again with plot as random effect. The "lmfor" package contains 20 two- and three parameter model forms, and the most suited forms for our data were selected based on the Akaike information criterion. The selected model forms (Equations 1 and 2) described by Prodan (1968) and Winsor (1932) respectively,

were then re-fitted using the "nlme" function (Pinheiro et al., 2014) in R for FD1 and FD2. The selected models can be expressed as the mean (expected value) functions:

$$\mathrm{E[H]} = 1.3 + \mathrm{DBH}^2/(\mathrm{a} + \mathrm{b} * \mathrm{DBH} + \mathrm{c} * \mathrm{DBH}^2), \quad (1)$$

$$\mathrm{E[H]} = 1.3 + \mathrm{a} * \exp\big(-\mathrm{b} * \exp(-\mathrm{c} * \mathrm{DBH})\big). \quad (2)$$

This method of calibrating the H-D model is described by Lappi and Bailey (1988) and is able to include local effects. The H-D development of trees can for instance be affected by local soil conditions or by surrounding trees. To capture the local effects, field plot was specified as random effect and all three parameters of the model were allowed to describe the random effects.

2.2.2 Aboveground biomass

Aboveground biomass for individual trees ($\widehat{\mathrm{AGB}_t}$) was predicted using a locally developed allometric model (Equation 3) (Masota et al., 2015). The model is developed from 60 trees from 34 different species in the ANR and has a pseudo coefficient of determination of 0.84. The trees were felled and the green weights of stem, branches, twigs and leaves were recorded in the field, along with DBH. Wood samples from each of the three components were collected and the green-to-dry weight ratio calculated after oven drying of the wood samples. The tree biomass was then calculated by first multiplying the green weight with the green-to-dry weight ratio of each of the tree components and then summing these up for each tree. The applied model was:

$$\widehat{\mathrm{AGB}_t} = 0.402 * \mathrm{DBH}_t^{1.4365} * \mathrm{H}_t^{0.8613}, \quad (3)$$

where $\widehat{\mathrm{AGB}_t}$ is the predicted aboveground biomass in Mg for individual tree number *t*, DBH_t is the tree diameter at breast height in cm for tree number *t*, and H_t is the tree height in m for tree number *t*. For DF1 the $\widehat{\mathrm{AGB}_t}$ was then summed at field plot level and converted to per-hectare units of biomass (Table 1). For FD2 each tree was allocated to each of the concentric plot size based on the distance from the plot centre to the centre of the stem, computing per-hectare biomass values for all plots of 700, 900, …, 1900 m^2 (Table 2). Although this biomass is referred to as "observed biomass", the computed values are subject to errors related to the applied allometric model, and the subsampling and measurement of tree DBH and height.

Table 1. Characteristics of the 153 field plots in FD1.

Characteristic	Range	Mean	SD
Area (ha)	0.0639–0.1239	0.0914	0.011

N[a] (ha^{-1})	85.4–1085.7	471.5	161.5
DBH[b] (cm)	10.0–270.0	27.5	22.9
BA[c] ($m^2 \cdot ha^{-1}$)	5.4–144.9	47.3	22.2
Biomass ($Mg \cdot ha^{-1}$)	43.2–1147.1	461.9	214.7
H[d] (m)	8.3–51.3	19.2	8.9

[a] number of trees, [b] diameter at breast height (1.3 m), [c] basal area, [d] predicted tree height.

Table 2. Mean biomass and standard deviation (SD) in FD2 at plot sizes of 700, 900,…, 1900 m^2.

Plot size (m^2)	Mean biomass ($Mg \cdot ha^{-1}$)	SD ($Mg \cdot ha^{-1}$)
700	371.8	221.5
900	366.1	216.3
1100	365.6	203.0
1300	361.0	190.5
1500	354.2	180.4
1700	355.0	170.2
1900	351.1	159.6

2.2.3 Positioning of the field plots

During the fieldwork in August 2011–April 2012, the plot corners of the rectangular plots in FD1 and the centre point of the circular plots in FD2 were georeferenced by means of differential global navigation satellite system (dGNSS). A 40-channel dual frequency survey grade receiver (Topcon Legacy-E+) was used as a field unit (Figure 4) and a second receiver, functioning as a base station, was placed on the roof of a house at the ANR headquarters with a distance of <14 km from the plots. Before the georeferencing started, the coordinates of the base station antenna were determined with precise point positioning with GPS and global navigation satellite system data collected continuously for 24 hours according to Kouba (2009). The field unit was placed at each point on a 2.9 m rod for a minimum of 30 minutes, and a one second logging rate was used. Horizontal errors of the georeferenced points were estimated to an average of 0.57 m based on random errors reported from the post-processing using Pinnacle software (Anon., 1999) and empirical experience of the relationship between reported error and the true error documented by Næsset (2001). Mean precision in the vertical direction after post-processing in Pinnacle (Anon., 1999) was reported to 0.39 m.

Figure 4. Field unit of the differential global navigation satellite system (dGNSS) used for positioning of field plots.

Figure 5. Measuring tree height using a Vertex IV hypsometer.

2.2.4 Remotely sensed data

The ALS data used in all three papers was collected as complete coverage using a Leica ALS70 sensor mounted on a Cessna 404 twin engine, fixed wing aircraft. The acquisition was carried out in the period 19–25 January 2012 with additional flights in the period 2–18 February 2012 to fill minor gaps in the data. Average flight speed was 70 m s^{-1} at a mean altitude of 800 m above ground level and with a laser pulse repetition frequency of 339 kHz. From each pulse the sensor registered up to five echoes. A maximum scan angle of ±16° from nadir yielded an average swath width of 460 m. The beam divergence was 0.28 mrad, which produced an average footprint size on the ground of about 22 cm.

In Paper III, interferometric synthetic aperture radio detection and ranging (InSAR) was assessed as an alternative source of remotely sensed data. The InSAR data were acquired by the Tandem-X satellite mission on 6th August 2011. The incidence angle was 46°, and the polarization was horizontal transmit and horizontal receive. The normal baseline was 210 m, which corresponded to a 2π height of ambiguity of 38 m.

3 Methods

The basis for the analyses in all three papers was the conventional method for biomass modelling and estimation known as the "area-based method" described section 1.5. The method is based on modelling the relationship between attributes of interest that have been measured or calculated from measurements on field plots, and explanatory variables derived from the remotely sensed data. It is vital that the remotely sensed data is extracted from the horizontal area matching the field plot. Discrepancy in this matching is often referred to as co-registration errors, and has been identified as an important source of error in the "area-based method" (Gobakken & Næsset, 2009). To apply the model on the area of interest, the remotely sensed data are tessellated into units, usually of the same size as the size of the field plots, and the explanatory variables are derived for each unit. The model is then applied to predict the response variable on each population unit.

3.1 Construction of digital terrain models

A prerequisite for the retrieval of useful remotely sensed 3D information for biomass estimation is a high quality DTM. In Papers I and III the DTM was derived from the ALS data by the supplier of the ALS data, Terratec AS, Norway. ALS echoes reflected from the ground were identified and classified using the progressive triangulated irregular network (TIN) densification algorithm (Axelsson, 2000) in the TerraScan software (Anon., 2012). The DTM was derived from the ALS as a TIN from the planimetric coordinates and corresponding heights of the ALS echoes classified as ground echoes. In Paper II a similar classification and construction of a DTM was performed using the "GroundFilter" program in the FUSION toolkit (McGaughey, 2013). The study involved repeated reduction of the ALS pulse density, and DTMs were constructed from pulse densities of 8, 4, 2, 1, 0.5, and 0.25 pulses·m^{-2}. The algorithm presented by Kraus and Pfeifer (1998) and implemented in the "GroundFilter" program initially makes an average surface based on all ALS echoes. Further, weights are given to all echoes based on their vertical distance to the initial surface. Low weight is given to echoes above the surface, and high weight to echoes below. The weights are then used in re-fitting the surface. Two parameters in the algorithm can be adjusted to determine which echoes are weighted. Echoes located below the surface with a distance larger than parameter *g* are assigned the maximum weight value of 1.0, while echoes located above the surface with a distance larger than the parameter *w* plus the parameter g are assigned weights of 0.0 (McGaughey, 2013). To adjust for the different pulse densities the two parameters were controlled while leaving the

other parameters at the program default setting. The *g* and *w* parameter settings at different pulse densities are given in Table 4. Visual inspection of initial classifications of ground echoes showed large outliers and a smoothing filter of 3 m was applied to remove these outliers. From the echoes classified as ground, a 1 m gridded surface was created using the "TINSurfaceCreate" program in FUSION (McGaughey, 2013).

3.2 Explanatory variables derived from remotely sensed data

After creation of a DTM the elevation of the DTM was subtracted from the elevation of all ALS echoes resulting in an elevation above the ground for each echo. From the five echoes per pulse registered by the ALS sensor, each echo was classified into one of three categories: "single", "first of many" or "last of many". The "single" and "first of many" were merged into one dataset, denoted as "first echoes" while the "single" and "last of many" were merged into another dataset and denoted as "last echoes". The two classes of ALS echoes formed the basis for derivation of conventional explanatory variables from the echoes. These variables comprise two main types of variables, canopy height variables and canopy density variables, and were computed separately from the "first echoes" and "last echoes". Both variable types describe the vertical distribution of ALS echoes. Canopy height variables including maximum and mean values (E.max, E.mean), standard deviation (E.sd), coefficients of variation (E.cv), kurtosis (E.kurt), skewness (E.skewness) and percentiles at 10% intervals (E.10, E.20,…, E.90) were derived from the laser echoes above a threshold of 2 m (Paper III) or 4 m (Papers I and II) above ground. Canopy density variables were derived by dividing the height between a 95% percentile height and the threshold into 10 equally spaced vertical layers and calculating the proportion of echoes above each layer to the total number of echoes of each echo category ("first echoes", "last echoes"), including echoes below the threshold (D.0, D.1,…, D.9). To denote whether the variables were derived from the first or last echo category, a subscript L or F was used as notation, e.g. E.mean.F. This computation of ALS variables follows the procedure presented in Næsset and Gobakken (2008) and is frequently implemented in practical forest inventories (Næsset, 2014). In Paper I, additional variables describing horizontal distribution of the echoes from an ALS-derived canopy surface model were computed. Firstly, a rasterized canopy surface model with 1 m resolution was computed from the top-of-canopy ALS echoes. The raster was then converted into grey level images from the field plots, and variables originally presented by Haralick et al. (1973) were calculated using the "glcm" package (Zvoleff, 2014) in R. The texture variables were calculated using a 3 × 3 m window size and averaged in all directions (0, 45, 90 and 135°). Shifts of 3, 6, 9, 12, and 15 m were tested and variables included mean (MN),

homogeneity (HG), variance (VAR), contrast (CONT), dissimilarity (DS), entropy (ENT), angular second moment (SM) and correlation (COR) for each of the shifts. The subscript 3, 6, 9, 12, or 15 was used as notation for the shifts. These variables, originating from image analysis, were proposed as additional information to the conventional height and density variables.

As part of the analysis in Paper II ALS variables from four concentric circular plot sizes of 0.07, 0.14, 0.21, and 0.28 ha were derived. These concentric plots were centred in the centre of the 153 rectangular field plots. A set of ALS variables was derived for each concentric plot using the "CloudMetrics" program in FUSION (McGaughey, 2013). Frequently used variables were selected for analysis. These included E.mean, E.max, E.10, E.90, D.0, D.5, and the variance of the elevation above ground (E.var). The first and last echo categories were not used in the variables in Paper II.

In Paper III, the results from ALS-assisted estimation were compared to use of remotely sensed data from satellite radar imagery. Only one explanatory variable, the mean height, was derived from the InSAR data. SAR image pairs were processed, using a kind of stereo imaging known as interferometry, resulting in a digital surface model (DSM). Further, removal of phase noise and offset and ramp errors was performed using a Goldstein filter (Goldstein & Werner, 1998) and ground control points, respectively. Phase unwrapping was carried out using the minimum cost flow method, and the DSM was geocoded to a ground resolution of 10 × 10 m. Following the construction of the DSM, the DTM derived from the ALS TIN was subtracted from the DSM, resulting in obtained InSAR heights, i.e. heights of the centre of the radar echo above ground. Mean InSAR height was then derived for each field plot by weighting the height of each 10 × 10 m units of the normalized InSAR DSM by the area of the unit intersected by the field plot.

3.3 Statistical analyses

3.3.1 Modelling the relationship between biomass and remotely sensed variables

Linear least-square multiple regression analysis was used for developing biomass models in Papers I and III. To account for heteroscedasticity and non-linear relationships between the response and explanatory variables, a transformation of the response is often used. Natural-log transformations of both response and explanatory variables were performed in Papers I and III. In addition, square-root transformation of the response was tested in Paper I. These transformations introduce a bias when back-transformed to arithmetic scale and procedures for bias-adjustment, described by Goldberger (1968), Gregoire et al. (2008), and Snowdon (1991), were therefore applied. In Paper I the selection of explanatory variables to be included in the

models was performed using a best-subset regression procedure implemented in the "leaps" package (Lumley & Miller, 2009) in R. To avoid multicollinearity, variance inflation factors were controlled and models were selected based on the Bayesian information criterion (BIC). The aptness for prediction of the selected models was validated by 10-fold cross-validation. The accuracy of the models was assessed by the RMSE:

$$\mathrm{RMSE} = \sqrt{\sum_{i=1}^{n}(\hat{y}_i - y_i)^2/n}, \quad (4)$$

where n is number of plots, y_i is the observed value for plot i, $\hat{y}_i$ is the predicted value for plot i. Precision was assessed by the MD:

$$\mathrm{MD} = \sum_{i=1}^{n}(\hat{y}_i - y_i)/n. \quad (5)$$

The relative RMSE (RMSE%) and relative MD (MD%) were calculated as percentages by dividing the absolute RMSE and MD values, respectively, by the observed means.

In a study utilising FD2, Mauya et al. (2015) found that E.60.F and D.1.L were the most frequently selected variables in modelling biomass using plot sizes from 700 to 1900 m^2. E.60.F and D.1.L were therefor selected a priori for the biomass models in paper III.

To explore the relative importance of the explanatory variables, an analysis was performed in Paper I by fitting a separate simple linear model for a random sample of 1/3 of the plots. The single explanatory variable which resulted in the lowest BIC value was included in the model. Random sampling of observations, performed without replacement and model-fitting, was repeated 1000 times. The frequency with which each variable appeared in the model was used as a measure of importance for each individual variable.

3.3.2 Effects of pulse density on DTM and canopy variables

The cost of acquiring ALS data is largely governed by the flight time. By flying higher and/or faster the costs can be reduced, resulting in cheaper but lower pulse density data. The effects of reduced pulse density on the ALS-derived DTM and canopy variables were investigated in Paper II. A random thinning procedure was incorporated in a Monte Carlo simulation, in which the thinning and the subsequent analysis were repeated 50 times per pulse density level, to quantify the effects of the reduced pulse density. To study the effects of reduced pulse densities on the DTMs, the elevation z in the DTMs from reduced pulse densities (z^{DTM}) were subtracted from the elevation of each point (k) measured with dGNSS (z^{dGNSS}) to obtain the difference for each point (D_k, Equation 6):

$$D_k = z_k^{DTM} - z_k^{dGNSS}. \quad (6)$$

The mean difference ($\overline{D}$) and standard deviation (S_D) of the differences (D_k) were calculated. To compare the $\overline{D}$ at each pulse density level a t-test was performed using the Holm-Bonferroni procedure (Holm, 1979) for correction of p-values for multiple comparisons.

Conventional measures of accuracy, $\overline{D}$ and S_D, assumes no outliers and a normal distribution of errors. As pointed out by e.g. Zandbergen (2008), errors in DTMs are not normally distributed. Q-Q plots were therefore produced and checked for non-normality. In addition, robust measures of accuracy suited for characterisation of non-normal distributions suggested by Höhle and Höhle (2009) were produced. The 50% sample quantile of the errors ($P50_D$, i.e., the median value) is a robust estimator for a systematic shift of the DTM (Höhle & Höhle, 2009). The 95% quantile of the absolute value of the errors ($P95_{|D|}$) and the normalized median absolute deviation (NMAD, Equation (7)), a robust estimator for S_D, are estimators resilient to outliers (Höhle & Höhle, 2009).

$$\mathrm{NMAD} = 1.4826 * \mathrm{median}_i(|D_k - P50_D|). \quad (7)$$

The mean value ($\overline{M}$) and standard deviation of each canopy variable (S_M) on plot level were calculated from the Monte Carlo simulations across the 50 repetitions. Even though the canopy variables derived from ALS have been shown to be relatively unaffected by the density of echoes (Lim et al., 2008), reduced pulse density increase the S_M. As explained by Magnussen et al. (2010), random factors affecting the canopy variables suggests that the variables should be considered as random variables instead of fixed, as is commonly the case. These random factors can be referred to as replication effects. Replication effects weaken the fit of the biomass models with a factor termed as the reliability ratio (Fuller, 1987, p. 3). By calculating the replication variance in the variables, estimates of the reliability ratios for the variables were calculated. The method was used by Magnussen et al. (2010), in which the reliability ratio was calculated as the ratio of the variance of each variable among sample plots, to the total variance of the corresponding variable (Equation (8)):

$$\text{Reliability ratio} = (\hat{\sigma}_u^2)/(\hat{\sigma}_u^2 + \hat{\sigma}_w^2), \quad (8)$$

where $\hat{\sigma}_u^2$ is the estimated among-plot variance of the variable and $\hat{\sigma}_w^2$ is the estimated average within-plot variance. High within-plot variance in a variable compared to the variance among plots for the same variable results in a low reliability ratio, indicating that the variable is less reliable as an explanatory variable.

To assess the effect of plot size on the reliability ratio of the variables derived from concentric circles of 0.07, 0.14, 0.21, and 0.28 ha were computed.

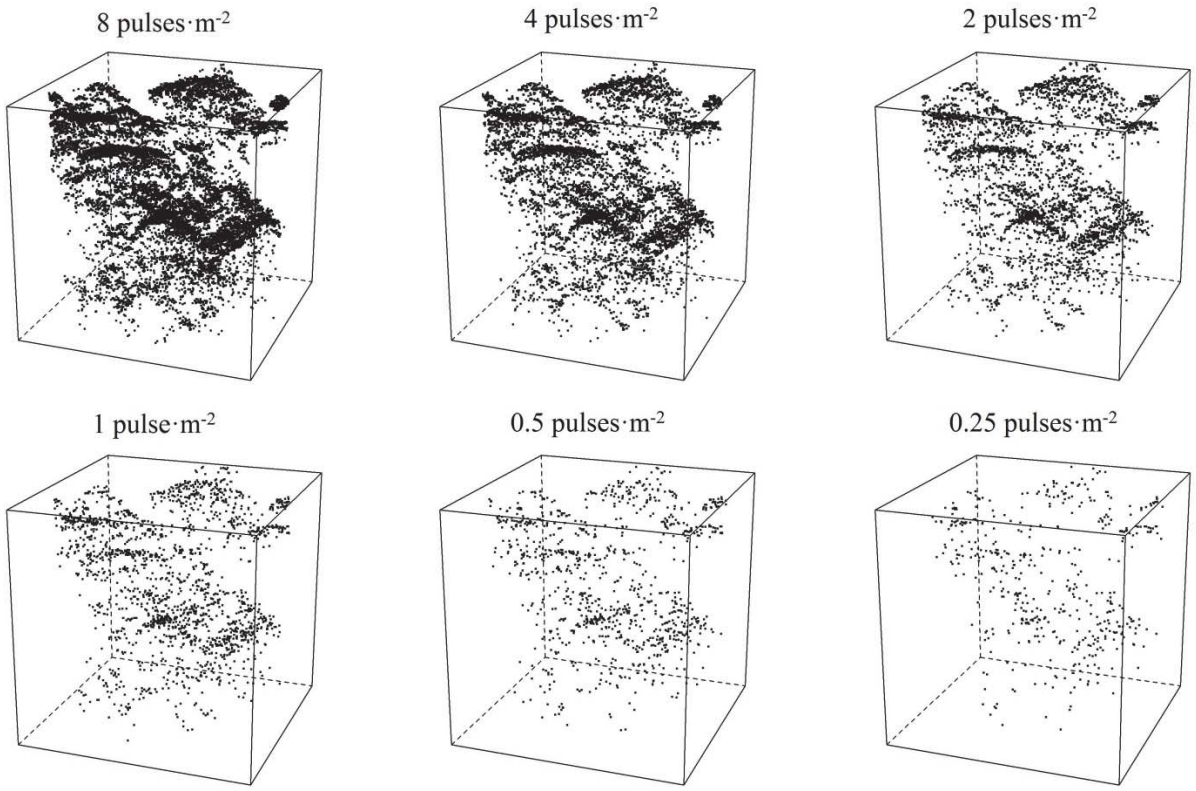

Figure 6. Illustration of thinned ALS echo cloud for plot number 49 with a plot size of 1400 m^2.

3.3.3 Variance estimation

As described in section 1.5, application of an estimated biomass model using the area-based method yields a biomass prediction for each population unit. The biomass predictions for the population elements are subsequently used to derive an estimate for the population, either as a mean or total biomass estimate. Accompanying the estimate, a variance estimate is calculated to state the precision of the estimate. Two main approaches to variance estimation have been used in forest inventories: design-based and model-based variance estimation. In the design-based approach the population, from which samples are taken, is regarded as fixed. The only source of variance is the random selection of elements included in the sample. Thus, the estimated variance is derived from the inventory sample and the probability of each population element to be included in the sample, referred to as the inclusion probability. This inclusion probability is assumed to be positive and known for all population elements. Such samples are often referred to as probability samples.

It is often the case, however, that the sample has been acquired in a non-probabilistic manner (Clark & Kellner, 2012), resulting in zero- or unknown inclusion probabilities. The

zero- or unknown inclusion probability can be the result of opportunistic sampling, i.e. sampling close to roads for economic and/or practical reasons. Similarly, purposive sampling, established to investigate a specific subject, often result in samples acquired in a non-probabilistic manner. Furthermore, the inclusion probability can be affected by the accessibility of the area (Köhl et al., 2006, p. 76). In the case where the sample data does not meet the requirements for a design-based approach to variance estimation, a model-based approach may be a viable alternative. Model-based inference does not, as opposed to design-based inference, rely on a probabilistic sample that represents the population. Instead the statistical inference relies on the model itself as a valid model of the distribution of possible observations for each population element. The population is not viewed as fixed, but rather as a result of a random process, referred to as a "superpopulation" model. This "superpopulation" model cannot be observed, but the parameters of the model can be estimated from the survey sample. The surveyed population is viewed as only one random realisation of this "superpopulation".

Because the field plots in FD2 were distributed in order to cover the height gradient in the ANR, the inclusion probabilities of the plots were unknown, and a model-based approach to estimation and inference was used in Paper III.

The approach followed the notation in Ståhl et al. (2011), where an element of the "superpopulation" was expressed as:

$$y_i = g(x_i, \alpha, \varepsilon_i), \tag{9}$$

where y is a vector of the observed plot biomass on plot i, x is a vector of variables derived from the auxiliary data, α is a vector of model parameters and ε is a vector of errors, and g is a function describing the "superpopulation". It is assumed that the errors are independent, normally distributed, with a constant variance, and without spatial auto-correlation. The parameters α were estimated with $\hat{\alpha}$ using least square regression, and used to estimate the population mean by:

$$\hat{\mu} = \frac{1}{N}\sum_{i=1}^{N} g(x_i, \hat{\alpha}), \tag{10}$$

where i indexes the population elements and N is the number of elements, i.e., i = 1, 2, …, N. Assuming that the estimated $\hat{\alpha}$ is accurate, the g function was linearized in the neighbourhood of the true function using first order Taylor series expansion:

$$\begin{aligned} g(x, \hat{\alpha}) \approx g(x, \alpha) + (\hat{\alpha}_1 - \alpha_1) * g_1'(x, \alpha) + (\hat{\alpha}_2 - \alpha_2) * g_2'(x, \alpha) \\ +\ldots+ \left(\hat{\alpha}_p - \alpha_p\right) * g_p'(x, \alpha), \end{aligned} \tag{11}$$

where $g'_j(x,\alpha) = \partial g(x,\alpha)/\partial\alpha_j$, j indexes the parameters and p is the number of parameters, i.e.,

j = 1, 2, …, k, …, p. The variance of the population mean was then estimated by:

$$\widehat{\mathrm{var}}(\hat{\mu}) = \sum_{j=1}^{p}\sum_{k=1}^{p}\widehat{\mathrm{Cov}}\left(\hat{\alpha}_j,\hat{\alpha}_k\right)\hat{\bar{g}}'_j\hat{\bar{g}}'_k, \quad (12)$$

where $\hat{\bar{g}}'_j$ and $\hat{\bar{g}}'_k$ are the estimated mean values of the first order derivatives of the g function for parameters j and k, respectively (cf. Ståhl et al., 2011).

Unlike design-based estimators, which often are unbiased or nearly unbiased, the unbiasedness of model-based estimators depends on the model being correctly specified. It was therefore paramount to assess how well the model fitted the field plot observations. Assessment of the fit of the models followed the approach used by McRoberts et al. (2013a). Scatterplots of observed *vs.* predicted biomass were produced for each plot size. Correctly specified models should result in points falling closely along a 1:1 line with intercept 0 and slope 1. Further, pairs of observations and predictions were ordered with respect to the predicted values and grouped into three classes of 10 pairs. The mean of the observed *vs.* predicted biomass was plotted for each group. A correctly specified model should again result in points falling along a 1:1 line.

3.3.4 Relative efficiency

To assess the gain in precision of using remotely sensed data to enhance the estimates, relative efficiency was calculated for both ALS ($RE_{TE:ALS}$) and InSAR ($RE_{TE:InSAR}$). Simple log-log models with the terrain elevation from the DTM as explanatory variable were developed for each plot size of 700, 900, …, 1900 m^2. These models were denoted as TE models. The relative efficiencies were calculated as ratios of the estimated variance for the mean biomass estimate ($\hat{\mu}$) for each plot size using the TE models divided by the variance estimates for each plot size using the ALS models:

$$RE_{TE:ALS_s} = \widehat{\mathrm{var}}(\hat{\mu}_{TE})_s/\widehat{\mathrm{var}}(\hat{\mu}_{ALS})_s, \quad (13)$$

where s is an indicator of the plot sizes 700, 900, …, 1900 m^2. Similarly, relative efficiency for InSAR was computed as:

$$RE_{TE:InSAR_s} = \widehat{\mathrm{var}}(\hat{\mu}_{TE})_s/\widehat{\mathrm{var}}(\hat{\mu}_{InSAR})_s. \quad (14)$$

Efficiency of ALS was also calculated relative to InSAR ($RE_{InSAR:ALS}$) in the same way by dividing the variance estimates for each plot size using the InSAR models by the variance estimates for each plot size using the ALS models:

$$\mathrm{RE}_{\mathrm{InSAR:ALS_s}} = \widehat{\mathrm{var}}(\hat{\mu}_{\mathrm{InSAR}})_s / \widehat{\mathrm{var}}(\hat{\mu}_{\mathrm{ALS}})_s. \quad (15)$$

In a design-based framework, applying simple random sampling (SRS), the relative efficiency can be used directly to calculate the additional number of field observations needed to compensate for the contribution of the remotely sensed data, which is a fundamental quantity in cost comparisons. This is because the SE of the mean estimate under SRS is proportional to the square root of the sample size minus the number of explanatory variables minus one (Stoltzenberg, 2009, p. 181). In practice, a relative efficiency of two would mean that the gain of the remotely sensed data could be compensated by twice as many field plots, assuming that the sample variance remain constant.

In the model-based framework used in Paper III the SE of the mean estimate is also assumed to reduce with increased number of observations. However, the number of observations needed to reach the same SE for the different models cannot be deduced by analytical means. Instead a basic Pólya-urn resampling scheme was applied as described in Köhl et al. (2006, pp. 195–196) to simulate the variance of the TE models. The Pólya-urn resampling scheme generates a design-consistent posterior predictive distribution of the property in interest, given that the sample is reasonably large and representative of the population (Ghosh & Meeden, 1997, p. 44–46). The field sample of u = 30 observations were considered as representative of the population, and the Pólya-urn resampling generated posterior predictive distributions of biomass for U = 60, 120, and 180 observations based on the sample. From a virtual urn, containing the 30 observations, one observation was randomly drawn, duplicated, and returned to the urn together with the duplicate. The urn thus contained u + 1 = 31 observations. The selection scheme was repeated until the desired number U of observations in the urn was reached. The simulations were repeated 200 times and the mean variance of observed biomass reported.

4 Results and discussion

Results presented in the papers constituting this thesis cover different aspects of using remotely sensed data in support of forest surveys in a dense tropical rainforest in Tanzania. With regards to the main objective in this thesis, the assessment of ALS as an auxiliary source of data, all three papers contributed to an increased knowledge in the use of ALS in dense tropical forests.

As pointed out in section 2.2.2, the observed biomass in the present thesis is subject to uncertainty not accounted for related to the allometric models and field measurements of DBH and tree height. Thus, errors related to the biomass observations are not accounted for. Overlooking these errors lead to overoptimistic precision of the variance estimates. In a study conducted in a tropical forest in Ghana, and with a plot size of 1600 m^2, Chen et al. (2015) found that the impact of allometric error contributed about 11% to the total relative prediction error. With similar forest conditions and plot sizes, it is reasonable to assume errors of similar influence in the present thesis.

4.1.1 Modelling aboveground biomass using ALS data

Paper I documented the relationship between ALS-derived variables and biomass calculated from measurements on field plots. In terms of accuracy and precision (Table 3), the results were similar to those of other recent studies in similar forests and with similar field plot sizes (Clark et al., 2011; Ioki et al., 2014; Laurin et al., 2014).

The study that was reported in Paper I also identified some modelling challenges when using the field observations in FD1. Firstly, the size of the field plots, together with their rectangular shape, possibly resulted in large negative boundary effects. These effects are due to a discrepancy between trees included in the field inventory and parts of their crown being outside the vertical boundary of the plot, and *vice versa*. Secondly, in a natural forest that has reached a climax state, old and aging trees will have reduced or even negative height and crown development. Because of the asymptotic relationship between height and diameter, canopy height variables are less suitable for discriminating between tall trees with various diameters. It is generally the large trees in a tropical forest that show this asymptotic H-D development (Poorter et al., 2006; Iida et al., 2011). Since the largest trees have great influence on the biomass in the observed biomass, this could explain the underestimation on field plots with a high biomass value, as observed in Paper I. Similar observations were made by Skowronski et al. (2007) in a temperate forest with a weak relationship between tree height and tree diameter. An analysis of the relative importance of ALS variables was therefore performed in Paper I. This analysis showed that most of the information for explaining biomass was found in

variables describing the vertical density of the full vegetation layer, and in variables from the last return echoes (Figure 8). Variables describing the height of the vegetation, which have been found to be important in boreal studies (Næsset & Gobakken, 2008), were found to be less useful in explaining the forest biomass. Similar results with regards to variable importance as those in Paper I, have also been presented by Laurin et al. (2014) for a tropical forest in Sierra Leone, West Africa.

Table 3. Summary of regression models for biomass using ALS variables.

Model	Response variable	Predictive model[a]	Model fit		10-fold cross-validation[b]			
			R^2	BIC	RMSE	RMSE%	MD	MD%
A	ln biomass	3.815 + 1.755·D.2.L+ 1.498·D.9.L + 0.016·E.90.F	0.70	98.8	149.18	32.3	−2.40	0.5
B	ln biomass	3.984 + 3.222·MN.3	0.52	160.6	173.84	37.6	−8.57	1.9
C	ln biomass	3.665 + 1.530·D.2.L + 1.231·D.9.L + 0.013·E.90.F + 0.737·MN.15	0.71	98.7	158.02	34.4	−2.85	0.6
D	sqrt(biomass)	3.796 + 11.294·D.2.L + 13.321·D.9.L+ 0.249·E.mean.L	0.62	814.4	154.44	33.4	6.12	1.3
E	sqrt(biomass)	7.563 + 0.054·MN.3 − 0.072·CONT.3	0.48	857.0	169.77	36.8	8.17	1.8
F	sqrt(biomass)	3.796 + 11.294·D.2.L + 13.321·D.9.L + 0.249·E.mean.L	0.62	814.4	156.59	33.9	5.57	1.2

[a] Explanatory variables presented in section 3.2; [b] Values after back-transformation to arithmetic scale.

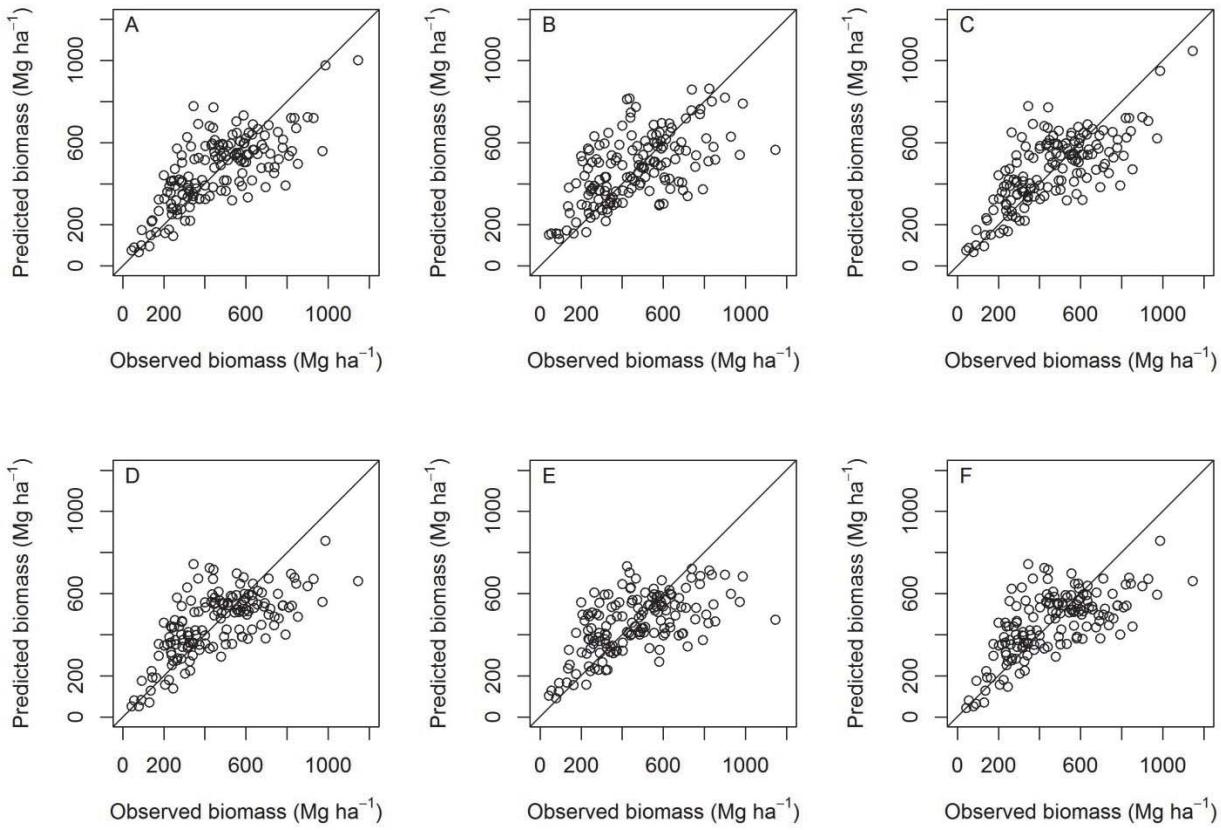

Figure 7. Scatter plots of observed *vs.* predicted biomass using logarithmic (A–C) or square root transformations of the response (D–F) in combination with vertical variables (A, D), texture variables (B, E) and both vertical and texture variables (C, F).

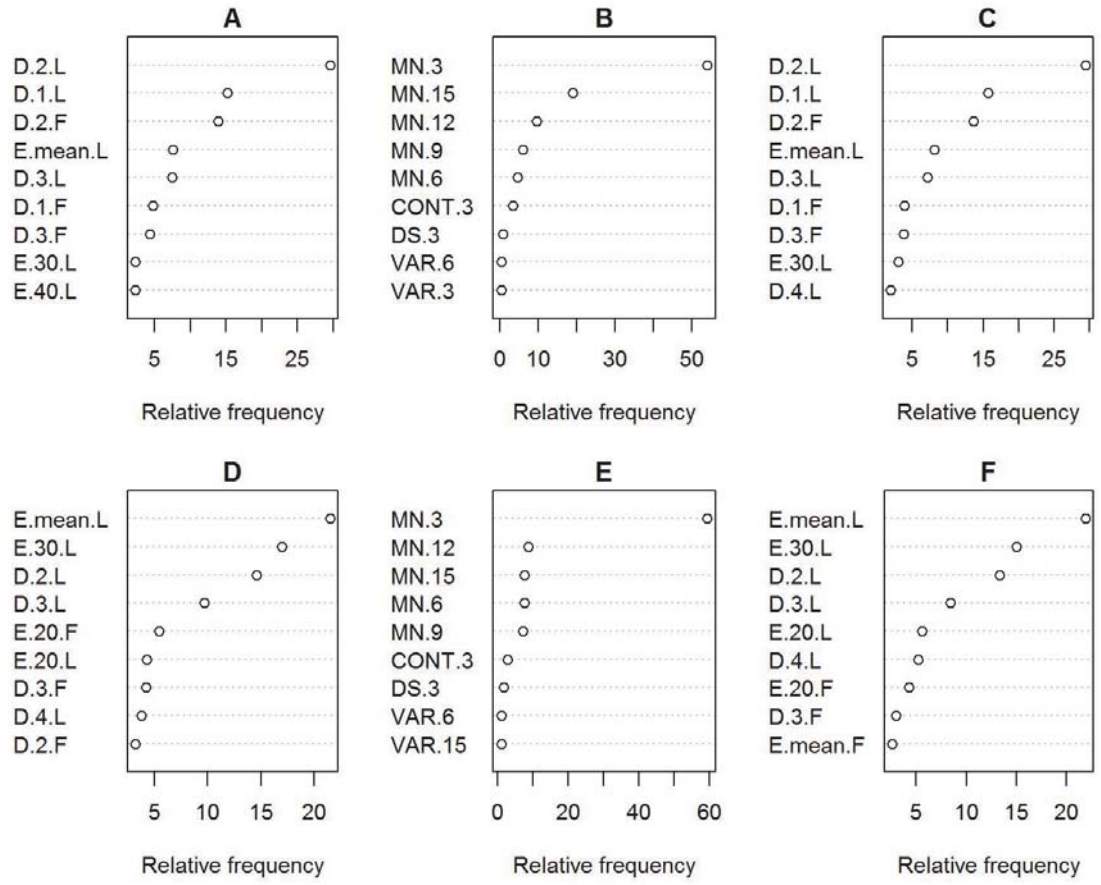

Figure 8. Dot charts of the relative frequency of the nine most frequently selected explanatory variables in a simple linear model fitting procedure with logarithmic (A–C) and square root transformation of the response (D–F) in combination with vertical variables (A, D), texture variables (B, E) and both vertical and texture variables (C, F). Variables are explained in Section 3.2.

4.1.2 Effects of pulse density on DTM quality and ALS variables

Effects of reduced pulse density on the DTMs and canopy variables derived from ALS data were assessed in Paper II. Reduced pulse density, assessed by Monte Carlo simulation, resulted in a $\overline{D}$ between the elevation of 612 point measurements recorded by the dGNSS and the elevation of the same points in the ALS-derived DTM of 1.81 m for a pulse density of 8 pulses·m^{-2} (Table 4). Thus, the elevation recorded by the dGNSS was higher than the ALS-derived DTM. Reduction of pulse density from 8 to 0.25 pulses·m^{-2} gave no significant effect on the $\overline{D}$.

Q-Q plot of the distribution of errors (Figure 9) showed non-normality and justified the presentation of robust measures of accuracy. A loss of precision was observed when the pulse density was reduced from 8 to 0.25 pulses·m^{-2}. This loss of precision was expressed both by the conventional measure of precision, S_D, and the more robust measure NMAD (Table 4).

Table 4. Summary of the difference in elevation between the dGNSS measurements and the DTM elevation for different pulse densities.

						Parameter settings[1]	
Pulses·m^{-2}	$\overline{D}$ (m)	S_D (m)	$P50_D$ (m)	$P95_{\|D\|}$ (m)	NMAD (m)	*g* (m)	*w* (m)
0.25	1.77	3.20	0.90	7.72	2.15	-1.0	1.5
0.5	1.77	3.02	0.92	7.50	1.97	-1.5	2.0
1	1.79	2.93	0.94	7.34	1.85	-2.0	2.5
2	1.81	2.90	0.96	7.28	1.80	-2.5	3.0
4	1.81	2.88	0.95	7.20	1.75	-3.0	3.5
8	1.81	2.89	0.95	7.35	1.81	-3.5	4.0

Mean difference ($\overline{D}$), standard deviation (S_D), 50% quantile of the difference ($P50_D$), 95% quantile of the absolute value of the difference ($P95_{|D|}$) and the normalized median absolute deviation (NMAD).
[1] Settings of the *g* and *w* parameters in the applied ground classification algorithm.

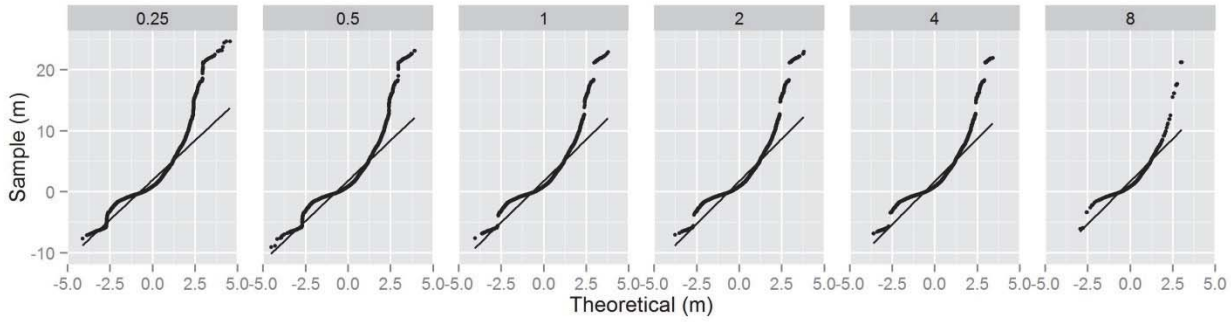

Figure 9. Normal Q-Q-plot for the distribution of the difference in elevation between the elevation recorded by the dGNSS and the elevation of the corresponding ALS-derived DTM at pulse densities of 0.25, 0.5, 1, 2, 4, and 8 pulses·m^{-2}.

Mean values from repeated simulations showed that most of the explanatory variables were unaffected by a reduced pulse density (Table 5). E.max, however, decreased with reduced pulse density, and showed a significant difference of 0.58 m at 1 pulse·m^{-2} compared to the value at 8 pulses·m^{-2} at a plot size of 0.07 ha. This effect was reduced with increased plot size, but was still significant for 1 pulse·m^{-2} at a plot size of 0.28 ha.

Reduced pulse density resulted in increased variance in the canopy variables on plot level (Figure 10). The standard deviations for the explanatory variables (S_M) showed that the variable describing the canopy elevation in the middle of the canopy (E.mean) was more stable than the elevation of the top and bottom of the canopy (E.max, E.10, E.90). Reduction of the

pulse density from 8 to 0.25 pulses·m^{-2} increased the S_M for E.mean from 0.09 to 0.90 m on a 0.07 ha plot size (Figure 10). The S_M of E.max increased from 0.16 to 1.03 m at a plots size of 0.07 ha.

Further, reduced pulse density resulted in decreased reliability ratio, the ratio of the estimated among-plot variance to the estimated total variance (Figure 11). At pulse densities ≥2 pulses·m^{-2}, and a plot size of 0.07 ha, the reliability ratio was >0.95 for all explanatory variables. At a pulse density of 0.5 pulses·m^{-2}, and a plot size of 0.07 ha, the reliability ratios of E.var and D.0 were reduced down to 0.60 and 0.90, respectively. At a pulse density of 0.25 pulses·m^{-2}, and a plot size of 0.07 ha, E.var, E.10, and D.0 had an estimated reliability ratio of <0.9, while the rest of the variables had a reliability ratio of >0.9.

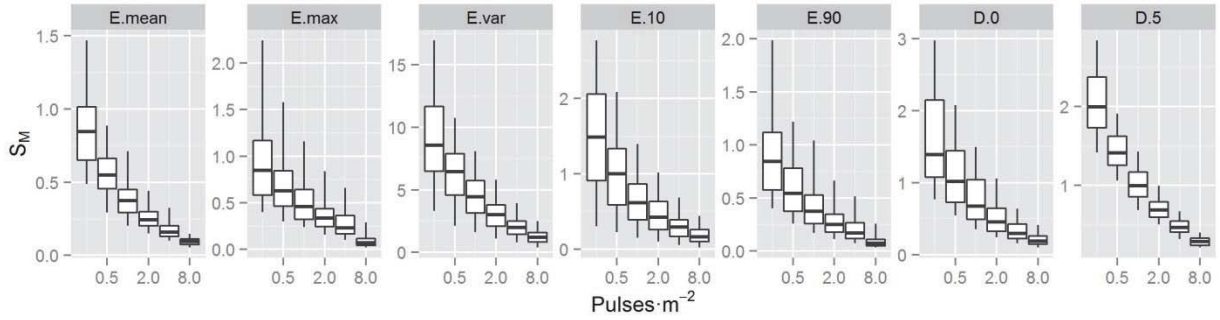

Figure 10. Box and whisker plots of standard deviations (S_M) (whiskers at 5th and 95th percentile) of ALS-derived explanatory variables for plot size of 0.07 ha and pulse densities of 0.25, 0.5, 1, 2, 4, and 8 pulses·m^{-2}. E.mean (mean elevation above ground), E.max (maximum elevation above ground), E.var (variance of the elevation above ground), E.10 and E.90 (10th and 90th height percentile of canopy points), D.0 and D.5 (the proportion of points above the ground and above the mean canopy height).

Table 5. Mean values ($\overline{M}$) of explanatory variables for plot sizes of 0.07, 0.14, 0.21, and 0.28 ha and pulse densities of 0.25, 0.5, 1, 2, 4, and 8 pulses·m^{-2}.

		$\overline{M}$						
Plot size (ha)	Pulses·m^{-2}	E.mean	E.max	E.var	E.10	E.90	D.0	D.5
0.07	0.25	24.59	41.42	107.59	10.06	36.15	89.99	55.18
0.07	0.5	24.49	41.75	108.79	9.79	36.18	90.01	55.25
0.07	1	24.47	41.98	108.93	9.72	36.16	90.09	55.39
0.07	2	24.49	42.22	109.17	9.70	36.19	90.17	55.47
0.07	4	24.59	42.36	108.72	9.82	36.21	90.29	55.68
0.07	8	24.69	42.56	108.17	9.93	36.26	90.33	55.73
0.14	0.25	24.59	43.44	112.27	9.48	36.64	90.07	54.67
0.14	0.5	24.47	43.70	113.24	9.28	36.60	90.07	54.74
0.14	1	24.45	43.92	113.60	9.21	36.60	90.15	54.80
0.14	2	24.49	44.11	113.67	9.24	36.63	90.23	54.89
0.14	4	24.60	44.23	113.15	9.40	36.68	90.38	55.05
0.14	8	24.70	44.39	112.60	9.52	36.74	90.44	55.14
0.21	0.25	24.60	44.38	114.04	9.33	36.93	90.16	54.35
0.21	0.5	24.47	44.61	114.91	9.12	36.86	90.14	54.42
0.21	1	24.43	44.81	115.22	9.04	36.84	90.18	54.50
0.21	2	24.49	45.03	115.35	9.07	36.88	90.28	54.59
0.21	4	24.59	45.17	114.83	9.22	36.93	90.40	54.72
0.21	8	24.70	45.33	114.22	9.35	37.00	90.48	54.82
0.28	0.25	24.59	45.01	115.87	9.13	37.05	90.01	54.31
0.28	0.5	24.45	45.23	116.54	8.93	36.97	89.97	54.36
0.28	1	24.44	45.47	116.95	8.87	36.98	90.04	54.45
0.28	2	24.48	45.68	116.93	8.91	37.00	90.12	54.52
0.28	4	24.59	45.85	116.40	9.05	37.05	90.24	54.66
0.28	8	24.69	45.98	115.84	9.18	37.12	90.33	54.75

Mean elevation above ground (E.mean), maximum elevation above ground (E.max), variance of the elevation above ground (E.var), 10th and 90th percentile of elevation (E.10 and E.90), and the proportion of points above the ground (D.0) and above the mean canopy height (D.5).

The statistics for the canopy variables, resulting from the Monte Carlo simulations, showed that the variances of the variables were reduced with plot size for all variables and at all pulse densities (Figure 11). Increasing the plot size means that the probability of including larger trees increase. As a result, the maximum elevation (E.max) and the elevation of the top

of the canopy (E.90) were found to increase in value with increased plot size (Table 5). Increasing the plot size also means that more of the variability in the elevation of ALS-echoes is captured by the plot, resulting in increased E.var. Variables describing the elevation of the lowest part of the canopy (E.10) and the proportion of points above the mean canopy height (D.5), however, decreased in value with increasing plot size. E.mean and D.0 did not show any trend with increased plot size. The reliability ratio increased for all variables with increasing plot size.

Dense vegetation obstructs the ALS pulses and results in fewer pulses reaching the ground and being available for DTM construction. The effect of vegetation on ALS-derived DTMs has been studied in different conditions and has resulted in both an over-prediction of terrain elevation (Bowen & Waltermire, 2002; Reutebuch et al., 2003; Töyrä et al., 2003) and under-prediction of terrain elevation (Hodgson et al., 2005; Tinkham et al., 2011). Hodgson et al. (2005) found that ALS-derived elevation was significantly under-predicted in all studied land cover classes. The under-prediction was largest in pine forest areas, by up to 0.24 m. Tinkham et al. (2011) also found an under-prediction of 0.9–0.16 m in coniferous areas, when comparing two different ground classification algorithms. In their discussion of observed under-predicted terrain elevation in heavily vegetated areas, Hodgson et al. (2005) suggested that the error was a result of echo density, and/or the accuracy of correct classification of echoes as ground.

The analysis in Paper II showed that the mean DTM elevation was unaffected by the reduction in pulse density from 8 to 0.25 pulses·m^{-2}. This was in contradiction with results from other studies on reducing ALS data density (Hyyppä et al., 2005; Anderson et al., 2006; Leitold et al., 2015). In a tropical forest with similar conditions as in the present study, Leitold et al. (2015) found an increased DTM elevation of 3.02 m at 1 pulse·m^{-2}, compared to a DTM from 20 pulses·m^{-2}. Leitold et al. (2015) attributed the increased elevation to the morphological filter algorithm (Zhang et al., 2003) used to classify ground points. Hyyppä et al. (2005), who used data collected in three separate flights, attributed an increased DTM elevation to the beam size and sensitivity of the laser.

From the analysis of the DTMs in Paper II and the results in several different studies related to construction of DTMs in different conditions, it seems clear that systematic effects of pulse thinning could be the result of the algorithm used to classify ground echoes or the parameter settings in the algorithm. Thus, great care is needed when using ALS data from different sensors and flying conditions, in diverse vegetation, and with different sensor-settings in terms of correctly classifying the ground echoes.

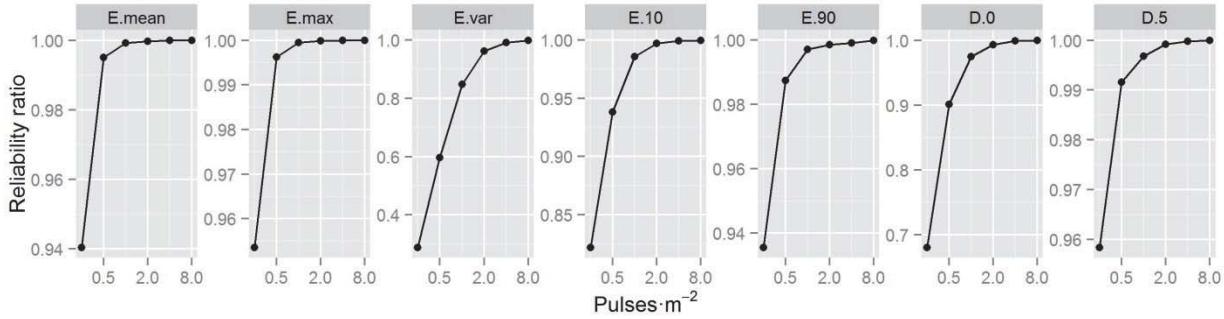

Figure 11. Plots of reliability ratios for ALS-derived variables at a plot size of 0.07 ha and pulse densities of 0.25, 0.5, 1, 2, 4, and 8 pulses·m^{-2}. E.mean (mean elevation above ground), E.max (maximum elevation above ground), E.var (variance of the elevation above ground), E.10 and E.90 (10th and 90th height percentile of canopy points), D.0 and D.5 (the proportion of points above the ground and above the mean canopy height).

Valbuena et al. (2012) assessed the vertical accuracy of a dGNSS receiver (Topcon Hiperpro), similar to the receiver used in the present thesis, under pine canopies in Spain. By using true coordinates obtained in a total station traverse, they found the accuracy to be 1.18 m with a standard deviation of 1.55 m. It is therefore expected that recordings under dense rainforest canopies with the reception of fewer satellite signals and more problems with multipath signals, result in lower accuracy.

Recent studies of biomass in tropical forests using ALS have been conducted using different pulse densities and plot sizes. Pulse densities from 25 pulses·m^{-2} (d'Oliveira et al., 2012) down to about 1.5 pulses·m^{-2} (Asner & Mascaro, 2014) have been used. The results from these studies are similar in terms of biomass prediction performance and show that high pulse density is not a requisite for estimation of forest biomass. In biomass studies where the key information is the vegetation height relative to the terrain elevation derived from the same ALS data, a systematic shift in the modelled surface is not a problem in itself. Of greater concern is the random error of the modelled terrain elevation. As expected, the standard deviation of $\overline{D}$ (S_D) increased with reduced pulse density. S_D increased from 2.9 m to 3.2 m when pulse density was reduced from 8 and 0.25 pulses·m^{-2}, respectively. This variation will directly translate into variation in the ALS-derived canopy variables.

Analysis of commonly applied canopy variables showed that the variables were affected differently by pulse density. As previously documented by Gobakken and Næsset (2008), E.max, which characterizes the maximum elevation of the canopy, decreases with decreasing pulse density. Mean values of the other variables assessed in the present study were found to

be stable. Reduced pulse density increased the variation in canopy variables and will result in models with increased residual variance. The estimated reliability of the explanatory variables, expressed by the reliability ratio, showed that all variables were reliable (reliability ratio >0.9) at pulse densities of down to 2 pulses·m^{-2}. Further reduction of pulse density resulted in some canopy variables becoming less reliable although most variables retain a reliability ratio of >0.9 at 0.5 pulses·m^{-2}. In low pulse density conditions (<1·m^{-2}), and with use of explanatory variables with a reliability ratio <0.9 Magnussen et al. (2010) proposed the use of a model calibration procedure.

Increasing the field plot size reduces the variation in ALS-derived variables and could counter the effects in low pulse density missions, concurring with the results of Gobakken and Næsset (2008). However, larger field plots are costly and finding the optimal balance between costs and desired accuracy has for decades been an issue of interest in designing forest inventories. Zeide (1980) presented how to optimize the plot size for systematic sampling. The optimal plot size is a function of the coefficient of variation between plots, plot measurement time, and travelling time between plots, under budgetary restraints or for a desired accuracy.

Although the study in Paper II aimed to simulate the effects caused by various flight elevations and speeds on the DTM and canopy variables derived from ALS data, effects such as increased footprint size and reduced pulse energy were not simulated and studied. Studies of the effects of footprint size on derived tree heights have shown that increased footprint size reduces the derived tree height estimates (Andersen et al., 2006). Andersen et al. (2006) found that this effect was stronger for trees with narrow crowns, and thus, we can expect that the effect is small in a tropical forest with wide tree crowns. Larger footprint sizes will, however, also have less energy per area unit and be less able to penetrate through the canopy (Hyyppä et al., 2005; Goodwin et al., 2006), resulting in a lower proportion of ground points. The influence of footprint size and pulse energy is likely to be of importance and should be investigated in future studies.

4.1.3 Effects of plot size on relative efficiency of ALS and InSAR data

In Paper III the main objective was to assess the effect of plot size on the relative efficiency of using auxiliary data from ALS and InSAR in estimation of biomass. Using FD2, separate log-log models were constructed for plot sizes of 700, 900, …, 1900 m^2 with auxiliary data from (1) the terrain elevation from a DTM (TE), (2) ALS, and (3) InSAR. TE models showed a positive correlation between biomass and elevation, and the explanatory variable was increasingly significant from $p = 0.044$ at 700 m^2 to $p = 0.002$ at 1900 m^2. Biomass was also

positively correlated to the two explanatory variables in the ALS models and the InSAR-height used in the InSAR models. All variables were significant at a 95% level except one of the ALS variables (D.1.L) at plot sizes of 1100–1700 m^2.

Inspection of the scatterplots of observed *vs.* predicted biomass (Figures 12–14) showed that the models had a lack of fit resulting in over-prediction of biomass in areas of low biomass and under-prediction in areas of high biomass. Similar lack of fit has been reported in studies from areas with high forest density (e.g. Nord-Larsen & Schumacher, 2012; Vincent et al., 2012). The plots of the grouped means of observations *vs.* predictions (Figures 15–17), however, showed small differences.

Increasing the plot size from 700 to 1900 m^2 reduced the SE of the mean estimates from 15.3 to 10.6% using TE, from 10.1 to 5.1% using ALS, and from 11.3 to 6.4% using InSAR (Figure 18). Both ALS and InSAR performed well compared to TE in terms of SE. ALS and InSAR estimates had an SE of about 5 and 4 percentage points lower than TE, respectively. Further, InSAR performed well compared to the ALS with only 0.4–1.3 percentage points higher SE depending on plot size. The differences in SE translated into relative efficiencies of 3.6–6.7 using ALS and 2.6–4.0 using InSAR, compared to TE (Figure 19). The relative efficiency of the ALS data also increased with increased plot size relative also to the InSAR data (Figure 19). At a plot size of 1900 m^2 the ALS was 6.7 times as efficient as using TE and 1.7 times as efficient as InSAR. The fact that the relative efficiency of ALS and InSAR increased with increased plot size may partly be due to reduced relative influence of boundary effects and co-registration errors. The slight increase in relative efficiency of ALS compared to InSAR may also indicate that the relative influence of boundary effects and co-registration errors is stronger for ALS than for InSAR. The relative efficiency of ALS compared to InSAR is modest compared to studies in Norway that have found the relative efficiency of ALS to be about twice to that of InSAR (Næsset et al., 2011; Rahlf et al., 2014).

As stated by Gregoire et al. (2015), information about the approach to statistical inference, design- or model-based, is essential in assessing the estimated variance. Taking the design-based approach to variance estimation d'Oliveira et al. (2012) reported a relative efficiency of 3.4 in a study utilising 50 plots of ∼0.25 ha in the Brazilian Amazon. A relative efficiency of 2.1 can similarly by computed from the variance estimates in Paper I. Large negative boundary effects in the ALS variables would contribute to a lower relative efficiency for smaller plots like the plots of ∼0.1 ha used in Paper I.

The relative efficiencies computed in Paper III in the model-based framework cannot be used as a factor for calculating the contribution of the remotely sensed data in terms of added

observations (see section 3.3.4). Instead a Pólya-urn resampling scheme was used to simulate the effect of additional field observations on the TE models. To reach similar levels of variance as for the ALS models with the TE models, the number of field plots would have to be increased by a factor of 3.5–6 depending on plot size (Figure 20).

The DTM used directly to derive the TE variable in the TE-models, and to derive the InSAR elevation above the terrain, was derived from the ALS data. DTMs constructed from ALS data have generally high accuracy (Meng et al., 2010). In the absence of an ALS-derived DTM, a DTM derived from other sources would have influenced the results. A DTM derived from sources like P-band SAR (e.g. Neeff et al., 2005) or the topographic map series of Tanzania, would most likely have resulted in substantially increased SE of the InSAR and TE estimates. In a study using InSAR height to estimate forest biomass in Norway Næsset et al. (2011) it was found that relative RMSE was approximately seven percentage points higher using a DTM from topographic maps with a contour interval of 20 m, compared to using an ALS-derived DTM. P-band SAR, used with good results in Neeff et al. (2005), is currently only available from airborne platforms, and was not collected in ANR.

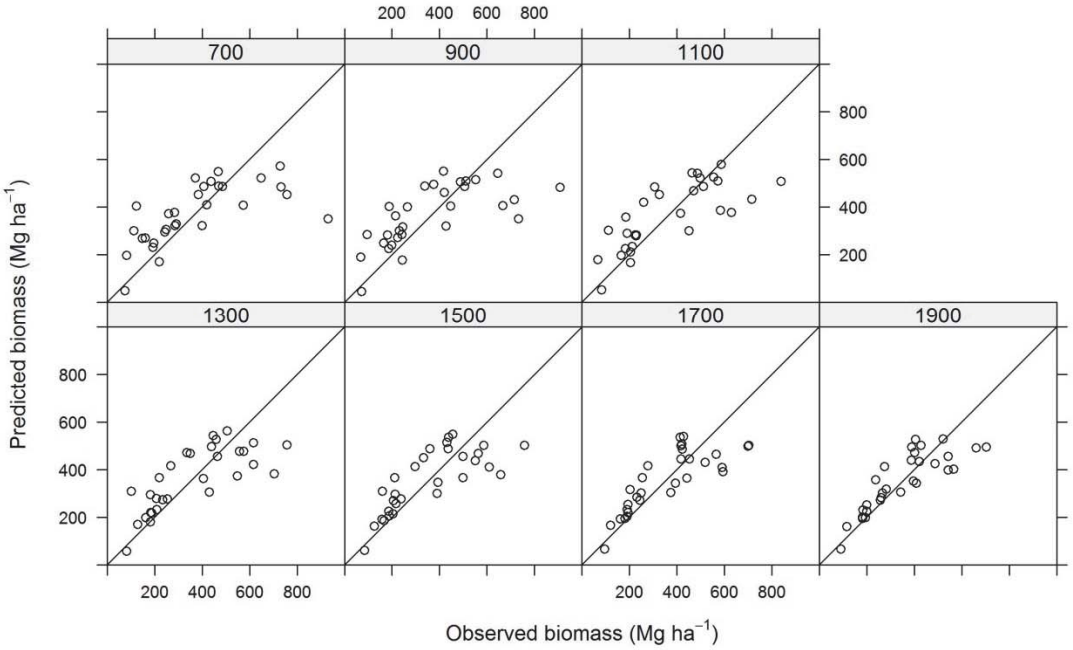

Figure 12. Observed *vs.* predicted biomass values using ALS for plot sizes of 700, 900,…, 1900 m^2.

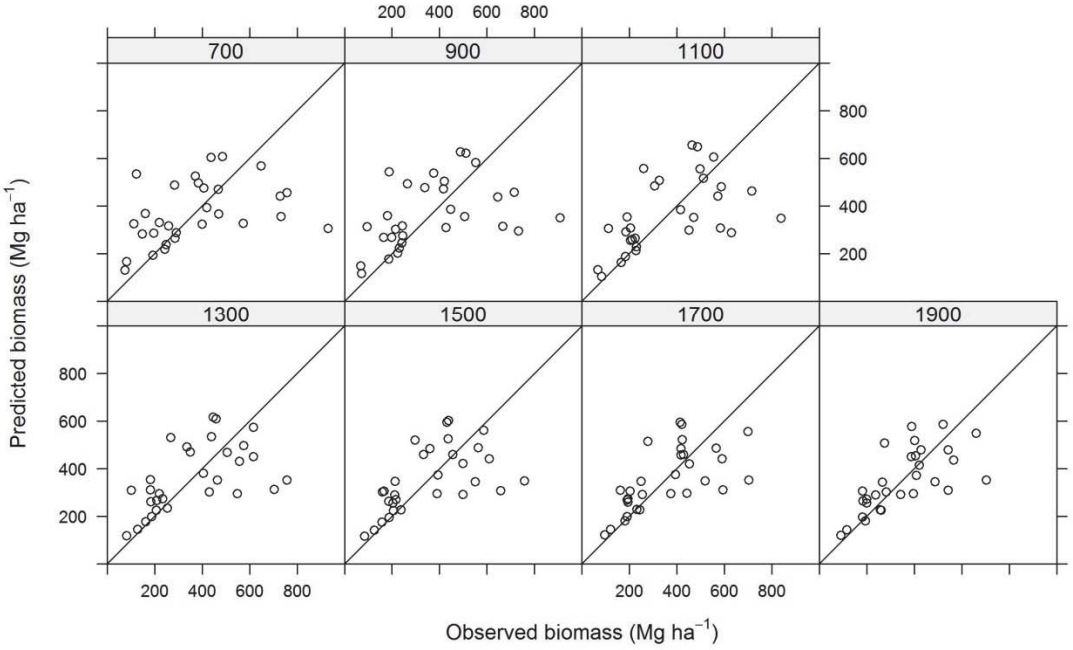

Figure 13. Observed *vs.* predicted biomass values using InSAR for plot sizes of 700, 900,…, 1900 m^2.

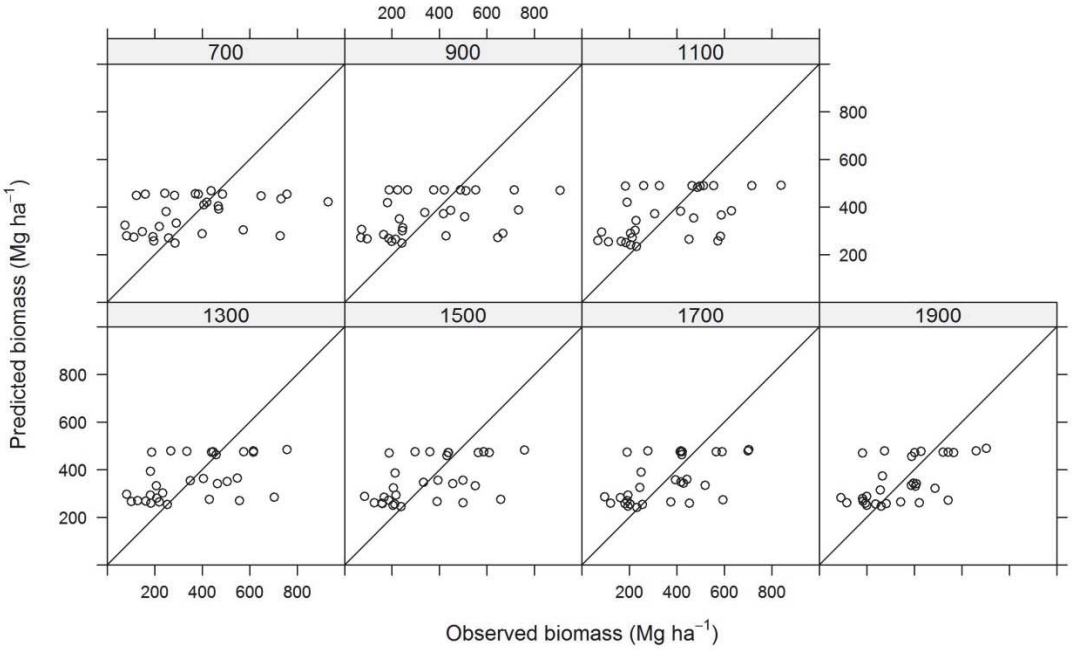

Figure 14. Observed *vs.* predicted biomass values using TE for plot sizes of 700, 900,…, 1900 m^2.

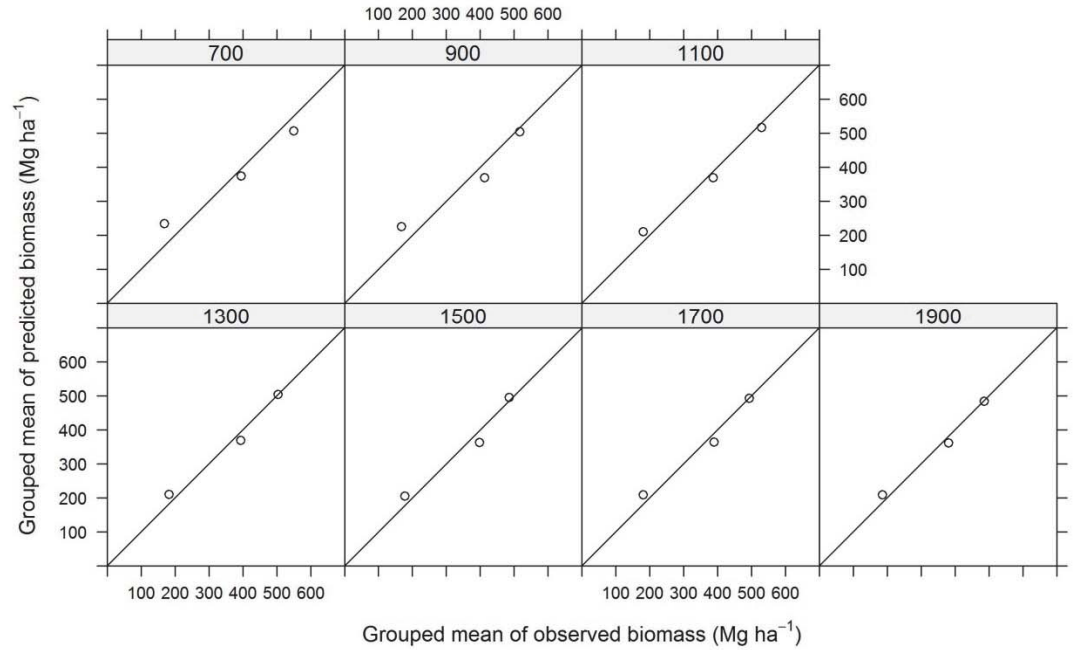

Figure 15. Grouped means of observed *vs.* predicted biomass values using ALS for plot sizes of 700, 900,…, 1900 m^2.

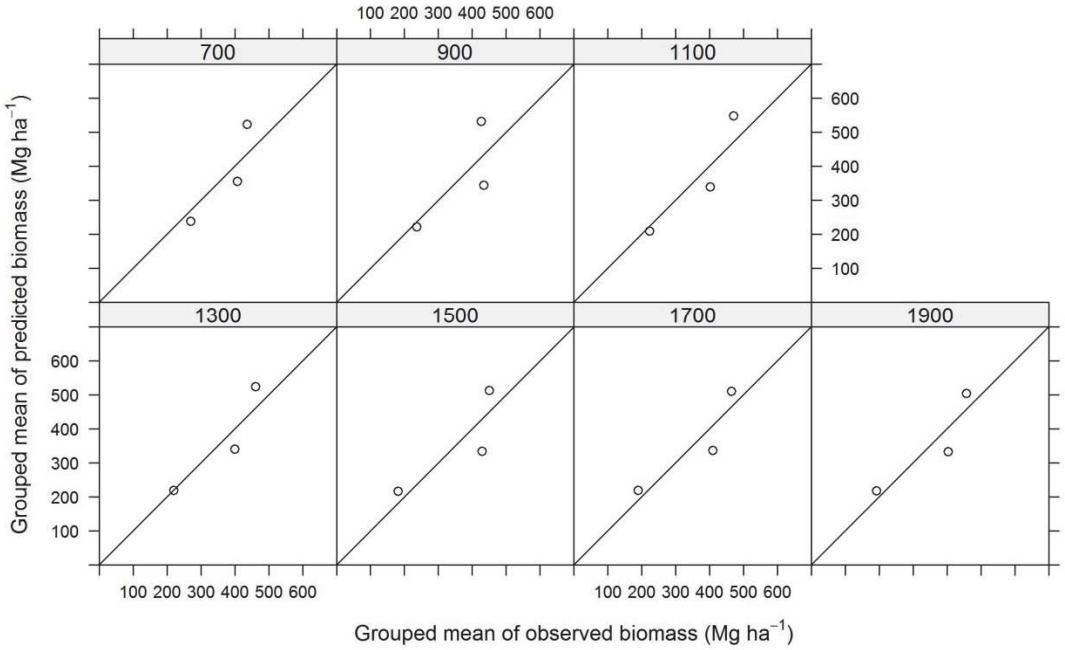

Figure 16. Grouped means of observed *vs.* predicted biomass values using InSAR for plot sizes of 700, 900,…, 1900 m^2.

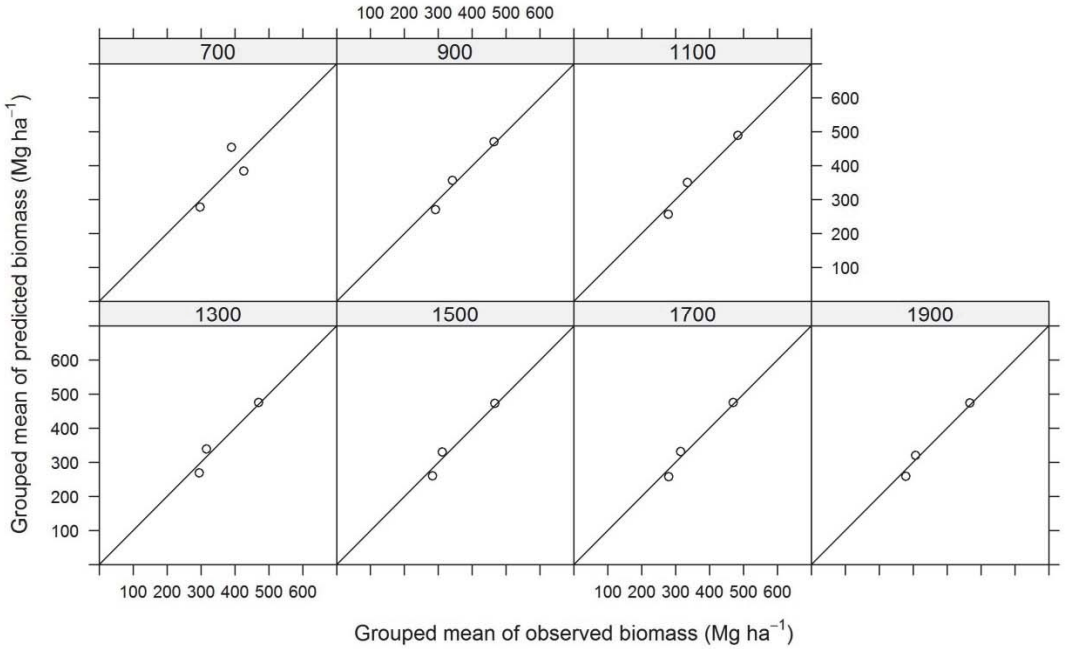

Figure 17. Grouped means of observed *vs.* predicted biomass values using TE for plot sizes of 700, 900,…, 1900 m^2.

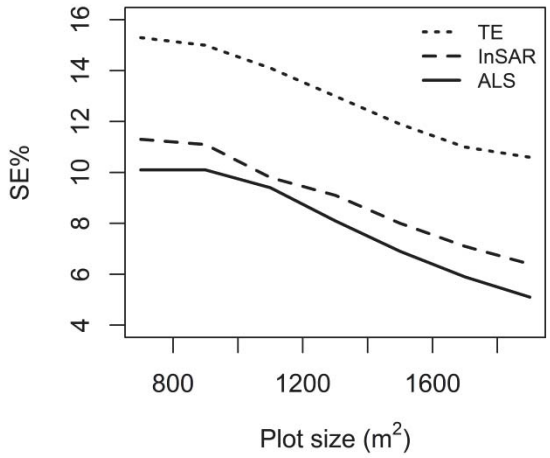

Figure 18. Relative standard error of biomass estimates (SE%) using models with auxiliary data of terrain elevation (TE) derived from a digital terrain model (dotted line), InSAR (dashed line), and ALS (solid line).

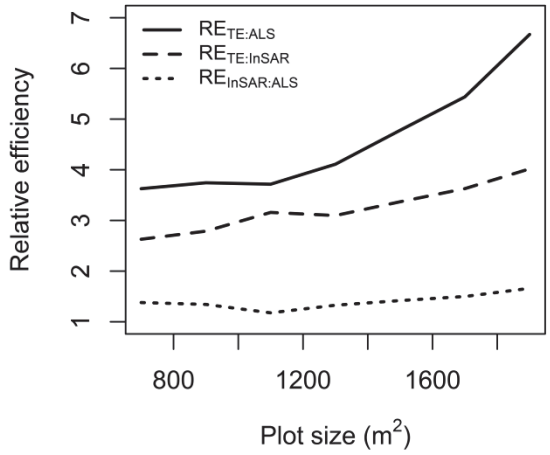

Figure 19. Relative efficiency of using InSAR ($RE_{TE:InSAR}$, dashed line) and ALS ($RE_{TE:ALS}$, solid line) relative to TE for biomass estimation, and ALS relative to InSAR ($RE_{InSAR:ALS}$, dotted line).

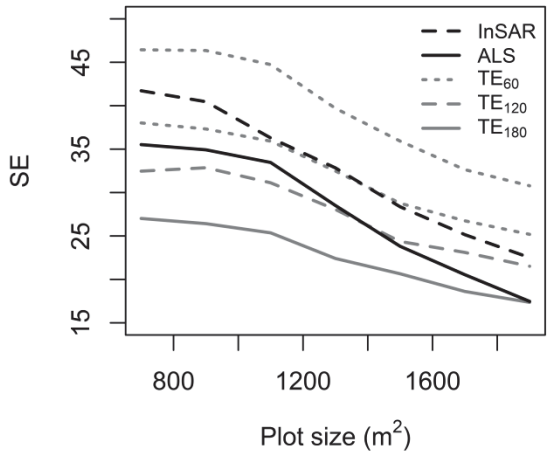

Figure 20. Standard error of biomass estimates (SE) using models with auxiliary data of InSAR (dashed line), ALS (solid line), and TE. TE model SE is derived from 60 (dotted grey line), 120 (dashed grey line), and 180 (solid grey line) simulated observations.

5 Final comments and future prospects

The analyses undertaken in the three papers which constitute this thesis have increased the understanding and basis for forest sample surveys in high-biomass tropical rainforests supported by remotely sensed auxiliary ALS- and InSAR-data. The studies shed light on important aspects of the relationship between biomass observed in the field and the remotely sensed data. A particular focus was directed at how the size of field plots affects this relationship.

Initially, Paper I established that aboveground biomass could be estimated using ALS and field plots of ca. 0.1 ha, at an accuracy of approximately 33% RMSE. Furthermore, the analyses in Paper II demonstrated that similar accuracies could be achieved using potentially cheaper ALS data, with lower pulse densities. Lastly, comparisons of estimated precision in estimation of biomass using both ALS and InSAR data documented that ALS gave the highest precision. The study reported in Paper III further documented that larger plots were relatively more efficient in improving the precision of estimates supported by remotely sensed data, compared to estimates from field observations supported by terrain elevation.

Although the use of ALS data as auxiliary information can reduce the number of field observations needed to obtain a desired accuracy level, the cost of field labour in Tanzania is low. With a cost of establishing an additional inventory plot of only 100–150 USD per plot (E. Mauya 2015, pers. comm. 19 Jan.) increasing the number of field observations is the cheapest way of increasing the accuracy of biomass estimates. However, there are still good reasons for investing in ALS as an auxiliary source of data. Firstly, the ALS DTM can be utilized with other, cheaper sources of remotely sensed data, such as SAR or optical satellite images. Secondly, stability in measurement of InSAR height over time as documented in Solberg et al. (2015) presents a potential of repeatedly estimating biomass without the need of repeated field surveys. This would permit biomass stock estimates at short intervals, annually or bi-annual for instance. Finally, the ALS-assisted inventory can, in addition to the total biomass estimate, provide a map of desired forest parameters. Maps of other forest traits, such as structure, are increasingly being used for improving our understanding of a range of ecological subjects (Maltamo et al., 2014; Pettorelli et al., 2014; Potts et al., 2014).

Collection of remotely sensed data using aircraft is inevitably relatively expensive. With an increasing demand for cheaper and more available information about forest ecosystems, satellite based sensors such as the ICESat-2 and Global Ecosystem Dynamics Investigation (GEDI) LiDARs of National Aeronautics and Space Administration and the P-band SAR

BIOMASS mission of the European Space Agency, are planned for launching in 2017, 2018 and 2020 respectively. In addition, new ALS missions are continuously being carried out and calls have been made for greater coverage of ALS (Mascaro et al., 2014) financed under a REDD+ framework. This gives us great possibilities of understanding further aspects of these important ecosystems.

Knowledge of how the remote sensing technologies are related to ground observations at different scales can be utilized to optimize both plot- and sampling design, in order to minimize the total inventory cost whilst still reaching the required level of precision.

References

Andersen, H.-E., Reutebuch, S. E. & McGaughey, R. J. (2006). A rigorous assessment of tree height measurements obtained using airborne lidar and conventional field methods. *Canadian Journal of Remote Sensing*, 32 (5): 355-366.

Andersen, H.-E., Reutebuch, S. E., McGaughey, R. J., d'Oliveira, M. V. N. & Keller, M. (2013). Monitoring selective logging in western Amazonia with repeat lidar flights. *Remote Sensing of Environment*, 151: 157-165.

Anderson, E. S., Thompson, J. A., Crouse, D. A. & Austin, R. E. (2006). Horizontal resolution and data density effects on remotely sensed LIDAR-based DEM. *Geoderma*, 132 (3–4): 406-415.

Anon. (1999). *Pinnacle user's manual*. San Jose, CA: Javad Positioning Systems.

Anon. (2012). *TerraScan user's guide*. Jyvaskyla, Finland: Terrasolid Oy. p. 311.

Asner, G. P., Powell, G. V. N., Mascaro, J., Knapp, D. E., Clark, J. K., Jacobson, J., Kennedy-Bowdoin, T., Balaji, A., Paez-Acosta, G., Victoria, E., et al. (2010). High-resolution forest carbon stocks and emissions in the Amazon. *Proceedings of the National Academy of Sciences of the United States of America*, 107 (38): 16738-16742.

Asner, G. P., Clark, J., Mascaro, J., Vaudry, R., Chadwick, K. D., Vieilledent, G., Rasamoelina, M., Balaji, A., Kennedy-Bowdoin, T., Maatoug, L., et al. (2012). Human and environmental controls over aboveground carbon storage in Madagascar. *Carbon Balance and Management*, 7 (2).

Asner, G. P., Knapp, D. E., Martin, R. E., Tupayachi, R., Anderson, C. B., Mascaro, J., Sinca, F., Chadwick, K. D., Higgins, M., Farfan, W., et al. (2014). Targeted carbon conservation at national scales with high-resolution monitoring. *Proceedings of the National Academy of Sciences of the United States of America*, 111 (47): E5016-E5022.

Asner, G. P. & Mascaro, J. (2014). Mapping tropical forest carbon: Calibrating plot estimates to a simple LiDAR metric. *Remote Sensing of Environment*, 140: 614-624.

Axelsson, P. (2000). DEM generation from laser scanner data using adaptive TIN models. *International Archives of the Photogrammetry and Remote Sensing*, 33: 110-117.

Bohlin, J., Wallerman, J. & Fransson, J. E. S. (2012). Forest variable estimation using photogrammetric matching of digital aerial images in combination with a high-resolution DEM. *Scandinavian Journal of Forest Research*, 27 (7): 692-699.

Bowen, Z. H. & Waltermire, R. G. (2002). Evaluation of light detection and ranging (LIDAR) for measuring river corridor topography. *Journal of the American Water Resources Association*, 38 (1): 33-41.

Boyd, D. S. & Danson, F. M. (2005). Satellite remote sensing of forest resources: three decades of research development. *Progress in Physical Geography*, 29 (1): 1-26.

Burgess, N. D., Butynski, T. M., Cordeiro, N. J., Doggart, N. H., Fjeldsa, J., Howell, K. M., Kilahama, F. B., Loader, S. P., Lovett, J. C., Mbilinyi, B., et al. (2007). The biological importance of the Eastern Arc Mountains of Tanzania and Kenya. *Biological Conservation*, 134 (2): 209-231.

Chen, Q., Vaglio Laurin, G. & Valentini, R. (2015). Uncertainty of remotely sensed aboveground biomass over an African tropical forest: Propagating errors from trees to plots to pixels. *Remote Sensing of Environment*, 160 (0): 134-143.

Ciais, P., Sabine, C., Bala, G., Bopp, L., Brovkin, V., Canadell, J., Chhabra, A., DeFries, R., Galloway, J., Heimann, M., et al. (2013). Carbon and Other Biogeochemical Cycles. In Stocker, T. F., Qin, D., Plattner, G.-K., Tignor, M., Allen, S. K., Boschung, J., Nauels, A., Xia, Y., Bex, V. & Midgley, P. M. (eds) *Climate Change 2013: The Physical Science Basis. Contribution of Working Group I to the Fifth Assessment Report of the Intergovernmental Panel on Climate Change*, pp. 465-570. Cambridge, UK and New York, NY, USA: Cambridge University Press.

Clark, D. B. & Kellner, J. R. (2012). Tropical forest biomass estimation and the fallacy of misplaced concreteness. *Journal of Vegetation Science*, 23 (6): 1191-1196.

Clark, M. L., Roberts, D. A., Ewel, J. J. & Clark, D. B. (2011). Estimation of tropical rain forest aboveground biomass with small-footprint lidar and hyperspectral sensors. *Remote Sensing of Environment*, 115 (11): 2931-2942.

d'Oliveira, M. V. N., Reutebuch, S. E., McGaughey, R. J. & Andersen, H. E. (2012). Estimating forest biomass and identifying low-intensity logging areas using airborne scanning lidar in Antimary State Forest, Acre State, Western Brazilian Amazon. *Remote Sensing of Environment*, 124: 479-491.

Dawson, W., Mndolwa, A. S., Burslem, D. & Hulme, P. E. (2008). Assessing the risks of plant invasions arising from collections in tropical botanical gardens. *Biodiversity and Conservation*, 17 (8): 1979-1995.

Ene, L. T., Næsset, E., Gobakken, T., Gregoire, T. G., Stahl, G. & Holm, S. (2013). A simulation approach for accuracy assessment of two-phase post-stratified estimation in large-area LiDAR biomass surveys. *Remote Sensing of Environment*, 133: 210-224.

FAO. (1948). *Forest resources of the world*. Unasylva, vol. 2, no. 4. Available at: http://www.fao.org/docrep/x5345e/x5345e00.htm (accessed: 16.01.2015).

FAO. (2011). *State of the World's Forests 2011*: Food and Agriculture Organization of the UN, Rome. 164 pp.

Fassnacht, F. E., Hartig, F., Latifi, H., Berger, C., Hernández, J., Corvalán, P. & Koch, B. (2014). Importance of sample size, data type and prediction method for remote sensing-based estimations of aboveground forest biomass. *Remote Sensing of Environment*, 154: 102-114.

Friedlingstein, P., Andrew, R. M., Rogelj, J., Peters, G. P., Canadell, J. G., Knutti, R., Luderer, G., Raupach, M. R., Schaeffer, M., van Vuuren, D. P., et al. (2014). Persistent growth of CO2 emissions and implications for reaching climate targets. *Nature Geosci*, 7 (10): 709-715.

Frontier Tanzania. (2001). Amani Nature Reserve: A biodiversity survey. In Doody, K. Z., Howell, K. M. & Fanning, E. (eds). *East Usambara Conservation Area Management Programme Technical Paper*. Dar es Salaam, Tanzania and Vantaa, Finland: Forestry and Beekeeping Division and Metsähallitus Consulting.

Fuller, W. A. (1987). *Measurement error models*. New York: John Wiley and Sons. 440 pp.

Ghosh, M. & Meeden, G. (1997). *Bayesian methods for finite population sampling*. London, UK: Chapman & Hall.

Gibbs, H. K., Brown, S., Niles, J. O. & Foley, J. A. (2007). Monitoring and estimating tropical forest carbon stocks: making REDD a reality. *Environmental Research Letters*, 2 (4).

Gobakken, T. & Næsset, E. (2008). Assessing effects of laser point density, ground sampling intensity, and field sample plot size on biophysical stand properties derived from airborne laser scanner data. *Canadian Journal of Forest Research*, 38 (5): 1095-1109.

Gobakken, T. & Næsset, E. (2009). Assessing effects of positioning errors and sample plot size on biophysical stand properties derived from airborne laser scanner data. *Canadian Journal of Forest Research*, 39 (5): 1036-1052.

Gobakken, T., Bollandsås, O. M. & Næsset, E. (2014). Comparing biophysical forest characteristics estimated from photogrammetric matching of aerial images and airborne laser scanning data. *Scandinavian Journal of Forest Research*: 1-14.

Goldberger, A. (1968). Interpretation and estimation of Cobb-Douglas functions. *Econometrica*, 36 (3-4): 464-472.

Goldstein, R. M. & Werner, C. L. (1998). Radar interferogram filtering for geophysical applications. *Geophysical Research Letters*, 25 (21): 4035-4038.

Goodwin, N. R., Coops, N. C. & Culvenor, D. S. (2006). Assessment of forest structure with airborne LiDAR and the effects of platform altitude. *Remote Sensing of Environment*, 103 (2): 140-152.

Grace, J., Mitchard, E. & Gloor, E. (2014). Perturbations in the carbon budget of the tropics. *Global Change Biology*, 20 (10): 3238-3255.

Grassi, G., Monni, S., Federici, S., Achard, F. & Mollicone, D. (2008). Applying the conservativeness principle to REDD to deal with the uncertainties of the estimates. *Environmental Research Letters*, 3 (3).

Gregoire, T. G., Lin, Q. F., Boudreau, J. & Nelson, R. (2008). Regression Estimation Following the Square-Root Transformation of the Response. *Forest Science*, 54 (6): 597-606.

Gregoire, T. G. & Valentine, H. T. (2008). *Sampling Strategies for Natural Resources and the Environment*. Chapman & Hall/CRC Applied Environmental Statistics. Boca Raton, Florida, USA: Chapman and Hall/CRC

Gregoire, T. G., Næsset, E., Ståhl, G., Andersen, H.-E., Gobakken, T., Ene, L., Nelson, R. F. & McRoberts, R. E. (2015). Statistical rigor in LiDAR-assisted estimation of aboveground forest biomass. *Remote Sensing of Environment*, under review.

Hamilton, A. C. & Bensted-Smith, R. (1989). *Forest conservation in the East Usambara Mountains, Tanzania*. Gland, Switzerland and Cambridge, UK: IUCN-The World Conservation Union ; Dar es Salaam, Tanzania : Forest Division, Ministry of Lands, Natural Resources, and Tourism, United Republic of Tanzania. 392 pp.

Hansen, M. C., Potapov, P. V., Moore, R., Hancher, M., Turubanova, S. A., Tyukavina, A., Thau, D., Stehman, S. V., Goetz, S. J., Loveland, T. R., et al. (2013). High-Resolution Global Maps of 21st-Century Forest Cover Change. *Science*, 342 (6160): 850-853.

Haralick, R. M., Shanmugam, K. & Dinsteein, J. (1973). Textural features for image classification. *IEEE Trans. Syst. Man Cybern*, 3: 610-621.

Henry, M., Besnard, A., Asante, W. A., Eshun, J., Adu-Bredu, S., Valentini, R., Bernoux, M. & Saint-Andre, L. (2010). Wood density, phytomass variations within and among trees, and allometric equations in a tropical rainforest of Africa. *Forest Ecology and Management*, 260 (8): 1375-1388.

Hodgson, M. E., Jensen, J., Raber, G., Tullis, J., Davis, B. A., Thompson, G. & Schuckman, K. (2005). An evaluation of lidar-derived elevation and terrain slope in leaf-off conditions. *Photogrammetric Engineering and Remote Sensing*, 71 (7): 817-823.

Holm, S. (1979). A simple sequentially rejective multiple test procedure. *Scandinavian Journal of Statistics*, 6 (2): 65-70.

Hou, Z., Xu, Q. & Tokola, T. (2011). Use of ALS, Airborne CIR and ALOS AVNIR-2 data for estimating tropical forest attributes in Lao PDR. *Isprs Journal of Photogrammetry and Remote Sensing*, 66 (6): 776-786.

Houghton, R. A. (2012). Carbon emissions and the drivers of deforestation and forest degradation in the tropics. *Current Opinion in Environmental Sustainability*, 4 (6): 597-603.

Hyyppä, J., Yu, X., Hyyppä, H., Kaartinen, H., Honkavara, E. & Rönnholm, P. (2005). *Factors affecting the quality of DTM generation in forested areas*. Proceedings of ISPRS Workshop on Laser Scanning 2005, 12–14 September, Enschede, Netherlands. 85-90 pp.

Höhle, J. & Höhle, M. (2009). Accuracy assessment of digital elevation models by means of robust statistical methods. *ISPRS Journal of Photogrammetry and Remote Sensing*, 64 (4): 398-406.

Iida, Y., Kohyama, T. S., Kubo, T., Kassim, A., Poorter, L., Sterck, F. & Potts, M. D. (2011). Tree architecture and life-history strategies across 200 co-occurring tropical tree species. *Functional Ecology*, 25 (6): 1260-1268.

Ioki, K., Tsuyuki, S., Hirata, Y., Phua, M.-H., Wong, W. V. C., Ling, Z.-Y., Saito, H. & Takao, G. (2014). Estimating above-ground biomass of tropical rainforest of different degradation levels in Northern Borneo using airborne LiDAR. *Forest Ecology and Management*, 328: 335-341.

IPCC. (2014). Fifth Assessment Synthesis Report. 116 pp.

ISO. (2012). *ISO 5725-1. Accuracy (trueness and precision) of measurement methods and results — Part 1: General principles and definitions*: International Organization for Standardization,

Geneva, Switzerland. Available at: https://www.iso.org/obp/ui/#iso:std:iso:5725:-1:ed-1:v1:en (accessed: 15.01.2015).

Jubanski, J., Ballhorn, U., Kronseder, K., Franke, J. & Siegert, F. (2012). Detection of large above ground biomass variability in lowland forest ecosystems by airborne LiDAR. *Biogeosciences Discuss.*, 9 (8): 11815-11842.

Keith, H., Mackey, B. G. & Lindenmayer, D. B. (2009). Re-evaluation of forest biomass carbon stocks and lessons from the world's most carbon-dense forests. *Proceedings of the National Academy of Sciences*, 106 (28): 11635-11640.

Kouba, J. (2009). *A guide to using international GNSS service (IGS) products*. IGS Central Bureau, Jet Propulsion Laboratory, Pasadena, CA. p. 34.

Kraus, K. & Pfeifer, N. (1998). Determination of terrain models in wooded areas with airborne laser scanner data. *Isprs Journal of Photogrammetry and Remote Sensing*, 53 (4): 193-203.

Köhl, M., Magnussen, S. & Marchetti, M. (2006). *Sampling methods, remote sensing and GIS multiresource forest inventory*. Berlin: Springer. 365 pp.

Laurin, G. V., Chen, Q., Lindsell, J. A., Coomes, D. A., Frate, F. D., Guerriero, L., Pirotti, F. & Valentini, R. (2014). Above ground biomass estimation in an African tropical forest with lidar and hyperspectral data. *ISPRS Journal of Photogrammetry and Remote Sensing*, 89: 49-58.

Le Toan, T., Quegan, S., Davidson, M. W. J., Balzter, H., Paillou, P., Papathanassiou, K., Plummer, S., Rocca, F., Saatchi, S., Shugart, H., et al. (2011). The BIOMASS mission: Mapping global forest biomass to better understand the terrestrial carbon cycle. *Remote Sensing of Environment*, 115 (11): 2850-2860.

Leitold, V., Keller, M., Morton, D. C., Cook, B. D. & Shimabukuro, Y. E. (2015). Airborne lidar-based estimates of tropical forest structure in complex terrain: opportunities and trade-offs for REDD+. *Carbon Balance Manag*, 10 (1): 3.

Lim, K., Hopkinson, C. & Treitz, P. (2008). Examining the effects of sampling point densities on laser canopy height and density metrics. *The Forestry Chronicle*, 84 (6): 876-885.

Lumley, T. & Miller, A. (2009). *leaps: regression subset selection*. R package version 2.9.

Magnussen, S., Næsset, E. & Gobakken, T. (2010). Reliability of LiDAR derived predictors of forest inventory attributes: A case study with Norway spruce. *Remote Sensing of Environment*, 114 (4): 700-712.

Magnussen, S., Næsset, E., Gobakken, T. & Frazer, G. (2012). A fine-scale model for area-based predictions of tree-size-related attributes derived from LiDAR canopy heights. *Scandinavian Journal of Forest Research*, 27 (3): 312-322.

Maltamo, M., Næsset, E. & Vauhkonen, J. (2014). *Forestry Applications of Airborne Laser Scanning - Concepts and Case Studies. Part III Ecological Applications*. Managing Forest Ecosystems, vol. 27: Springer Netherlands. 335-462 pp.

Marshall, A. R., Willcock, S., Platts, P. J., Lovett, J. C., Balmford, A., Burgess, N. D., Latham, J. E., Munishi, P. K. T., Salter, R., Shirima, D. D., et al. (2012). Measuring and modelling above-ground carbon and tree allometry along a tropical elevation gradient. *Biological Conservation*, 154: 20-33.

Mascaro, J., Detto, M., Asner, G. P. & Muller-Landau, H. C. (2011). Evaluating uncertainty in mapping forest carbon with airborne LiDAR. *Remote Sensing of Environment*, 115 (12): 3770-3774.

Mascaro, J., Asner, G., Davies, S., Dehgan, A. & Saatchi, S. (2014). These are the days of lasers in the jungle. *Carbon Balance and Management*, 9 (1): 7.

Masota, A. M., Zahabu, E., Malimbwi, R., Bollandsås, O. M. & Eid, T. (2015). Tree Allometric Models for Above- and Belowground Biomass of Tropical Rainforests in Tanzania. *Submitted to: Southern Forests: a Journal of Forest Science*.

Matthews, H. D., Gillett, N. P., Stott, P. A. & Zickfeld, K. (2009). The proportionality of global warming to cumulative carbon emissions. *Nature*, 459 (7248): 829-832.

Mauya, E., Hansen, E. H., Gobakken, T., Bollandsås, O. M., Malimbwi, R. E. & Næsset, E. (2015). Effects of field plot size on prediction accuracy of aboveground biomass in airborne laser scanning-assisted inventories in tropical rain forests of Tanzania. *Submitted to: Carbon Balance Manage.*

McGaughey, R. J. (2013). *FUSION/LDV: Software for LIDAR Data Analysis and Visualization*. 3.30 ed. Available at: http://forsys.cfr.washington.edu/fusion (accessed: 09.01.2015).

McRoberts, R. E., Tomppo, E. O. & Næsset, E. (2010). Advances and emerging issues in national forest inventories. *Scandinavian Journal of Forest Research*, 25 (4): 368-381.

McRoberts, R. E., Næsset, E. & Gobakken, T. (2013a). Inference for lidar-assisted estimation of forest growing stock volume. *Remote Sensing of Environment*, 128: 268-275.

McRoberts, R. E., Tomppo, E. O., Vibrans, A. C. & de Freitas, J. V. (2013b). Design considerations for tropical forest inventories. *Brazilian journal of forestry research*, 33 (74): 189-202.

McRoberts, R. E., Andersen, H. E. & Næsset, E. (2014a). Using Airborne Laser Scanning Data to Support Forest Sample Surveys. In Maltamo, M., Næsset, E. & Vauhkonen, J. (eds) Managing Forest Ecosystems, vol. 27 *Forestry Applications of Airborne Laser Scanning*, pp. 269-292: Springer Netherlands.

McRoberts, R. E., Næsset, E. & Gobakken, T. (2014b). Estimation for inaccessible and non-sampled forest areas using model-based inference and remotely sensed auxiliary information. *Remote Sensing of Environment*, 154: 226-233.

Mehtatalo, L. (2012). *Forest biometrics functions of Lauri Mehtatalo*. R package version 1.1 ed. Available at: http://cs.uef.fi/~lamehtat/rcodes (accessed: 09.01.2015).

Meng, X. L., Currit, N. & Zhao, K. G. (2010). Ground Filtering Algorithms for Airborne LiDAR Data: A Review of Critical Issues. *Remote Sensing*, 2 (3): 833-860.

Mgumia, F. (2014). Implications of forestland tenure and status changes on resource base, forest govenance, and community livelihood sorrounding Amani Nature Reserve. *Unpublished draft*.

Minh, D. H. T., Le Toan, T., Rocca, F., Tebaldini, S., d'Alessandro, M. M. & Villard, L. (2014). Relating P-Band Synthetic Aperture Radar Tomography to Tropical Forest Biomass. *Geoscience and Remote Sensing, IEEE Transactions on*, 52 (2): 967-979.

Mitchard, E. T. A., Saatchi, S. S., Woodhouse, I. H., Nangendo, G., Ribeiro, N. S., Williams, M., Ryan, C. M., Lewis, S. L., Feldpausch, T. R. & Meir, P. (2009). Using satellite radar backscatter to predict above-ground woody biomass: A consistent relationship across four different African landscapes. *Geophysical Research Letters*, 36 (L23401).

Mpanda, M. M., Luoga, E. J., Kajembe, G. C. & Eid, T. (2011). Impact of forestland tenure changes on forest cover, stocking and tree species diversity in Amani Nature Reserve, Tanzania. *Forests, Trees and Livelihoods*, 20 (4): 215-229.

Myers, N., Mittermeier, R. A., Mittermeier, C. G., da Fonseca, G. A. B. & Kent, J. (2000). Biodiversity hotspots for conservation priorities. *Nature*, 403 (6772): 853-858.

Myhre, G., Shindell, D., Bréon, F.-M., Collins, W., Fuglestvedt, J., Huang, J., Koch, D., Lamarque, J.-F., Lee, D., Mendoza, B., et al. (2013). Anthropogenic and natural radiative forcing. In Stocker, T. F., Qin, D., Plattner, G.-K., Tignor, M., Allen, S. K., Boschung, J., Nauels, A., Xia, Y., Bex, V. & Midgley, P. M. (eds) *Climate change 2013: the physical science basis. Contribution of Working Group I to the fifth assessment report of the intergovernmental panel on climate change*, pp. 659-740. Cambridge, UK and New York, NY, USA: Cambridge University Press.

Neeff, T., Dutra, L. V., dos Santos, J. R., Freitas, C. d. C. & Araujo, L. S. (2005). Tropical Forest Measurement by Interferometric Height Modeling and P-Band Radar Backscatter. *Forest Science*, 51 (6): 585-594.

Newmark, W. D. (2002). *Conserving biodiversity in East African forests: a study of the eastern arc mountains*. Berlin: Springer. 197 pp.

Nord-Larsen, T. & Schumacher, J. (2012). Estimation of forest resources from a country wide laser scanning survey and national forest inventory data. *Remote Sensing of Environment*, 119: 148-157.

Næsset, E. (1997a). Determination of mean tree height of forest stands using airborne laser scanner data. *ISPRS Journal of Photogrammetry and Remote Sensing*, 52 (2): 49-56.

Næsset, E. (1997b). Estimating timber volume of forest stands using airborne laser scanner data. *Remote Sensing of Environment*, 61 (2): 246-253.

Næsset, E. (2001). Effects of differential single- and dual-frequency GPS and GLONASS observations on point accuracy under forest canopies. *Photogrammetric Engineering and Remote Sensing*, 67 (9): 1021-1026.

Næsset, E. (2002). Determination of Mean Tree Height of Forest Stands by Digital Photogrammetry. *Scandinavian Journal of Forest Research*, 17 (5): 446-459.

Næsset, E. & Gobakken, T. (2008). Estimation of above- and below-ground biomass across regions of the boreal forest zone using airborne laser. *Remote Sensing of Environment*, 112 (6): 3079-3090.

Næsset, E., Gobakken, T., Solberg, S., Gregoire, T. G., Nelson, R., Stahl, G. & Weydahl, D. (2011). Model-assisted regional forest biomass estimation using LiDAR and InSAR as auxiliary data: A case study from a boreal forest area. *Remote Sensing of Environment*, 115 (12): 3599-3614.

Næsset, E. (2014). Area-Based Inventory in Norway – From Innovation to an Operational Reality. In Maltamo, M., Næsset, E. & Vauhkonen, J. (eds) Managing Forest Ecosystems, vol. 27 *Forestry Applications of Airborne Laser Scanning*, pp. 215-240: Springer Netherlands.

Persson, H., Wallerman, J., Olsson, H. & Fransson, J. E. S. (2013). Estimating forest biomass and height using optical stereo satellite data and a DTM from laser scanning data. *Canadian Journal of Remote Sensing*, 39 (3): 251-262.

Pettorelli, N., Laurance, W. F., O'Brien, T. G., Wegmann, M., Nagendra, H. & Turner, W. (2014). Satellite remote sensing for applied ecologists: opportunities and challenges. *Journal of Applied Ecology*, 51 (4): 839-848.

Pinheiro, J., Bates, D., DebRoy, S., Sarkar, D. & R Development Core Team. (2014). nlme: Linear and Nonlinear Mixed Effects Models. R package version 3.1-115.

Plugge, D., Baldauf, T. & Köhl, M. (2011). Reduced Emissions from Deforestation and Forest Degradation (REDD): Why a Robust and Transparent Monitoring, Reporting and Verification (MRV) System is Mandatory. In Blanco, J. (ed.) *Climate Change - Research and Technology for Adaptation and Mitigation*, pp. 155-170: InTech.

Poorter, L., Bongers, L. & Bongers, F. (2006). Architecture of 54 moist-forest tree species: Traits, trade-offs, and functional groups. *Ecology*, 87 (5): 1289-1301.

Potts, J. R., Mokross, K., Stouffer, P. C. & Lewis, M. A. (2014). Step selection techniques uncover the environmental predictors of space use patterns in flocks of Amazonian birds. *Ecology and Evolution*, 4 (24): 4578-4588.

Prodan, M. (1968). *Forest biometrics*. Oxford, UK: Pergamon Press. 447 pp.

R Development Core Team. (2013). *R: A language and environment for statistical computing*. Vienna, Austria: R Foundation for Statistical Computing. Available at: http://www.R-project.org/ (accessed: 10.01.2015).

Rahlf, J., Breidenbach, J., Solberg, S., Næsset, E. & Astrup, R. (2014). Comparison of four types of 3D data for timber volume estimation. *Remote Sensing of Environment*, 155: 325-333.

Reutebuch, S. E., McGaughey, R. J., Andersen, H. E. & Carson, W. W. (2003). Accuracy of a high-resolution lidar terrain model under a conifer forest canopy. *Canadian Journal of Remote Sensing*, 29 (5): 527-535.

Skowronski, N., Clark, K., Nelson, R., Hom, J. & Patterson, M. (2007). Remotely sensed measurements of forest structure and fuel loads in the Pinelands of New Jersey. *Remote Sensing of Environment*, 108 (2): 123-129.

Snowdon, P. (1991). A ratio estimator for bias correction in logarithmic regressions. *Canadian Journal of Forest Research*, 21 (5): 720-724.

Solberg, S., Lohne, T.-P. & Karyanto, O. (2015). Temporal stability of InSAR height in a tropical rainforest. *Remote Sensing Letters*, 6 (3): 209-217.

Stoltzenberg, R. M. (2009). Multiple Regression Analysis. In Hardy, M. A. & Bryman, A. (eds) *Handbook of Data Analysis*, pp. 165-207. London: SAGE Publications Ltd.

Ståhl, G., Holm, S., Gregoire, T. G., Gobakken, T., Næsset, E. & Nelson, R. (2011). Model-based inference for biomass estimation in a LiDAR sample survey in Hedmark County, Norway. *Canadian Journal of Forest Research*, 41 (1): 96-107.

Tinkham, W. T., Huang, H. Y., Smith, A. M. S., Shrestha, R., Falkowski, M. J., Hudak, A. T., Link, T. E., Glenn, N. F. & Marks, D. G. (2011). A Comparison of Two Open Source LiDAR Surface Classification Algorithms. *Remote Sensing*, 3 (3): 638-649.

Toutin, T. & Gray, L. (2000). State-of-the-art of elevation extraction from satellite SAR data. *ISPRS Journal of Photogrammetry and Remote Sensing*, 55 (1): 13-33.

Töyrä, J., Pietroniro, A., Hopkinson, C. & Kalbfleisch, W. (2003). Assessment of airborne scanning laser altimetry (lidar) in a deltaic wetland environment. *Canadian Journal of Remote Sensing*, 29 (6): 718-728.

UNFCCC. (2006). *Good practice guidance and adjustments under Article 5, paragraph 2, of the Kyoto Protocol. FCCC/KP/CMP/2005/8/Add.3 Decision 20/CMP.1*.

UNFCCC. (2010). *Report of the Conference of the Parties on its fifteenth session, held in Copenhagen from 7 to 19 December 2009. Addendum. Part Two: Action taken by the Conference of the Parties at its fifteenth session*: United Nations Office, Geneva, Switzerland. p. 43.

UNFCCC. (2011). *Report of the Conference of the Parties on its sixteenth session, held in Cancun from 29 November to 10 December 2010. Addendum. Part two: Action taken by the Conference of the Parties at its sixteenth session*: United Nations Office, Geneva, Switzerland. p. 31.

Valbuena, R., Mauro, F., Rodriguez-Solano, R. & Antonio Manzanera, J. (2012). Partial Least Squares for Discriminating Variance Components in Global Navigation Satellite Systems Accuracy Obtained Under Scots Pine Canopies. *Forest Science*, 58 (2): 139-153.

Vauhkonen, J., Maltamo, M., McRoberts, R. & Næsset, E. (2014). Introduction to Forestry Applications of Airborne Laser Scanning. In Maltamo, M., Næsset, E. & Vauhkonen, J. (eds) Managing Forest Ecosystems, vol. 27 *Forestry Applications of Airborne Laser Scanning*, pp. 1-16: Springer Netherlands.

Vincent, G., Sabatier, D., Blanc, L., Chave, J., Weissenbacher, E., Pélissier, R., Fonty, E., Molino, J. F. & Couteron, P. (2012). Accuracy of small footprint airborne LiDAR in its predictions of tropical moist forest stand structure. *Remote Sensing of Environment*, 125: 23-33.

Winsor, C. P. (1932). The Gompertz Curve as a Growth Curve. *Proceedings of the National Academy of Sciences of the United States of America*, 18 (1): 1-8.

Zandbergen, P. A. (2008). Positional Accuracy of Spatial Data: Non-Normal Distributions and a Critique of the National Standard for Spatial Data Accuracy. *Transactions in GIS*, 12 (1): 103-130.

Zeide, B. (1980). Plot size optimization. *Forest Science*, 26 (2): 251-257.

Zhang, K., Chen, S.-C., Whitman, D., Shyu, M.-L., Yan, J. & Zhang, C. (2003). A progressive morphological filter for removing nonground measurements from airborne LIDAR data. *IEEE Transactions on Geoscience and Remote Sensing*, 41 (4): 872-882.

Zolkos, S. G., Goetz, S. J. & Dubayah, R. (2013). A meta-analysis of terrestrial aboveground biomass estimation using lidar remote sensing. *Remote Sensing of Environment*, 128: 289-298.

Zvoleff, A. (2014). *Calculate textures from grey-level co-occurrence matrices (GLCMs) in R*. R package version 0.3.1 ed. Available at: http://cran.r-project.org/web/packages/glcm/.

PAPER I

Remote Sens. **2015**, *7*, 788-807; doi:10.3390/rs70100788

OPEN ACCESS

remote sensing

ISSN 2072-4292

www.mdpi.com/journal/remotesensing

Article

Modeling Aboveground Biomass in Dense Tropical Submontane Rainforest Using Airborne Laser Scanner Data

Endre Hofstad Hansen [1,*], Terje Gobakken [1], Ole Martin Bollandsås [1], Eliakimu Zahabu [2] and Erik Næsset [1]

[1] Department of Ecology and Natural Resource Management, Norwegian University of Life Sciences, P.O. Box 5003, NO-1432 Ås, Norway; E-Mails: terje.gobakken@nmbu.no (T.G.); ole.martin.bollandsas@nmbu.no (O.M.B.); erik.naesset@nmbu.no (E.N.)

[2] Department of Forest Mensuration and Management, Sokoine University of Agriculture, P.O. Box 3013, Chuo Kikuu, Morogoro, Tanzania; E-Mail: zahabue@yahoo.com

***** Author to whom correspondence should be addressed; E-Mail: endre.hansen@nmbu.no; Tel.: +47-6496-5756; Fax: +47-6496-8890.

Academic Editors: Lars T. Waser and Prasad S. Thenkabail

Received: 9 September 2014 / Accepted: 7 January 2015 / Published: 14 January 2015

Abstract: Successful implementation of projects under the REDD+ mechanism, securing payment for storing forest carbon as an ecosystem service, requires quantification of biomass. Airborne laser scanning (ALS) is a relevant technology to enhance estimates of biomass in tropical forests. We present the analysis and results of modeling aboveground biomass (AGB) in a Tanzanian rainforest utilizing data from a small-footprint ALS system and 153 field plots with an area of 0.06–0.12 ha located on a systematic grid. The study area is dominated by steep terrain, a heterogeneous forest structure and large variation in AGB densities with values ranging from 43 to 1147 $Mg \cdot ha^{-1}$, which goes beyond the range that has been reported in existing literature on biomass modeling with ALS data in the tropics. Root mean square errors from a 10-fold cross-validation of estimated values were about 33% of a mean value of 462 $Mg \cdot ha^{-1}$. Texture variables derived from a canopy surface model did not result in improved models. Analyses showed that (1) variables derived from echoes in the lower parts of the canopy and (2) canopy density variables explained more of the AGB density than variables representing the height of the canopy.

Keywords: aboveground biomass; airborne laser scanning; canopy surface; LiDAR; texture variables; tropical rainforest

1. Introduction

Moist and wet tropical forests have the potential to store large amounts of carbon as biomass. Quantification of biomass and knowledge about its spatial distribution provides important information about the forest that is useful for ecological and environmental applications as well as forest resource management. A detailed description of forest structure will help to understand the ecological functionality of these forests [1] and how structure is governed by edaphic and climatic factors. This knowledge can be used in the development of models for local natural resource management, such as water management [2,3], or in modeling of the response of forests to climate change [4]. In some countries, timber and wood products from tropical forest are important export commodities [5] and inventories assisted by remote sensing data can provide valuable information for decision making. Even in areas in which forest products and ecosystem services are not part of a market system, forest resource information might be useful, for example for fuel wood management [6]. The carbon sequestration potential of tropical forests has received a lot of attention and has resulted in the policy and economic incentive mechanism known as REDD+. The aim of REDD+, described in the 16th session of the Conference of Parties to the United Nations Framework Convention on Climate Change, is to encourage reduction of emissions from deforestation and forest degradation, conservation and enhancement of forest carbon stocks and sustainable management of forests in developing countries [7]. Reporting of emissions from loss of forest carbon at the national level will be required [8], but many countries are likely to benefit from more local monitoring programs within the countries as well, assessing the effects of national policies and local financial mechanisms aimed at reaching goals for emission control for the nation as a whole.

Accessing carbon finances through REDD+ requires, among other factors, measurement of carbon stock changes in forests [9]. Furthermore, a mechanism for commercial trading of forest carbon credits earned through enhancement of forest carbon stocks, conservation of forests or sustainable forest management require trustworthy systems for verification of carbon offsets. In addition, application of the conservativeness principle, which takes into account the uncertainty of estimates to minimize the risk of overestimating emission reductions [10,11], and lack of accurate biomass estimates may result in loss of carbon credits for the project developer [12]. Establishing a robust and transparent system for measuring, reporting and verification (MRV) is therefore a requirement for successful implementation of a REDD+ regime [13]. A central part of such an MRV system would be the use of remote sensing data for monitoring both forest area changes and changes within forested areas [14] because remote sensing data can greatly improve the precision of estimates and change estimates of areas as well as of biomass and carbon stocks—and especially so if the remote sensing data are strongly correlated with the parameter of interest.

A variety of remote sensing technologies for determination of forest biomass exists, whereof LiDAR (light detection and ranging) sensors have been found to produce the best results in terms of

precision [15,16]. The use of LiDAR, which is most commonly mounted on a small aircraft and with a scanning capability—known as airborne laser scanning (ALS)—has proven to be both effective and accurate for determining biomass in different forest types [15–17]. ALS is also used as an integral part of operational forest management inventories in several countries [18]. Most of the published studies on ALS to estimate AGB have been carried out in boreal and sub-boreal coniferous forests with relatively low biomass and open forest structure. However, in the last five years use of ALS for AGB estimation has been demonstrated in tropical forests in South America [19–23], Asia [24] and Africa [25]. The maximum biomass densities in these studies were about 500 $Mg \cdot ha^{-1}$, while biomass densities in tropical rainforests can go far beyond 500 $Mg \cdot ha^{-1}$.

Due to the fact that ALS does not measure biomass directly, there is a need for field data for modeling the relationship between remotely sensed observables and biomass from ground observations. The models are subsequently used for estimation of forest biomass. Taking the area-based approach [26], commonly used for ALS-based forest inventory, attributes of interest are measured or calculated from measurements on field plots and a relationship between the ALS echoes and ground attribute is determined using statistical methods such as regression analysis, nearest neighbors, neural-networks or ensemble learning. The size of field plots varies, but has usually been in the range of 0.1–1.0 ha in tropical ALS studies.

Different types of variables are often derived from the ALS echoes and are tested to describe the relationship between the remotely sensed information and biomass. The most commonly used types of ALS-derived variables are percentiles of the height above ground above a certain threshold (canopy height variables), and fractions of echoes in the canopy to total number of echoes, including ground echoes (canopy density variables). Estimated models often include a canopy height variable describing the canopy height close to the top of the canopy or mean canopy height, in combination with a canopy density variable derived from the lower parts of the canopy, e.g., [26,27]. Alternative approaches have been to use the total canopy volume [28] or canopy height profile and canopy cover [29] calculated from the ALS echoes. The latter approach has been widely applied in tropical areas by Asner *et al.* [30] utilizing only one variable, namely the mean canopy profile height. Studies have documented positive relationships between AGB and forest structure diversity [31] and tree species diversity [32]. Textural information that capture structural information is commonly used in image analysis, and has been shown to be successful in modeling AGB using high-resolution satellite images [33]. Bohlin *et al.* [34] successfully used textural information from a canopy surface model in combination with ALS-derived height and density variables to model stem volume and basal area in Sweden. Based on these findings, we reasoned that texture variables might be able to capture information about the spatial distribution of trees and forest structure which could improve the model performance even in tropical rainforests.

When applying regression analysis, a transformation of the response and/or predictor variables is usually performed to account for non-normality and non-constant variance in the response variable. Logarithmic transformations of both response and predictor variables have been applied in several studies, e.g., [26,35]. Other strategies have been to transform the response only, and both logarithmic [24,36] and square root [19,37,38] transformations are commonly used.

In natural forests that have reached a climax state another challenge occurs when utilizing canopy height derived variables for biomass modeling. Tree height growth decreases with age, and because the decrease is stronger and starts earlier compared to a decrease in diameter growth [39], trees with

similar crown height may have very different diameters, and thus biomass. There might even be a negative change in canopy height as trees approaches mortality and the tree crown starts to die off. Tree diameter, however, does not decrease. Thus, ALS-derived variables describing tree heights might be less correlated with AGB.

The overall objective of this study was to model AGB in a tropical forest with a wide range in AGB densities in rugged and steep terrain using ALS-derived variables. We explored the use of texture variables derived from a canopy surface model. To improve our understanding of the relationship between AGB and canopy height and density, we assessed the relative importance of different ALS-derived prediction variables.

2. Material and Methods

2.1. Study Area

The study area, Amani Nature Reserve (Figure 1) (S5°08', E38°37', 200–1200 m above sea level), covers around 8360 ha of tropical submontane rainforest and is located in the East Usambara Mountains in eastern Tanzania, which is a part of the Eastern Arc Mountains. The Eastern Arc Mountains is a global biodiversity hotspot area [40] and the forest, stretching from Udzungwa in Tanzania in the south to Taita Hills in Kenya in the north, contains many endemic species of both animals and plants. Within this mountain system, the East Usambara Mountains have been identified as one of three top priority areas for forest conservation [41]. In this forest ecosystem, rain falls throughout the year with two wet seasons, April to May and October to November, and the area receives around 2000 mm rainfall per year. Daily mean temperatures vary from about 16–25 °C. Amani Nature Reserve was gazetted in 1997 comprising of six former forest reserves, Amani-East, Amani-West, Amani-Sigi, Kwamsambia, Kwamkoro and Mnyusi Scarp. In addition, forest land from the neighboring tea estate, sisal estate and local village was included in the nature reserve. The area also includes the Amani Botanical Gardens, established in 1902 under German colonial rule and have contained over 500 indigenous and non-native tree species [42]. Very few of the non-native species have successfully spread from the area in which they were planted, but one species in particular, *Maesopsis eminii*, is found over the whole nature reserve and is the most common species in the reserve. The *M. eminii* originate from the lake region in eastern Congo and is a typical light demanding, pioneer species. It thrives in disturbed areas, but is not able to germinate under thick canopy [43] and is not found in the less disturbed areas of the reserve. In an inventory carried out in 1986/87, about half of the nature reserve was classified as logged or covered with *M. eminii* as a result of logging [44]. Logging was stopped in the late 1980s and most of the nature reserve is now covered by a closed forest cover.

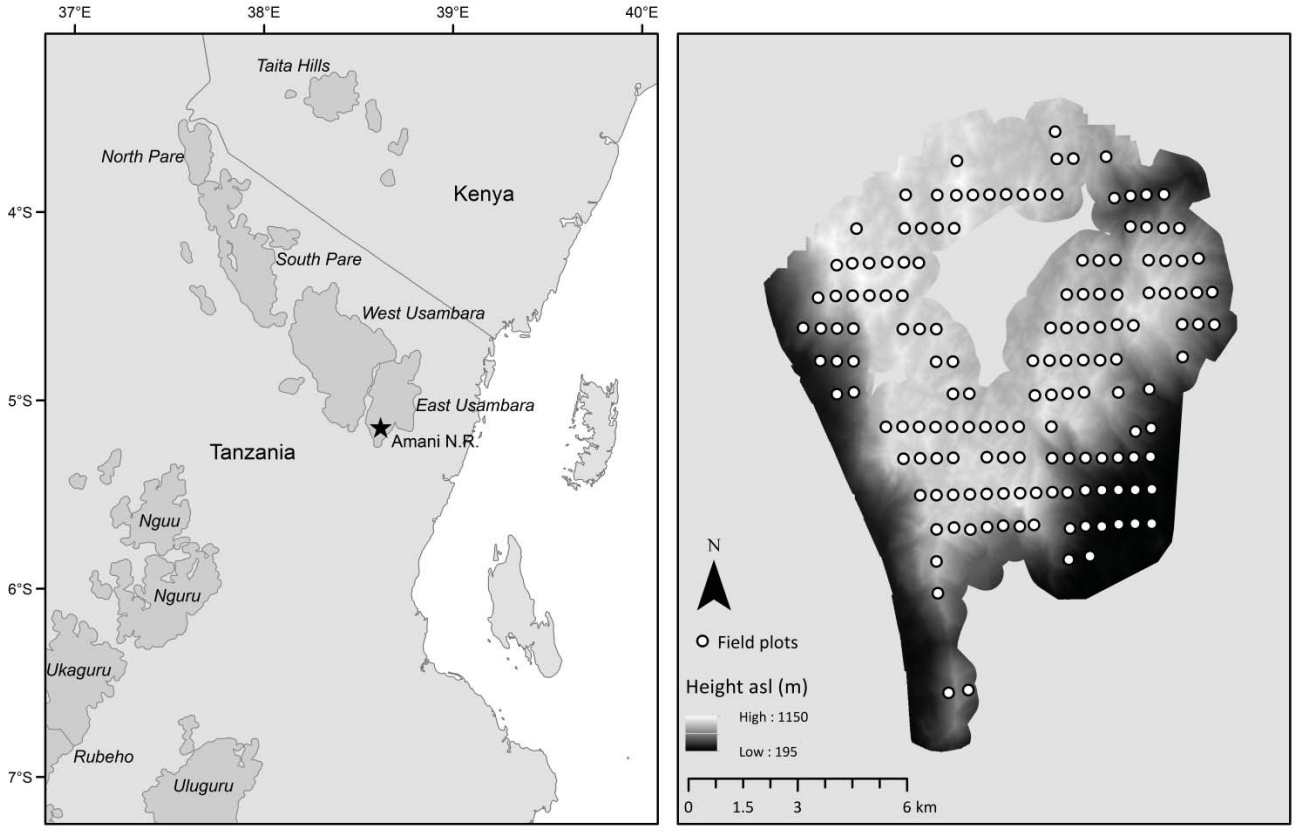

Figure 1. Left: study area (marked by star) situated in the Eastern Arc Mountains (dark grey areas). Right: field plot locations (marked by dots) inside the Amani Nature Reserve.

2.2. Field Data

During 1999–2000, a non-governmental conservation and development organization, Frontier Tanzania, established a grid of east/west and north/south transects for surveying flora and fauna in the reserve [45] as part of a larger biodiversity survey covering several of the tropical forest areas in Tanzania. At each crossing in the 450 by 900 m grid, a rectangular plot measuring 50 m west and 20 m north from the transect crossing, was established (Figure 1). The horizontal area of the plots varies from 0.0639–0.1239 ha because the plots were laid out along the terrain slope, without any slope correction. All trees with ≥10 cm diameter at breast height (DBH) were callipered, marked and species identified. During two campaigns in 2008 and 2009/2010, 143 of these plots were revisited and all trees re-measured [46,47]. Trees that had grown larger than 10 cm in DBH since the first survey were included, and dead or missing trees excluded. All of the initial 173 plot locations were again visited during August 2011–April 2012 and plots that were not re-measured during the 2008–2010 period were re-measured this time. All plots were identified in the field by local personnel that had been doing the establishment and the previous re-measurement. Plots which were not positively identified in the field were re-established and all the trees with a DBH ≥10 cm registered. This was also done for plots with an apparent change in the structure (due to landslide or human activity), or trees where added or removed where there was a clear error in the earlier records. Of the 173 plots, 15 plots had one or more corners with missing coordinates after completion of the field work due to reception of too few satellites during data recording from positioning satellites, see details below. One plot was also

discarded because one of the processed corner coordinates had a reported error of >10 m. Furthermore, four plots were found to be outside the forest. The DBH data from the remaining 153 plots contain measurements from four different years; 2008 (19 plots), 2009/2010 (91 plots) and 2011/2012 (43 plots).

Ten trees per plot were selected for height measurement. The trees were systematically selected by choosing the closest tree to each corner; one tree in the middle of each short end of the plot; and two trees along the sides, 15 m from each corner, respectively. Tree height (H) was measured using a Vertex IV hypsometer and trees with damage were noted. For plots with low stocking in which the same tree could be selected more than once, less than 10 heights were measured. A total of 1497 trees were measured during the fieldwork in 2011 and 2012. A summary of the field plot characteristics is presented in Table 1.

Table 1. Characteristics of 153 field plots.

Characteristic	Range	Mean	SD
Area (ha)	0.0639–0.1239	0.0914	0.011
N [a] (ha^{-1})	85.4–1085.7	471.5	161.5
DBH [b] (cm)	10.0–270.0	27.5	22.9
BA [c] ($m^2 \cdot ha^{-1}$)	5.4–144.9	47.3	22.2
AGB [d] ($Mg \cdot ha^{-1}$)	43.2–1147.1	461.9	214.7
H [e] (m)	8.3–51.3	19.2	8.9

[a] number of trees; [b] diameter at breast height (1.3 m); [c] basal area; [d] aboveground biomass; [e] predicted tree height.

2.2.1. Height-Diameter Models

Single tree predictions of AGB with both DBH and H as independent variables in the allometric models give more reliable and lower biomass levels than without height information [48,49]. From the trees measured for height, a nonlinear mixed effects height-diameter (H-D) model was developed with plot as random effect. Initially, five trees with H/DBH ratio of <2 m/cm were left out of the modeling. Thereafter, 20 two- and three-parameter H-D models were fit using the "fithd" function in the package "lmfor" [50] in the R software [51], and the best model form selected based on the Akaike Information Criterion (AIC). The selected model form (Equation (1)) described by Prodan [52] was then fit using the "nlme" function [53] in R, specifying a, b and c as random parameters because this resulted in the lowest AIC value. The selected model can be expressed as the mean (expected value) function

$$\mathrm{E[H]} = 1.3 + \frac{\mathrm{DBH}^2}{a + b * \mathrm{DBH} + c * \mathrm{DBH}^2} \quad (1)$$

This method of calibrating the H-D model is described by Lappi and Bailey [54] and is able to include local effects. The H-D development of trees can for instance be affected by local soil conditions or by surrounding trees. The mixed effects H-D model developed from 1492 trees had a correlation between observed and predicted height (pseudo coefficient of determination (pR^2)) of 0.75 (Table 2). To capture the local effects, field plot was specified as random effect and all three parameters of the model were allowed to describe the random effects.

Table 2. Estimated parameters, standard deviation (SD), pseudo coefficient of determination (pR^2, correlation coefficient between observed and predicted values) and root mean square error (RMSE) for applied height-diameter model.

Variable	Parameter estimate	SD
a	0.3376	(0.9032)
b	0.9834	(0.0855)
c	0.0172	(0.0012)
σ_a	4.9221	
σ_b	0.5905	
σ_c	0.0024	
σ_ε	0.3485	
pR^2	0.75	
RMSE	5.38	

2.2.2. Aboveground Biomass

Aboveground biomass for individual trees ($\widehat{\mathrm{AGB}_t}$) was predicted using a locally developed allometric model (Equation (2)) [55]. The model is developed from 60 trees from 34 different species in the Amani Nature Reserve and has a pR^2 of 0.84. The trees were felled and green weight of stem, branches, twigs, and leaves were recorded in the field along with DBH. Wood samples from each of the three components were collected and the green-to-dry weight ratio calculated after oven drying of the wood samples. The tree biomass was then calculated by multiplying the green weight with the green-to-dry weight ratio of each of the tree components and summed up for each tree. The applied model was

$$\widehat{\mathrm{AGB}_t} = 0.402 * \mathrm{DBH}^{1.4365} * \mathrm{H}^{0.8613} \quad (2)$$

where $\widehat{\mathrm{AGB}_t}$ is the predicted aboveground biomass in Mg for individual tree number *t*, DBH is the tree diameter at breast height in cm and H is the tree height in m. The $\widehat{\mathrm{AGB}_t}$ was then summed on field plot level and weighted to per hectare unit by the plot area (Table 1).

2.2.3. Positioning of the Field Plots

During the revisit of the field plots in the period August 2011–April 2012, the plot corners were georeferenced by means of differential global positioning system (GPS) and global navigation satellite system (GLONASS) using a 40-channel dual frequency survey grade receiver as field unit. A second receiver, acting as a base station, was placed on the roof of a house at the Amani Nature Reserve headquarters with a distance of <14 km from the plots. Before the positioning of the plots started, the coordinates of the base station antenna was determined with Precise Point Positioning with GPS and GLONASS data collected continuously for 24 h according to Kouba [56]. The field unit was placed at each corner of each plot on a 2.9 m rod for a minimum of 30 min, and a one second logging rate was used. Planimetric errors of the plot corner coordinates were estimated to an average of 57 cm based on random errors reported from the post-processing using Pinnacle software [57] and empirical experience of the relationship between reported error and the true error documented by Næsset [58].

2.3. ALS Data

Airborne laser scanning with complete coverage was performed using a Leica ALS70 sensor mounted on a Cessna 404 twin engine, fixed wing aircraft. The acquisition was carried out in the period 19–25 January 2012 with additional flights in the period 2–18 February 2012 to fill minor gaps in the data. Average flight speed was 70 $m \cdot s^{-1}$ at a mean flying altitude of 800 m above ground level and with a laser pulse repetition frequency of 339 kHz. From each pulse, the sensor registered up to five echoes. A maximum scan angle of ±16° from nadir yielded an average swath width of 460 m. The beam divergence was 0.28 mrad which produced an average footprint size on the ground of about 22 cm. Following the acquisition, a post processing was performed by the contractor (Terratec AS, Norway). Echoes reflected from the ground were identified and classified using the progressive triangulated irregular network (TIN) densification algorithm [59] of TerraScan software [60]. An ALS terrain model was created as a TIN from the planimetric coordinates and corresponding heights of the ALS echoes classified as ground echoes. The TIN model was then used to calculate the height relative to the ground for all echoes by subtracting the TIN model height from the height of the echoes. ALS echoes classified according to Anon. [61] as "overlapping", "low", and "error" were omitted, resulting in an average pulse density of 10 echoes$\cdot m^{-2}$. From the five echoes registered per pulse, we used only echoes of the three categories "single", "first of many", and "last of many". Single and first of many were merged into one dataset and denoted as "first echoes" while single and last of many were merged into another dataset and denoted as "last echoes".

ALS data for the canopy layer were extracted for each field plot, and a number of variables describing the vertical distribution of ALS echoes (vertical variables) were derived from the height distribution of echoes for each of the two echo categories (first, last). Vertical variables were further divided into variables describing the height (canopy height variables) and density (canopy density variables) of the forest canopy. Canopy height variables including maximum- and mean values (Hmax, Hmean), standard deviation (Hsd), coefficients of variation (Hcv), kurtosis (Hkurt), skewness (Hskewness) and percentiles at 10% intervals (H10, H20,…, H90) were derived from the laser echoes above a threshold of 4 m above ground. It has been common in boreal forests to use a threshold of 2 m to distinguish between the tree layer and below-canopy vegetation [26,62], however, the minimum DBH of 10 cm and the overall size of the trees sampled justify the higher threshold of 4 m. In addition to the canopy height variables, canopy density variables were derived by dividing the height between a 95% percentile height and the 4 m threshold into 10 equally tall vertical layers and calculating the proportion of echoes above each layer to the total number of echoes of each echo category (first, last), including echoes below the 4 m threshold (D0, D1,…, D9). To denote if the variables were derived from the first or last echo category, a subscript L or F was used as notation, e.g., Hmean.F.

Variables describing horizontal distribution of the ALS canopy echoes, texture variables, were also computed. Firstly, a rasterized canopy surface model of 1 m resolution was computed from the top-of-canopy echoes. The raster was then converted into grey level images and variables originally presented by Haralick *et al.* [63] were calculated using the "glcm" package [64] in R. The texture variables were calculated using a 3 m window size and averaged in all directions (0, 45, 90 and 135°). The window size of 3 m was chosen because a 3 pixel window was the smallest available in the "glmc" package, and we considered that larger window sizes would provide less detailed metrics.

Shifts of 3, 6, 9, 12 and 15 m were tested and variables included mean (MN), homogeneity (HG), variance (VAR), contrast (CONT), dissimilarity (DS), entropy (ENT), angular second moment (SM) and correlation (COR) for each of the shifts. As an example MN.15 is the average of the height of the 3 m windows with a distance of 15 m between each window in all directions.

2.4. Multiple Regression Analysis

Different linear least-square multiple regression models for AGB were developed using vertical variables, texture variables and a combination of both vertical and texture variables (Table 3). Two alternative transformations of the response variable, logarithmic and square root were also performed for each set of predictor variable type (Table 3). For models A–C for which logarithmic transformations were applied, the transformation of the response variable introduced a bias when back-transformed to arithmetic scale. The models were therefore adjusted for logarithmic bias according to Goldberger [65] by adding half of the model mean square error to the constant term before transformation to arithmetic scale. For models D–F, with square root transformed response, the models were back-transformed according to Gregoire *et al.* [66] by squaring the prediction and adding the model mean square error.

Predictor variable selection was performed using a best subset regression procedure implemented in the "leaps" package [67] in R. The models were selected based on the Bayesian information criterion (BIC), allowing up to five predictor variables. To avoid multicollinearity the variance inflation factors (VIF) were controlled. For the selected model, a 10-fold cross-validation was performed, and assessment of accuracy was done by estimating the RMSE (Equation (3)) and mean difference ($\overline{\mathrm{D}}$) (Equation (4)):

$$\mathrm{RMSE} = \sqrt{\frac{\sum_{i=1}^{n}(\hat{y}_i - y_i)^2}{n}} \tag{3}$$

$$\overline{\mathrm{D}} = \frac{\sum_{i=1}^{n}(\hat{y}_i - y_i)}{n} \tag{4}$$

where n is number of plots, y_i is the observed value for plot i, $\hat{y}_i$ is the predicted value for plot i. The relative RMSE (RMSE%) and relative $\overline{\mathrm{D}}$ ($\overline{\mathrm{D}}$%) were calculated as a percentage by dividing the absolute RMSE and $\overline{\mathrm{D}}$, respectively, by the observed mean.

Table 3. Summary of tested model forms and predictor variables.

Model	Transformation	Predictor variables
A	Logarithmic	Vertical
B	Logarithmic	Texture
C	Logarithmic	Vertical + Texture
D	Square root	Vertical
E	Square root	Texture
F	Square root	Vertical + Texture

2.5. Analysis of ALS Variables

In a natural forest that has reached a climax state, and where the height growth of some of the trees has stopped, the asymptotical H-D relationship will introduce problems when using ALS variables derived from canopy height for predicting AGB. The canopy height information is likely to be less correlated with the response variable of interest so that variables capturing other features—for example canopy density—could be better suited as predictor variables. The diversity in forest structure expressed by texture variables could also provide important information for AGB prediction.

To explore the relative importance of the predictor variables, an analysis was performed by fitting a separate simple linear model for a random sample of 1/3 of the plots. The single predictor variable resulting in the lowest BIC value was included in the model. Random sampling of observations, performed without replacement and model-fitting was repeated 1000 times. The rate of how often each variable appeared in the model was used as a measure of importance for each individual variable.

3. Results

Results for the six different models are presented in Table 4. Models with logarithmic and square root transformations of the response perform equally well, with an RMSE of estimated values of around 33% of a mean value of 462 Mg·ha^{-1} for both transformations. Multicollinearity was controlled by checking the VIF of the models. All models had a VIF value below 3. Models developed using vertical variables only (A and D) included three variables and variables describing the height and density of the forest canopy. Use of texture variables only did not perform as well as the standard vertical variables. The modeling procedure selected only one and two texture variables for models B and E, respectively.

In combination with the vertical variables, only MN.15 was selected together with vertical variables in model C. The cross-validation procedure generally resulted in overestimated AGB values of observation in the range of 200–500 Mg·ha^{-1} and underestimation of observation of above 500 Mg·ha^{-1} (Figure 2).

Table 4. Summary of regression models for aboveground biomass (AGB) using ALS variables.

Model	Response Variable	Predictive Model [a]	Model Fit		10-Fold Cross-Validation [b]			
			R^2	BIC	RMSE	RMSE%	$\overline{D}$	$\overline{D}$%
A	ln AGB	3.815 + 1.755 D2.L+ 1.498·D9.L + 0.016 H90.F	0.70	98.8	149.18	32.3	−2.40	0.5
B	ln AGB	3.984 + 3.222 MN.3	0.52	160.6	173.84	37.6	−8.57	1.9
C	ln AGB	3.665 + 1.530 D2.L + 1.231·D9.L + 0.013 H90.F+ 0.737 MN.15	0.71	98.7	158.02	34.4	−2.85	0.6
D	sqrt(AGB)	3.796 + 11.294 D2.L + 13.321·D9.L+ 0.249 Hmean.L	0.62	814.4	154.44	33.4	6.12	1.3

Table 4. *Cont.*

Model	Response Variable	Predictive Model [a]	Model Fit		10-Fold Cross-Validation [b]			
			R^2	BIC	RMSE	RMSE%	$\overline{D}$	$\overline{D}$%
E	sqrt(AGB)	7.563 + 0.054 MN.3 − 0.072·CONT.3	0.48	857.0	169.77	36.8	8.17	1.8
F	sqrt(AGB)	3.796 + 11.294 D2.L + 13.321·D9.L + 0.249 Hmean.L	0.62	814.4	156.59	33.9	5.57	1.2

Notes: [a] Variables explained in Section 2.3.; [b] Values after back transformation to arithmetic scale.

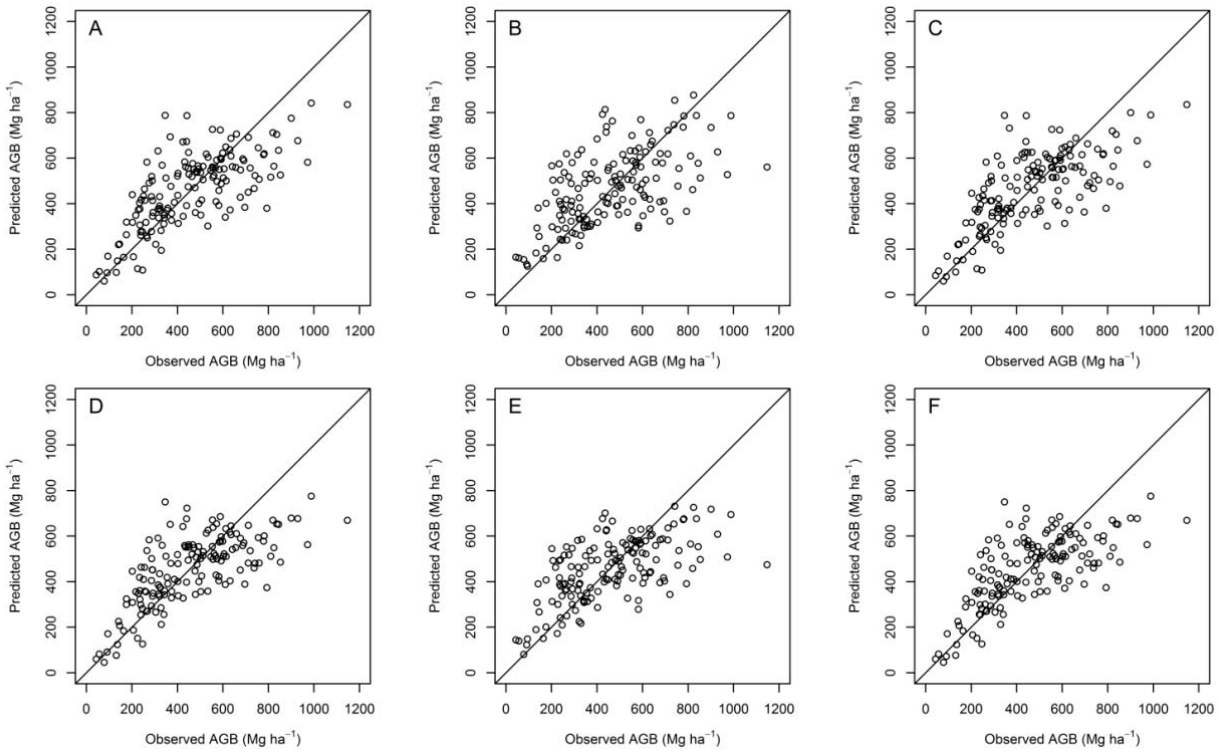

Figure 2. Scatter plots of observed *versus* predicted aboveground biomass (AGB) using logarithmic (**A–C**) or square root transformations of the response (**D–F**) in combination with vertical variables (A, D), texture variables (B, E) and both vertical and texture variables (C, F).

The analysis of the relative importance (Section 2.5) of the variables used to estimate AGB generally showed that density variables from the lower parts of the forest canopy and from the last echo category were frequently selected. For logarithmic transformation with both vertical and texture variables, D1.L, D2.L and D3.L were the most frequently selected variables and they were selected in 52% of the models. D1.F, D2.F and D3.F were selected in 22% of the models. Canopy height variables are less frequently selected and only Hmean.L and H30.L feature among the 10 most selected variables with a frequency of 9% and 4%, respectively. The most frequently selected texture variable was MN.3, which also is an expression of the mean canopy height and was selected in 2% of the models. The nine most frequently selected variables for each model strategy are presented in Figure 3.

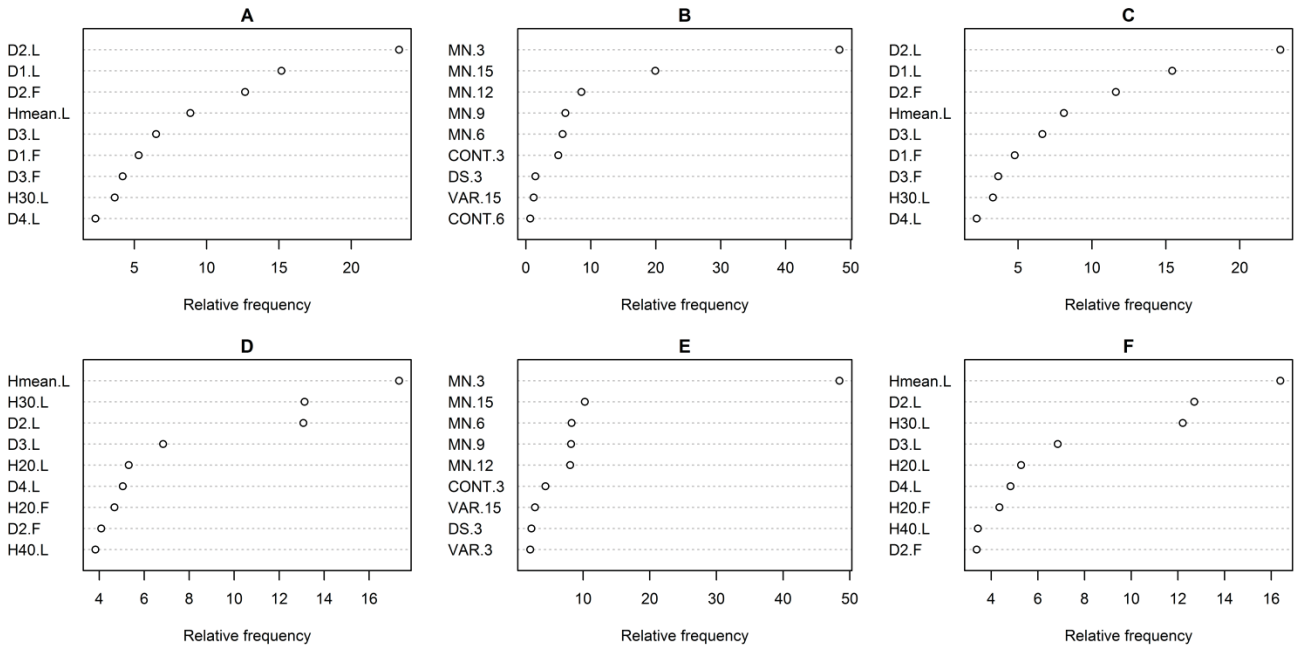

Figure 3. Dotchart of the relative frequency of the nine most frequently selected predictor variables in a simple linear model fitting procedure with logarithmic (**A–C**) and square root transformation of the response (**D–F**) in combination with vertical variables (A, D), texture variables (B, E) and both vertical and texture variables (C, F). Variables are explained in Section 2.3.

4. Discussion

From a REDD+ perspective, it is important to establish a robust and transparent system for estimating carbon stocks in all types of forest. The dataset used in this study is from a unique submontane tropical rainforest with a wide range in biomass densities and very high maximum levels of biomass. Regression models for AGB were developed with ALS-derived variables as predictors. The size of each plot (0.0639–0.1239 ha, Table 1) corresponds well with sizes that have been used frequently in forest sample surveys in tropical countries [68,69]. The plot size is smaller than what has been common practice in more ecologically oriented studies [70], and the wide range in AGB is a direct consequence of the limited plot size. Marshall *et al.* [48] reported a maximum AGB of about 600 Mg·ha^{-1} on 1-ha plots from the same forest area in Tanzania as in our study. In temperate areas the use of LiDAR has been shown to aid successful estimation of biomass up to 1200 Mg·ha^{-1} [29,71], and even though the mentioned studies applied large footprint full waveform LiDAR systems and the forest structure was very different (coniferous forest dominated by Douglas fir (*Pseudotsuga menziesii*)), this has set a standard for what could be achieved with the technology. In comparison to other studies, our results in terms of RMSE for estimated AGB are within in the ranges of what has been found in tropical forest areas. Clark *et al.* [19] reported an RMSE of 33% using small-footprint ALS and a field plot size of 0.09 ha in old-growth and managed tropical forest in Costa Rica. In the study by Asner *et al.* [30] findings in terms of RMSE% from Hawaii, Peru, Panama and Madagascar were 32%, 24%, 18% and 35%, respectively. Some caution should be exercised though, when comparing with other studies, especially with the one reported by Asner *et al.* [30], because the latter

study covered a smaller AGB range than our data and the reference plot size was larger, ranging from 0.1–0.36 ha. Studies based on large field plots will report lower RMSE due to spatial averaging as larger field plot sizes will decrease between-plot variance (cf. [72,73]). That means that all field observations will be more similar, covering a smaller range, and closer to the average value. In addition, larger plots have smaller ratios of the border zone to total plot area than smaller plots—a zone which is subject to edge effects [73,74]. This implies that the relative influences of edge effects are smaller for larger plots, regardless of plot shape. Negative consequences of GPS positioning errors are also smaller for large plots [72]. Likewise, edge effects will be more pronounced in forests with large tree crowns and for rectangular or quadratic plots than circular plots with a smallest possible circumference-to-area ratio.

Even though larger field plots result in models with better performance [16,73], the practical application is limited due to the difficulty of establishing larger field plots, *i.e.*, plots larger than, say, 0.25 ha. This is especially challenging in rugged and steep terrain, and in areas with very dense vegetation. Reducing the field plot size to a more practical and manageable size like in our case will however introduce more edge effects and reduced accuracy of model predictions, as indicated above. Circular plots—as opposed to rectangular plots that were used in this study—will have a smaller circumference-to-area ratio and thus reduce the edge effects and improve the results. It is clear though, that inventory applications, assuming support of ALS data in the estimation, will profit from larger plots than what traditionally have been used in pure field-based sample surveys in the tropics.

Measuring the height of trees is increasingly difficult as tree height increases because (1) an offset in the registered angle results in larger errors in absolute values and (2) the domed shapes and wide tree crowns, common for large and emergent trees, also increase the difficulty of determining the true top of the tree. Because of the dense vegetation in many tropical forests one is forced to stand relatively close to the tree when measuring the tree height. This increases the effect of both (1) and (2). Our H-D model accuracy is in line with the results reported by others, both in Tanzania [75] and other tropical areas [39]. However, the error in the H-D model will propagate and introduce errors in the field estimated AGB, reducing the fit of the AGB models.

Co-registration errors, *i.e.*, the mismatch between the positioning of the field plots and the ALS data, will also add to the total error of the AGB LiDAR models. Although the reported precision of the plot corner coordinates was 57 cm, the true accuracy is unknown, but probably lower (cf. [76]).

The time lag between the field inventory and the ALS survey will also introduce errors in the models. Most of the trees will increase in AGB, and some might die. We tried to correct for some of the most extreme changes (like tree mortality) during the field inventory. There are however most likely still errors in the data caused by the time lag that were not accounted for.

Forest canopy height and density are correlated with AGB, and ALS-derived variables describing the canopy height and density are useful for modeling forest AGB. In addition, forest structural diversity is positively correlated with AGB [31], and use of ALS-derived horizontal information has been explored for estimation of forest variables [34,77] and silvicultural treatment needs [78]. Bohlin *et al.* [34] found a small but significant improvement with inclusion of textural information in modeling forest volume and basal area in a coniferous forest in Sweden. Li *et al.* [77] tested a new ALS-derived horizontal variable in a Chinese spruce forest for biomass estimation and found it to improve the models at tree level. However, area-based estimates did not improve. It should be noted

that the previous studies were conducted in coniferous forests with relatively low structural diversity. We proposed that by adding textural variables, describing horizontal distribution of forest canopy, we would capture information about the spatial distribution of trees and of the forest structure which could improve the model performance. The result of including textural variables derived from an ALS surface model was; however, negative. None of the textural variables were selected in the multiple regression variable selection routine.

In a natural forest that has reached a climax state and in which some of the largest trees have reached their maximum height, the canopy height information from the ALS echoes will provide less information about the AGB. Because of the asymptotic relationship between height and diameter, canopy height variables are less suitable to discriminate between tall trees with various diameters. It is generally the large trees in a tropical forest that show this asymptotic H-D development [79,80] and since these trees have great influence on the AGB in our field plots, this effect could also explain the underestimation for the plots with the higher AGB values. Similar observations were made by Skowronski *et al.* [81] in a temperate forest with asymptotic relationship between height and diameter. Our analysis of the relative importance of the ALS variables showed that most of the information for explaining AGB is found in the variables describing the vertical density of the full vegetation layer, and in variables from the last return echoes. The height of the trees and the density of the vegetation in higher levels of the vegetation provide less explanatory power supporting the notion that the height information is less informative than the density of the forest in a high-biomass tropical forest in which the largest trees have reached their maximum height.

5. Conclusions

In this study, we modeled AGB in a dense tropical rainforests using ground observations from 153 relatively small field plots of 0.0639–0.1239 ha, and ALS-derived variables. The RMSE of the models was approximately 33% of the mean value of 462 $Mg \cdot ha^{-1}$. This result is similar to earlier studies in tropical rainforest areas. The AGB range however is larger than reported in previous studies. We explored the use of texture information derived from a canopy surface model and anticipated that these variables would capture information about the forest structure useful for modeling forest AGB. However, none of the texture variables were selected in models in which all predictor variables were available. The single most important variable available among the texture variables was MN.3, describing the mean canopy height on a 3 m spatial scale, which expresses much the same information as a mean canopy profile height. Nevertheless, this variable did not add new information to the models. Furthermore, analyses of the ALS variables showed that the most important variables were derived from the last echo category, from the lower parts of the canopy, and that they were variables describing the density of the forest canopy. This finding indicates that ALS-derived variables are less able to pick up on information about AGB in a natural forest in which a proportion of the trees has a reduced or even negative height and crown development.

The findings in the present study demonstrate the power of utilizing ALS data even in extreme conditions in dense tropical forests. However, the results also identified some challenges related to field plot size, plot edge effects and tree height–biomass relationship that warrant further research in this valuable biome.

Acknowledgments

This work is part of the project “Enhancing the measuring, reporting and verification (MRV) of forests in Tanzania through the application of advanced remote sensing techniques” funded by the Royal Norwegian Embassy in Tanzania as part of the Norwegian International Climate and Forest Initiative. Tree DBH data from 2008 to 2010 were provided by project “Assessing the impact of forestland tenure changes on forest resources and rural livelihoods in Tanzania” under the Tanzania-Norway NUFU program. We wish to thank Terratec AS, Norway, for acquiring and processing the ALS data and Nuru Hussein and the rest of the field crew for field data collection.

Author Contributions

Endre Hofstad Hansen has been the main author of the manuscript, carried out and supervised the field work and performed the calculations and analysis. Terje Gobakken has prepared the remote sensing data, co-authored and revised the manuscript. Ole Martin Bollandsås has planned and prepared the field data and revised parts of the manuscript. Eliakimu Zahabu has planned and supervised the study. Erik Næsset has planned and supervised the study and revised parts of the manuscript.

Conflicts of Interest

The authors declare no conflict of interest.

References

1. Lewis, S.L.; Sonké, B.; Sunderland, T.; Begne, S.K.; Lopez-Gonzalez, G.; van der Heijden, G.M.F.; Phillips, O.L.; Affum-Baffoe, K.; Baker, T.R.; Banin, L.; *et al*. Above-ground biomass and structure of 260 African tropical forests. *Philos. Trans. Royal Soc. B Biol. Sci.* **2013**, *368*, doi:10.1098/rstb.2012.0295.
2. Bastiaanssen, W.; Noordman, E.; Pelgrum, H.; Davids, G.; Thoreson, B.; Allen, R. SEBAL model with remotely sensed data to improve water-resources management under actual field conditions. *J. Irrig. Drain. Eng.* **2005**, *131*, 85–93.
3. De Jong, S.M.; Jetten, V.G. Estimating spatial patterns of rainfall interception from remotely sensed vegetation indices and spectral mixture analysis. *Int. J. Geogr. Inf. Sci.* **2007**, *21*, 529–545.
4. Doherty, R.M.; Sitch, S.; Smith, B.; Lewis, S.L.; Thornton, P.K. Implications of future climate and atmospheric CO_2 content for regional biogeochemistry, biogeography and ecosystem services across East Africa. *Glob. Change Biol.* **2010**, *16*, 617–640.
5. ITTO (International Tropical Timber Organization). *Annual Report 2012*; ITTO: Yokohama, Japan, 2012.
6. Masera, O.; Ghilardi, A.; Drigo, R.; Angel Trossero, M. WISDOM: A GIS-based supply demand mapping tool for woodfuel management. *Biomass Bioenergy* **2006**, *30*, 618–637.
7. UNFCCC. *Report of the Conference of the Parties on Its Sixteenth Session, Held in Cancun from 29 November to 10 December 2010. Addendum. Part Two: Action Taken by the Conference of the Parties at Its Sixteenth Session*; United Nations Office: Geneva, Switzerland, 2011; p. 31.

8. UNFCCC. *Outcome of the Work of the Ad Hoc Working Group on Long-Term Cooperative Action under the Convention—C. Policy Approaches and Positive Incentives on Issues Relating to Reducing Emissions from Deforestation and Forest Degradation in Developing Countries and the Role of Conservation, Sustainable Management of Forests and Enhancement of Forest Carbon Stocks in Developing Countries*; United Nations Office: Geneva, Switzerland, 2010.
9. UNFCCC. *Report of the Conference of the Parties on Its Fifteenth Session, Held in Copenhagen from 7 to 19 December 2009. Addendum. Part Two: Action taken by the Conference of the Parties at Its Fifteenth Session*; United Nations Office: Geneva, Switzerland, 2010; p. 43.
10. UNFCCC. *Good Practice Guidance and Adjustments Under Article 5, Paragraph 2, of the Kyoto Protocol*; FCCC/KP/CMP/2005/8/Add.3 Decision 20/CMP.1; United Nations Office: Geneva, Switzerland, 2006.
11. Grassi, G.; Monni, S.; Federici, S.; Achard, F.; Mollicone, D. Applying the conservativeness principle to REDD to deal with the uncertainties of the estimates. *Environ. Res. Lett.* **2008**, *3*, doi:10.1088/1748-9326/3/3/035005.
12. Gibbs, H.K.; Brown, S.; Niles, J.O.; Foley, J.A. Monitoring and estimating tropical forest carbon stocks: making REDD a reality. *Environ. Res. Lett.* **2007**, *2*, doi:10.1088/1748-9326/2/4/045023.
13. Plugge, D.; Baldauf, T.; Köhl, M. Reduced Emissions from Deforestation and Forest Degradation (REDD): Why a robust and transparent Monitoring, Reporting and Verification (MRV) System is mandatory. In *Climate Change—Research and Technology for Adaptation and Mitigation*; Blanco, J., Ed. InTech: Rijeka, Croatia, 2011; pp. 155–170.
14. GOFC-GOLD. A sourcebook of methods and procedures for monitoring and reporting anthropogenic greenhouse gas emissions and removals associated with deforestation, gains and losses of carbon stocks in forests remaining forests, and forestation. In *GOFC-GOLD Report Version COP18–1*; GOFC-GOLD Land Cover Project Office, Wageningen University: Wageningen, The Netherlands, 2012; p. 219.
15. Fassnacht, F.E.; Hartig, F.; Latifi, H.; Berger, C.; Hernández, J.; Corvalán, P.; Koch, B. Importance of sample size, data type and prediction method for remote sensing-based estimations of aboveground forest biomass. *Remote Sens. Environ.* **2014**, *154*, 102–114.
16. Zolkos, S.G.; Goetz, S.J.; Dubayah, R. A meta-analysis of terrestrial aboveground biomass estimation using lidar remote sensing. *Remote Sens. Environ.* **2013**, *128*, 289–298.
17. Koch, B. Status and future of laser scanning, synthetic aperture radar and hyperspectral remote sensing data for forest biomass assessment. *ISPRS-J. Photogramm. Remote Sens.* **2010**, *65*, 581–590.
18. McRoberts, R.E.; Tomppo, E.O.; Næsset, E. Advances and emerging issues in national forest inventories. *Scand. J. Forest Res.* **2010**, *25*, 368–381.
19. Clark, M.L.; Roberts, D.A.; Ewel, J.J.; Clark, D.B. Estimation of tropical rain forest aboveground biomass with small-footprint lidar and hyperspectral sensors. *Remote Sens. Environ.* **2011**, *115*, 2931–2942.
20. Asner, G.P.; Clark, J.K.; Mascaro, J.; Galindo García, G.A.; Chadwick, K.D.; Navarrete Encinales, D.A.; Paez-Acosta, G.; Cabrera Montenegro, E.; Kennedy-Bowdoin, T.; Duque, Á.; *et al*. High-resolution mapping of forest carbon stocks in the Colombian Amazon. *Biogeosciences Discuss.* **2012**, *9*, 2445–2479.

21. Mascaro, J.; Asner, G.P.; Muller-Landau, H.C.; van Breugel, M.; Hall, J.; Dahlin, K. Controls over aboveground forest carbon density on Barro Colorado Island, Panama. *Biogeosciences.* **2011**, *8*, 1615–1629.
22. Vincent, G.; Sabatier, D.; Blanc, L.; Chave, J.; Weissenbacher, E.; Pélissier, R.; Fonty, E.; Molino, J.-F.; Couteron, P. Accuracy of small footprint airborne LiDAR in its predictions of tropical moist forest stand structure. *Remote Sens. Environ.* **2012**, *125*, 23–33.
23. Asner, G.P.; Powell, G.V. N.; Mascaro, J.; Knapp, D.E.; Clark, J.K.; Jacobson, J.; Kennedy-Bowdoin, T.; Balaji, A.; Paez-Acosta, G.; Victoria, E.; Secada, L.; Valqui, M.; Hughes, R.F. High-resolution forest carbon stocks and emissions in the Amazon. *Proc. Natl. Acad. Sci. USA* **2010**, *107*, 16738–16742.
24. Hou, Z.; Xu, Q.; Tokola, T. Use of ALS, Airborne CIR and ALOS AVNIR-2 data for estimating tropical forest attributes in Lao PDR. *ISPRS-J. Photogramm. Remote Sens.* **2011**, *66*, 776–786.
25. Asner, G.P.; Clark, J.; Mascaro, J.; Vaudry, R.; Chadwick, K.D.; Vieilledent, G.; Rasamoelina, M.; Balaji, A.; Kennedy-Bowdoin, T.; Maatoug, L.; *et al*. Human and environmental controls over aboveground carbon storage in Madagascar. *Carbon Balance Manag.* **2012**, *7*, doi:10.1186/1750-0680-7-2.
26. Næsset, E. Predicting forest stand characteristics with airborne scanning laser using a practical two-stage procedure and field data. *Remote Sens. Environ.* **2002**, *80*, 88–99.
27. Næsset, E.; Gobakken, T. Estimation of above- and below-ground biomass across regions of the boreal forest zone using airborne laser. *Remote Sens. Environ.* **2008**, *112*, 3079–3090.
28. Hollaus, M.; Wagner, W.; Schadauer, K.; Maier, B.; Gabler, K. Growing stock estimation for alpine forests in Austria: A robust lidar-based approach. *Can. J. For. Res.* **2009**, *39*, 1387–1400.
29. Lefsky, M.A.; Cohen, W.B.; Harding, D.J.; Parker, G.G.; Acker, S.A.; Gower, S.T. Lidar remote sensing of above-ground biomass in three biomes. *Glob. Ecol. Biogeogr.* **2002**, *11*, 393–399.
30. Asner, G.P.; Mascaro, J.; Muller-Landau, H.C.; Vieilledent, G.; Vaudry, R.; Rasamoelina, M.; Hall, J.S.; van Breugel, M. A universal airborne LiDAR approach for tropical forest carbon mapping. *Oecologia* **2012**, *168*, 1147–1160.
31. Wang, W.F.; Lei, X.D.; Ma, Z.H.; Kneeshaw, D.D.; Peng, C.H. Positive relationship between aboveground carbon stocks and structural diversity in spruce-dominated forest stands in New Brunswick, Canada. *For. Sci.* **2011**, *57*, 506–515.
32. Kebede, M.; Kanninen, M.; Yirdaw, E.; Lemenih, M. Vegetation structural characteristics and topographic factors in the remnant moist Afromontane forest of Wondo Genet, south central Ethiopia. *J. For. Res.* **2013**, *24*, 419–430.
33. Bastin, J.-F.; Barbier, N.; Couteron, P.; Adams, B.; Shapiro, A.; Bogaert, J.; De Cannière, C. Aboveground biomass mapping of African forest mosaics using canopy texture analysis: Toward a regional approach. *Ecol. Appl.* **2014**, *24*, 1984–2001.
34. Bohlin, J.; Wallerman, J.; Fransson, J.E.S. Forest variable estimation using photogrammetric matching of digital aerial images in combination with a high-resolution DEM. *Scand. J. For. Res.* **2012**, *27*, 692–699.
35. Lim, K.S.; Treitz, P.M. Estimation of above ground forest biomass from airborne discrete return laser scanner data using canopy-based quantile estimators. *Scand. J. For. Res.* **2004**, *19*, 558–570.

36. Li, Y.Z.; Andersen, H.E.; McGaughey, R. A comparison of statistical methods for estimating forest biomass from light detection and ranging data. *West. J. Appl. For.* **2008**, *23*, 223–231.
37. Boudreau, J.; Nelson, R.F.; Margolis, H.A.; Beaudoin, A.; Guindon, L.; Kimes, D.S. Regional aboveground forest biomass using airborne and spaceborne LiDAR in Quebec. *Remote Sens. Environ.* **2008**, *112*, 3876–3890.
38. D'Oliveira, M.V.N.; Reutebuch, S.E.; McGaughey, R.J.; Andersen, H.E. Estimating forest biomass and identifying low-intensity logging areas using airborne scanning lidar in Antimary State Forest, Acre State, Western Brazilian Amazon. *Remote Sens. Environ.* **2012**, *124*, 479–491.
39. Feldpausch, T.R.; Banin, L.; Phillips, O.L.; Baker, T.R.; Lewis, S.L.; Quesada, C.A.; Affum-Baffoe, K.; Arets, E.; Berry, N.J.; Bird, M.; *et al*. Height-diameter allometry of tropical forest trees. *Biogeosciences* **2011**, *8*, 1081–1106.
40. Myers, N.; Mittermeier, R.A.; Mittermeier, C.G.; da Fonseca, G.A.B.; Kent, J. Biodiversity hotspots for conservation priorities. *Nature* **2000**, *403*, 853–858.
41. Burgess, N.D.; Butynski, T.M.; Cordeiro, N.J.; Doggart, N.H.; Fjeldsa, J.; Howell, K.M.; Kilahama, F.B.; Loader, S.P.; Lovett, J.C.; Mbilinyi, B.; *et al*. The biological importance of the Eastern Arc Mountains of Tanzania and Kenya. *Biol. Conserv.* **2007**, *134*, 209–231.
42. Dawson, W.; Mndolwa, A.S.; Burslem, D.; Hulme, P.E. Assessing the risks of plant invasions arising from collections in tropical botanical gardens. *Biodivers. Conserv.* **2008**, *17*, 1979–1995.
43. Newmark, W.D. *Conserving Biodiversity in East African Forests: A Study of the Eastern Arc Mountains*; Springer: Berlin, Germany, 2002; p. 197.
44. Hamilton, A.C.; Bensted-Smith, R. *Forest conservation in the East. Usambara Mountains, Tanzania*; IUCN-The World Conservation Union; Forest Division, Ministry of Lands, Natural Resources, and Tourism, United Republic of Tanzania: Dar es Salaam, Tanzania and Gland, Switzerland and Cambridge, UK, 1989; p. 392.
45. Frontier Tanzania. *Amani Nature Reserve: A biodiversity survey*; Forestry and Beekeeping Division and Metsähallitus Consulting: Dar es Salaam, Tanzania and Vantaa, Finland, 2001.
46. Mpanda, M.M.; Luoga, E.J.; Kajembe, G.C.; Eid, T. Impact of forestland tenure changes on forest cover, stocking and tree species diversity in Amani Nature Reserve, Tanzania. *For. Trees Livelihoods* **2011**, *20*, 215–229.
47. Mgumia, F. Implications of Forestland Tenure Reforms on Forest Conditions, Forest Govenance, and Community Livelihoods at Amani Nature Reserve. Ph.D. Thesis, Sokoine University of Agriculture, Tanzania, 2014; pp. 280.
48. Marshall, A.R.; Willcock, S.; Platts, P.J.; Lovett, J.C.; Balmford, A.; Burgess, N.D.; Latham, J.E.; Munishi, P.K.T.; Salter, R.; Shirima, D.D.; *et al*. Measuring and modelling above-ground carbon and tree allometry along a tropical elevation gradient. *Biol. Conserv.* **2012**, *154*, 20–33.
49. Henry, M.; Besnard, A.; Asante, W.A.; Eshun, J.; Adu-Bredu, S.; Valentini, R.; Bernoux, M.; Saint-Andre, L. Wood density, phytomass variations within and among trees, and allometric equations in a tropical rainforest of Africa. *For. Ecol. Manag.* **2010**, *260*, 1375–1388.
50. Mehtatalo, L. Forest Biometrics Functions of Lauri Mehtatalo, R Package Version 1.1. Available online: http://cs.uef.fi/~lamehtat/rcodes (accessed on 9 January 2015).
51. R Development Core Team. *R: A language and environment for statistical computing*; R Foundation for Statistical Computing: Vienna, Austria, 2013.

52. Prodan, M. *Forest Biometrics*; Pergamon Press: Oxford, UK, 1968; p. 447.
53. Pinheiro, J.; Bates, D.; DebRoy, S.; Sarkar, D.; R Development Core Team. nlme: Linear and Nonlinear Mixed Effects Models. R Package Version 3.1–115. Available online: http://cran.r-project.org/src/contrib/Archive/nlme (accessed on 9 January 2015).
54. Lappi, J.; Bailey, R.L. A height prediction model with random stand and tree parameters—An alternative to traditional site index methods. *For. Sci.* **1988**, *34*, 907–927.
55. Masota, A.M.; Zahabu, E.; Malimbwi, R.; Bollandsås, O.M.; Eid, T. Tree allometric models for above- and belowground biomass of tropical rainforests in Tanzania. *Southern For. A J. For. Sci.* **2015**, submitted.
56. Kouba, J. *A Guide to Using International Gnss Service (Igs) Products*; IGS Central Bureau, Jet Propulsion Laboratory: Pasadena, CA, USA, 2009; p. 34.
57. Anon. *Pinnacle User's Manual*; Javad Positioning Systems: San Jose, CA, USA, 1999.
58. Næsset, E. Effects of differential single- and dual-frequency GPS and GLONASS observations on point accuracy under forest canopies. *Photogramm. Eng. Remote Sens.* **2001**, *67*, 1021–1026.
59. Axelsson, P. DEM generation from laser scanner data using adaptive TIN models. *Int. Arch. Photogramm. Remote Sens.* **2000**, *33*, 110–117.
60. Anon. *Terrascan User's Guide*; Terrasolid Oy: Jyvaskyla, Finland, 2012; p. 311.
61. Anon. *LAS specification, Version 1.2*; American Society for Photogrammetry and Remote Sensing (ASPRS): Bethesda, MA, USA, 2008; p. 13.
62. Nilsson, M. Estimation of tree heights and stand volume using an airborne lidar system. *Remote Sens. Environ.* **1996**, *56*, 1–7.
63. Haralick, R.M.; Shanmugam, K.; Dinsteein, I.H. Textural features for image classification. *IEEE Trans. Syst. Man Cybern.* **1973**, *3*, 610–621.
64. Zvoleff, A. Calculate Textures from Grey-Level Co-Occurrence Matrices (Glcms) In R, R Package Version 0.3.1. Available online: http://cran.r-project.org/src/contrib/Archive/glmc (accessed on 9 January 2015).
65. Goldberger, A. Interpretation and estimation of Cobb-Douglas functions. *Econometrica* **1968**, *36*, 464–472.
66. Gregoire, T.G.; Lin, Q.F.; Boudreau, J.; Nelson, R. Regression estimation following the square-root transformation of the response. *For. Sci.* **2008**, *54*, 597–606.
67. Lumley, T.; Miller, A. Leaps: Regression Subset Selection, R Package Version 2.9. Available online: http://cran.r-project.org/src/contrib/Archive/leaps (accessed on 9 January 2015).
68. Tomppo, E.; Katila, M.; Mäkisara, K.; Peräsaari, J.; Malimbwi, R.; Chamuya, N.; Otieno, J.; Dalsgaard, S.; Leppänen, M. A Report to the Food and Agriculture Organization of the United Nations (FAO) in Support of Sampling Study for National Forestry Resources Monitoring and Assessment (NAFORMA) in Tanzania. Available online: http://www.mp-discussion.org/NAFORMA.pdf (accessed on 10 March 2010).
69. Freitas, J.; Oliveira, Y.M.D.; Rosot, M.A.; Gomide, G.; Mattos, P. Development of the national forest inventory of Brazil. In *National Forest Inventories: Pathways for Common Reporting*; Tomppo, E., Gschwantner, T., Lawrence, M., McRoberts, R.E., Eds.; Springer: Heidelberg, Germany, 2010; pp. 89–95.

70. Laurance, S.G.W.; Laurance, W.F.; Nascimento, H.E.M.; Andrade, A.; Fearnside, P.M.; Expedito, R.G.R.; Condit, R. Long-term variation in Amazon forest dynamics. *J. Veg. Sci.* **2009**, *20*, 323–333.
71. Means, J.E.; Acker, S.A.; Harding, D.J.; Blair, J.B.; Lefsky, M.A.; Cohen, W.B.; Harmon, M.E.; McKee, W.A. Use of large-footprint scanning airborne lidar to estimate forest stand characteristics in the Western Cascades of Oregon. *Remote Sens. Environ.* **1999**, *67*, 298–308.
72. Gobakken, T.; Næsset, E. Assessing effects of positioning errors and sample plot size on biophysical stand properties derived from airborne laser scanner data. *Can. J. For. Res.* **2009**, *39*, 1036–1052.
73. Mascaro, J.; Detto, M.; Asner, G.P.; Muller-Landau, H.C. Evaluating uncertainty in mapping forest carbon with airborne LiDAR. *Remote Sens. Environ.* **2011**, *115*, 3770–3774.
74. McRoberts, R.E.; Andersen, H.E.; Næsset, E. Using Airborne Laser Scanning data to support forest sample surveys. In *Forestry Applications of Airborne Laser Scanning*; Maltamo, M., Næsset, E., Vauhkonen, J., Eds.; Springer Netherlands: Burlin, Germany, 2014; Volumn 27, pp. 269–292.
75. Mugasha, W.; Bollandsås, O.M.; Eid, T. Relationships between diameter and height of trees in natural tropical forest in Tanzania. *Southern For A J. For. Sci.* **2013**, *75*, 221–237.
76. Valbuena, R.; Mauro, F.; Rodriguez-Solano, R.; Manzanera, J.A. Accuracy and precision of GPS receivers under forest canopies in a mountainous environment. *Span. J. Agric. Res.* **2010**, *8*, 1047–1057.
77. Li, W.; Niu, Z.; Gao, S.; Huang, N.; Chen, H. Correlating the horizontal and vertical distribution of lidar point clouds with components of biomass in a picea crassifolia forest. *Forests* **2014**, *5*, 1910–1930.
78. Pippuri, I.; Kallio, E.; Maltamo, M.; Peltola, H.; Packalen, P. Exploring horizontal area-based metrics to discriminate the spatial pattern of trees and need for first thinning using airborne laser scanning. *Forestry* **2012**, *85*, doi:10.1093/forestry/cps005.
79. Iida, Y.; Kohyama, T.S.; Kubo, T.; Kassim, A.; Poorter, L.; Sterck, F.; Potts, M.D. Tree architecture and life-history strategies across 200 co-occurring tropical tree species. *Funct. Ecol.* **2011**, *25*, 1260–1268.
80. Poorter, L.; Bongers, L.; Bongers, F. Architecture of 54 moist-forest tree species: Traits, trade-offs, and functional groups. *Ecology* **2006**, *87*, 1289–1301.
81. Skowronski, N.; Clark, K.; Nelson, R.; Hom, J.; Patterson, M. Remotely sensed measurements of forest structure and fuel loads in the Pinelands of New Jersey. *Remote Sens. Environ.* **2007**, *108*, 123–129.

PAPER II

Remote Sens. **2015**, *7*, 1-x manuscripts; doi:10.3390/rs70x000x

OPEN ACCESS

remote sensing

ISSN 2072-4292

www.mdpi.com/journal/remotesensing

Article

Effects of Pulse Density on Digital Terrain Models and Canopy Metrics using Airborne Laser Scanning in a Tropical Rainforest

Endre Hofstad Hansen*, Terje Gobakken and Erik Næsset

Department of Ecology and Natural Resource Management, Norwegian University of Life Sciences, P.O. Box 5003, NO-1432 Ås, Norway; E-Mails: endre.hansen@nmbu.no (E.H.H.); terje.gobakken@nmbu.no (T.G.); erik.naesset@nmbu.no (E.N.)

***** Author to whom correspondence should be addressed; E-Mail: endre.hansen@nmbu.no; Tel.: +47-6496-5756;

Academic Editor:

Received: / Accepted: / Published:

Abstract: Airborne laser scanning (ALS) is increasingly being used to enhance the accuracy of biomass estimates in tropical forests. Although the technological development of ALS instruments has resulted in ever higher pulse densities, studies in boreal and sub-boreal forests have shown consistent results even at relatively low pulse densities. The objective of the present study was to assess the effects of reduced pulse density on (1) the digital terrain model (DTM), and (2) canopy metrics derived from ALS data collected in a tropical rainforest in Tanzania. We utilized a total of 612 points measured with a differential dual frequency Global Navigation Satellite System receiver to analyse the effects on DTMs at pulse densities of 8, 4, 2, 1, 0.5, and 0.025 pulses·m^{-2}. Furthermore, canopy metrics derived for each pulse density and from four different field plot sizes (0.07, 0.14, 0.21, and 0.28 ha) were analysed. Random variation in DTMs and canopy metrics increased with reduced pulse density. Increased plot size similarly reduced variation in canopy metrics. A reliability ratio, quantifying replication effects in the canopy metrics, indicated that most of the common metrics assessed were reliable at pulse densities >0.5 pulses·m^{-2} at a plot size of 0.07 ha.

Keywords: ALS; airborne laser scanning; digital terrain model; DTM; LiDAR; reliability ratio; tropical rainforest

---

1. Introduction

Tropical forests store large amounts of carbon as biomass and regrowth of tropical forests sequester 1.85 ± 0.09 Pg of carbon annually [1]. However, the annual loss of forest carbon due to deforestation and forest degradation in tropical areas is estimated to 2.01 ± 1.1 Pg [1]. In response to the important role of forests both as a source of carbon emissions and as a potential sink source, the UNFCCC negotiations has resulted in a policy and economic incentive mechanism for creating economic incentives for reducing loss of forest biomass and increasing the net sink of carbon in forests [2]. A key component in the proposed mechanism is monitoring that ensures reliable measurement, reporting, and verification of the reduced loss, or net increase of forest biomass. In order to provide precise estimates of forest biomass the use of airborne laser scanning (ALS) has become increasingly popular as several studies have demonstrated its good performance in tropical areas [3-10].

Modern ALS instruments are able to emit pulses at a rate of up to around 800 kHz and are usually flown over the area of interest mounted on a small airplane. From each pulse the instrument is normally set to record up to 5–9 echoes from each pulse, herein referred to as points. Acquisition of ALS data is costly compared to for instance optical satellite images or radar data. This cost is largely governed by the flight time which can be reduced by flying higher and/or faster resulting in cheaper, but lower pulse density data. To study how lower pulse densities affect the quality of the biomass estimates, reduction of ALS density by controlled thinning of the data has been used to assess the effect on model prediction accuracy [11-22]. Findings from such controlled experiments have resulted in reduced pulse density and lowered cost for ALS acquisitions for operational forest inventory purposes, making the technology more widely applied while providing biomass estimates at acceptable precision levels. Lowered costs and well documented precision levels have resulted in low density ALS missions covering large areas and even entire countries [23], providing valuable data for decision making in forestry. Most studies of pulse density have been conducted in boreal coniferous forests [11-14, 16-17] with examples also from temperate mixed-conifer forest [18, 20] and subtropical pine plantation [15]. The main conclusions from the studies in coniferous forests have been that reducing pulse density down to, say, 0.1 pulses·m^{-2} has hardly any effect on the accuracy of timber volume prediction.

To our knowledge, the recent study by Leitold *et al.* [21], is the only study assessing effects of pulse density in tropical broadleaved forests. The study, conducted in the Brazilian Atlantic forest, reported a systematic effect of pulse density in the construction of the digital terrain model (DTM). Leitold *et al.* [21] concluded that this systematic error in the DTM was propagated to the canopy metrics, resulting in underestimation of forest biomass with reduced pulse density.

A prerequisite for successful application of ALS data for biomass modelling is a good quality terrain model, as information about vegetation height is derived relative to the modelled terrain surface. The quality of the terrain model is determined by the number of pulses that successfully reach the ground and is naturally affected by the density of the vegetation [e.g. 24, 25]. In a recent study by the Norwegian Mapping Authority the percentage of ground points in dense spruce forest was in the range of 4–14% and for dense broadleaved forest in leaf-on conditions 3–9% [26]. In addition to the number of pulses that reach the ground, the quality of the terrain model is dependent on a correct classification of these points as ground. There are several algorithms for classifying individual points

as ground and they differ in performance under different terrain and vegetation conditions [27-28]. Algorithm parameter settings also affect the proportion of points classified as ground. Comparison of five vendors applying the same classification software on the same ALS data showed a difference in the proportion of ground points of 17 percentage points [29]. This difference is most likely due to the parameter settings in the applied algorithm. Part of the result, however, may also be attributed to differences in data analysis routines not documented in the ALS data processing reports [29]. With high biomass and dense broadleaved canopies, the proportion of points classified as ground is expected to be small in tropical rainforests. Furthermore, a low ground point density, due to dense canopy, has been shown to result in increased error in the constructed DTM [25, 30].

When applying ALS data for biomass estimation following the commonly used area-based approach [31], a relationship between biomass measured on field plots on the ground and canopy metrics derived from ALS data from the corresponding area is modelled using statistical methods such as regression analysis, nearest neighbour classification, neural networks or ensemble learning [32-34]. It is possible to derive a large number of canopy metrics from the ALS data to be used in the modelling. However, since these metrics are highly correlated, only a few are usually selected in the final models. Common metrics for biomass estimation in tropical forests have been found to be different expressions of the canopy mean elevation above ground [35-37] and canopy maximum elevation above ground [3, 38]. Other metrics used include percentiles and variance of the canopy elevation above ground [7, 35]. In the present study, we therefore chose to assess canopy metrics similar to those used in the aforementioned studies. Because these metrics describe the vertical distribution of ALS points, they remain relatively unaffected by point density [39].

In addition to pulse density, performance of ALS based biomass estimation is also affected by the field plot size [15, 40-41]. Combined effects of pulse density and plot size was assessed by Watt *et al.* [15] who concluded that reduced pulse density and plot size had little effect on model fit for pulse densities >0.1 pulses·m^{-2} and plot sizes of >0.03 ha. Gobakken and Næsset [11] documented that canopy metrics have lower variation on larger plots and that increasing plot size could compensate for low pulse density. The size of field plots applied in studies of biomass in tropical forests utilizing ALS data usually range between 0.1 and 1.0 ha [42]. To assess the effect of plot size on the mean values and variation of ALS-derived canopy metrics we computed and analysed metrics derived from plot sizes of 0.07, 0.14, 0.21, and 0.28 ha. The smallest plot size of 0.07 ha was chosen because it corresponds to the plot size used in the Tanzanian national forest inventory [43].

The objectives of the present study were to assess the effects of reduced ALS pulse densities on (1) the DTMs and (2) the canopy metrics derived from the ALS data used for biomass estimation in a dense tropical rainforest in East Africa. We reduced the pulse density from an initial density of about 13 pulses·m^{-2}, to 8, 4, 2, 1, 0.5, and 0.25 pulses·m^{-2}. Following the pulse density reduction, we assessed the differences between the DTMs derived from ALS data and the elevation obtained from 612 ground points measured using a survey-grade differential Global Navigation Satellite System (dGNSS) receiver. Furthermore, we produced standard canopy metrics commonly used for forest biomass modelling and compared the effect of reduced pulse densities on four different field plot sizes (0.07, 0.14, 0.21, and 0.28 ha).

2. Materials and Methods

2.1. Study Area

The study area is located in eastern Tanzania in the Amani Nature Reserve (S 5°08', E 38°37', 200–1200 m above sea level) and covers around 8360 ha of tropical submontane rainforest. Most of the annual precipitation of around 2000 mm is received in two main rain seasons. Daily mean temperatures vary from about 16 to 25 °C. In an inventory carried out in 1986/87, about half of the nature reserve was classified as logged or covered with an non-indigenous tree species *Maesopsis eminii* as a result of logging [44]. The logging was stopped in the late 1980s and most of the nature reserve is now covered by closed forest.

2.2. Field Data

A total of 612 point measurements (x, y, and z positions) were collected in the corners of 153 rectangular field plots positioned in the period August 2011–April 2012. On plot level, the distance between each point was approximately 20 m in the north-south direction and 50 m in the east-west direction. The distance between plots was approximately 900 m in the north-south direction 450 m in the east-west direction. The points were measured by means of dGNSS using two 40-channel survey-grade receivers (Topcon Legacy-E+). One receiver was placed at each plot corner (k) on a 2.9 m carbon rod for a minimum of 30 minutes, and a one second logging rate was used. A second receiver, acting as a base station, was placed on the roof of a house at the Amani Nature Reserve headquarters with a distance of <14 km from the plots. Prior to measuring the points, the position of the base station antenna was determined with Precise Point Positioning with Global Positioning System and Global Navigation Satellite System data collected continuously for 24 hours according to Kouba [45]. Due to the sloped terrain and dense biomass conditions the elevation measured at each point with the dGNSS (z^{dGNSS}) had a mean precision (standard deviation) of 0.39 m reported from the post-processing using Pinnacle software [46]. Further details about the field data can be found in Hansen *et al.* [47].

2.3. ALS Data

Complete coverage ALS data were collected in January and February 2012 using a Leica ALS70 (Leica Geosystems AG, Switzerland) sensor mounted on a fixed wing aircraft. Average altitude and speed were 800 m above ground level and 70 $m \cdot s^{-1}$, respectively. The sensor was operated using a laser pulse repetition frequency of 339 kHz and up to five echoes were recorded for each emitted pulse. Planned pulse density at acquisition was set to 10 $pulses \cdot m^{-2}$, but due to overlap between adjacent strips the average pulse density in the area of the field plots was 13 $pulses \cdot m^{-2}$.

2.4. Monte Carlo Simulation

In order to study the effects of reduced pulse densities, a thinning procedure was employed by which individual pulses were randomly discarded (section 2.5). The random thinning procedure was

incorporated in a Monte Carlo simulation by which we repeated the thinning and the subsequent analysis on the thinned data 50 times to quantify the effects of the data reduction (sections 2.5–2.7).

2.5. Reduction of Laser Pulse Density

The thinning of ALS data was executed on pulse level using the "ThinData" program in the FUSION toolkit [48]. ALS data were thinned from an initial density of about 13 pulses·m^{-2} to pulse densities of 8, 4, 2, 1, 0.5, and 0.25 pulses·m^{-2}. To mimic and maintain the fairly regular spatial distribution of ALS pulses inherent in the initial data, the thinning was performed on a grid size of 0.1, 0.2, 0.5, 1, 2, 10, and 20 m, for pulse densities of 8, 4, 2, 1, 0.5, and 0.25·m^{-2}, respectively. Following the thinning, a classification of ground points was conducted using the "GroundFilter" program in FUSION. The interpolating algorithm [49] implemented in "GroundFilter" initially makes an average surface based on all ALS points. Further, weights are given to all points based on their vertical distance to the initial surface. Low weight is given to points above the surface, and high weight to points below. The weights are then used in re-fitting the surface. Two parameters in the algorithm can be adjusted to determine which points are given weights. Points located below the surface with a distance larger than parameter *g* are assigned the maximum weight value of 1.0, while points located above the surface with a distance larger than the parameter *w* + the parameter *g* are assigned weights of 0.0 [48]. To adjust for the different pulse densities we controlled the two parameters while leaving the other parameters at the program default setting. The *g* and *w* parameter settings at different pulse densities are given in Table 1. Visual inspection of initial classifications of ground points showed large outliers and a smoothing filter of 3 m was applied to remove these outliers. From the points classified as ground, a 1 m gridded surface was created using the "TINSurfaceCreate" program in FUSION.

2.6. Assessing Effects of Pulse Density on DTM Quality

Reduction of the pulse density will affect the quality of the DTM since less ground points are available for constructing the DTM surface. To study the effects of reduced pulse densities on the DTMs we subtracted the elevation in the DTMs resulting from the reduced pulse densities (z^{DTM}), from the elevation of each plot corner (k) measured with dGNSS (z^{dGNSS}) to get the difference for each point (D_k, Equation (1)):

$$D_k = z_k^{DTM} - z_k^{dGNSS}. \quad (1)$$

The mean difference ($\overline{D}$) and standard deviation (S_D) of the differences (D_k) were calculated. To compare the $\overline{D}$ at each pulse density level a t-test was performed using the Holm-Bonferroni procedure [50] for correction of p-values for multiple comparisons.

The conventional measures of accuracy, $\overline{D}$ and S_D, assumes no outliers and a normal distribution of errors. As pointed out by e.g. Zandbergen [51], errors in DTMs are often not normally distributed. We therefore checked for non-normality by inspecting a Q-Q plot and calculated robust accuracy measures suited for characterisation of non-normal distributions suggested by Höhle and Höhle [52]. The 50% sample quantile of the errors ($P50_D$, i.e., the median value) is a robust estimator for a systematic shift of the DTM [52]. The 95% quantile of the absolute value of the errors ($P95_{|D|}$) and the normalized

median absolute deviation (NMAD, Equation (2)), a robust estimator for S_D, are estimators resilient to outliers [52].

$$\mathrm{NMAD} = 1.4826 * \mathrm{median}_i(|D_k - P50_D|). \quad (2)$$

2.7. Assessing Effects of Pulse Density on Canopy Metrics

After creating a gridded DTM, the elevation of the DTM was subtracted from the elevation for all ALS points resulting in an elevation above the ground for each individual point. Together these points form a "cloud" of points, referred to as the point cloud. At the centre of each of the 153 rectangular field plots we extracted the point clouds from four concentric circles of 0.07, 0.14, 0.21, and 0.28 ha. For each plot centre, and for each plot size, a set of canopy metrics was computed using the "CloudMetrics" program in FUSION. Frequently used canopy metrics for biomass estimation in tropical forests include mean elevation above ground (E.mean) and maximum elevation above ground (E.max). Other commonly used metrics also includes variance of the elevation above ground (E.var), percentiles of elevation and canopy density. The canopy density metrics are commonly derived by dividing the canopy into 10 vertical parts of equal height and calculating the proportion of points above each vertical part. We selected the 10th and 90th percentile of elevation (E.10, E.90), the proportion of points above the ground (D.0) and above the mean canopy height (D.5), along with E.mean, E.max, and E.var for analysis.

From the simulations described in section 2.4, we calculated the mean ($\overline{M}$) and standard deviation of each canopy metric (S_M) on plot level across the 50 Monte Carlo repetitions. Even though the canopy metrics are relatively unaffected by point density [39], reduced pulse density will increase S_M. As explained by Magnussen *et al.* [19], random factors affecting the canopy metrics suggests that the metrics should be considered as random variables instead of fixed, as is commonly the case. These random factors can be referred to as replication effects. Replication effects will weaken the fit of the biomass models with a factor termed as the reliability ratio [53, p. 3]. By calculating the replication variance in the metrics, estimates of the reliability ratios for the metrics were calculated. The method was used by Magnussen *et al.* [19], in which the reliability ratio was calculated as the ratio of the variance of each metric among sample plots, to the total variance of the corresponding metric (Equation (3)):

$$\text{Reliability ratio} = (\hat{\sigma}_u^2)/(\hat{\sigma}_u^2 + \hat{\sigma}_w^2), \quad (3)$$

where $\hat{\sigma}_u^2$ is the estimated among-plot variance of the metric and $\hat{\sigma}_w^2$ is the estimated average within-plot variance. High within-plot variance in a metric compared to the variance among plots for the same metric results in a low reliability ratio, indicating that the metric is less reliable as a predictor.

3. Results

3.1. Effects of Pulse Density on DTM Quality

Effects of reduced pulse density, assessed by Monte Carlo simulation, resulted in a $\overline{D}$ between the elevation of the 612 point measurements recorded by the dGNSS and the elevation of the same points in the ALS-derived DTM of 1.81 m for a pulse density of 8 pulses·m^{-2} (Table 1). Thus, the elevation recorded by the dGNSS was higher than the ALS-derived DTM. Reduction of pulse density from 8 to 0.25 pulses·m^{-2} gave no significant effect on the $\overline{D}$.

The Q-Q plot of the distribution of errors (Figure 1) showed non-normality and justified the presentation of robust measures of accuracy. We observed loss of precision when reducing the pulse density from 8 to 0.25 pulses·m^{-2}, expressed by both the conventional measure of precision (S_D) and the more robust measure NMAD (Table 1).

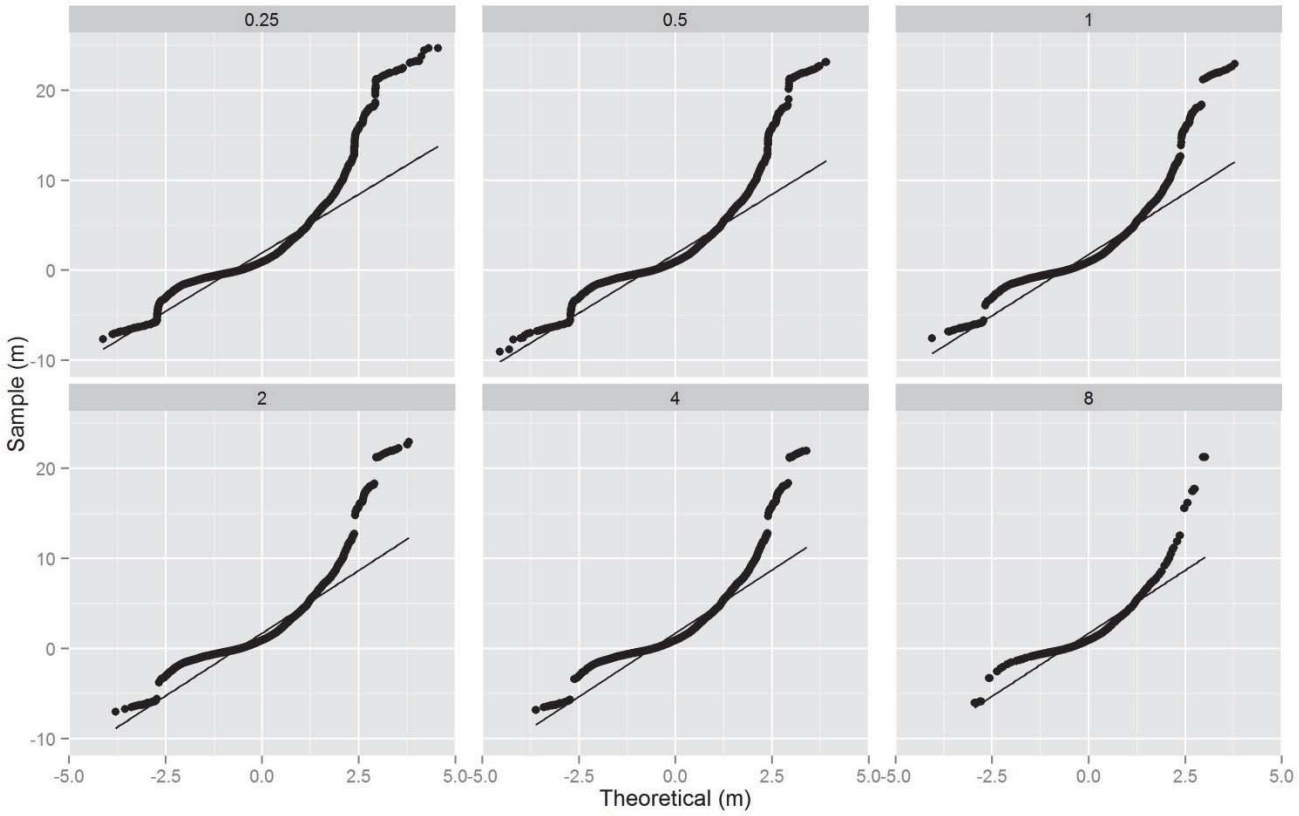

Figure 1. Normal Q-Q-plot for the distribution of the difference in elevation between the elevation recorded by the dGNSS and the elevation of the corresponding ALS-derived DTM at pulse densities of 0.25, 0.5, 1, 2, 4, and 8 pulses·m^{-2}.

Table 1. Summary of the difference in elevation between the dGNSS measurements and the DTM elevation for different pulse densities.

						Parameter settings[1]	
Pulses·m^{-2}	$\overline{D}$ (m)	S_D (m)	$P50_D$ (m)	$P95_{\|D\|}$ (m)	NMAD (m)	*g* (m)	*w* (m)
0.25	1.77	3.20	0.90	7.72	2.15	-1.0	1.5
0.5	1.77	3.02	0.92	7.50	1.97	-1.5	2.0
1	1.79	2.93	0.94	7.34	1.85	-2.0	2.5
2	1.81	2.90	0.96	7.28	1.80	-2.5	3.0
4	1.81	2.88	0.95	7.20	1.75	-3.0	3.5
8	1.81	2.89	0.95	7.35	1.81	-3.5	4.0

Mean difference ($\overline{D}$), standard deviation (S_D), 50% quantile of the difference ($P50_D$), 95% quantile of the absolute value of the difference ($P95_{|D|}$) and the normalized median absolute deviation (NMAD).

[1] Settings of the *g* and *w* parameters in the applied ground classification algorithm.

3.2. Effects of Pulse Density on Canopy Metrics

Canopy metrics were derived from the ALS data from field plot sizes of 0.07, 0.14, 0.21, and 0.28 ha. Mean values from the repeated simulations showed that most of the assessed metrics were unaffected by the reduced pulse density (Table 2). E.max, however, decreased with reduced pulse density, and showed a significant difference ($p = 0.00072$) of 0.58 m at 1 pulse·m^{-2} compared to the value at 8 pulses·m^{-2}, at a plot size of 0.07 ha. This effect was reduced with increased plot size, but was still significant ($p = 0.00298$) for 1 pulse·m^{-2} at the plot size of 0.28 ha.

Reduced pulse density resulted in an increased variation in the canopy metrics on plot level (Figure 2). The standard deviation for the canopy metrics (S_M) showed that the metric describing the canopy elevation in the middle of the canopy (E.mean) was more stable than the elevation of the top and bottom of the canopy (E.max, E.10, E.90). Reduction of the pulse density from 8 to 0.25 pulses·m^{-2} increased the S_M for E.mean from 0.09 to 0.90 m on a 0.07 ha plot size. The effect for E.max, on the 0.07 ha plot size, was an increase of S_M from 0.16 to 1.03 m (Figure 2).

Further, reduced pulse density resulted in decreased reliability ratio, the ratio of the estimated among-plot variance to the estimated total variance (Figure 3). At pulse densities ≥2 pulses·m^{-2} and a plot size of 0.07 ha, the reliability ratio was >0.95 for all canopy metrics. At a pulse density of 0.5 pulses·m^{-2} and a plot size of 0.07 ha, the reliability ratios of E.var and D.0 were reduced down to 0.60 and 0.90, respectively. At a pulse density of 0.25 pulses·m^{-2} and a plot size of 0.07 ha, E.var, E.10, and D.0 had an estimated reliability ratio of <0.9, while the rest of the metrics had a reliability ratio of >0.9.

Table 2. Mean values ($\overline{M}$) of canopy metrics for plot sizes of 0.07, 0.14, 0.21, and 0.28 ha and pulse densities of 0.25, 0.5, 1, 2, 4, and 8 pulses·m^{-2}.

		$\overline{M}$						
Plot size (ha)	Pulse density	E.mean	E.max	E.var	E.10	E.90	D.0	D.5
0.07	0.25	24.59	41.42	107.59	10.06	36.15	89.99	55.18
0.07	0.5	24.49	41.75	108.79	9.79	36.18	90.01	55.25
0.07	1	24.47	41.98	108.93	9.72	36.16	90.09	55.39
0.07	2	24.49	42.22	109.17	9.70	36.19	90.17	55.47
0.07	4	24.59	42.36	108.72	9.82	36.21	90.29	55.68
0.07	8	24.69	42.56	108.17	9.93	36.26	90.33	55.73
0.14	0.25	24.59	43.44	112.27	9.48	36.64	90.07	54.67
0.14	0.5	24.47	43.70	113.24	9.28	36.60	90.07	54.74
0.14	1	24.45	43.92	113.60	9.21	36.60	90.15	54.80
0.14	2	24.49	44.11	113.67	9.24	36.63	90.23	54.89
0.14	4	24.60	44.23	113.15	9.40	36.68	90.38	55.05
0.14	8	24.70	44.39	112.60	9.52	36.74	90.44	55.14
0.21	0.25	24.60	44.38	114.04	9.33	36.93	90.16	54.35
0.21	0.5	24.47	44.61	114.91	9.12	36.86	90.14	54.42
0.21	1	24.43	44.81	115.22	9.04	36.84	90.18	54.50
0.21	2	24.49	45.03	115.35	9.07	36.88	90.28	54.59
0.21	4	24.59	45.17	114.83	9.22	36.93	90.40	54.72
0.21	8	24.70	45.33	114.22	9.35	37.00	90.48	54.82
0.28	0.25	24.59	45.01	115.87	9.13	37.05	90.01	54.31
0.28	0.5	24.45	45.23	116.54	8.93	36.97	89.97	54.36
0.28	1	24.44	45.47	116.95	8.87	36.98	90.04	54.45
0.28	2	24.48	45.68	116.93	8.91	37.00	90.12	54.52
0.28	4	24.59	45.85	116.40	9.05	37.05	90.24	54.66
0.28	8	24.69	45.98	115.84	9.18	37.12	90.33	54.75

Mean elevation above ground (E.mean), maximum elevation above ground (E.max), variance of the elevation above ground (E.var), 10th and 90th percentile of elevation (E.10 and E.90), and the proportion of points above the ground (D.0) and above the mean canopy height (D.5).

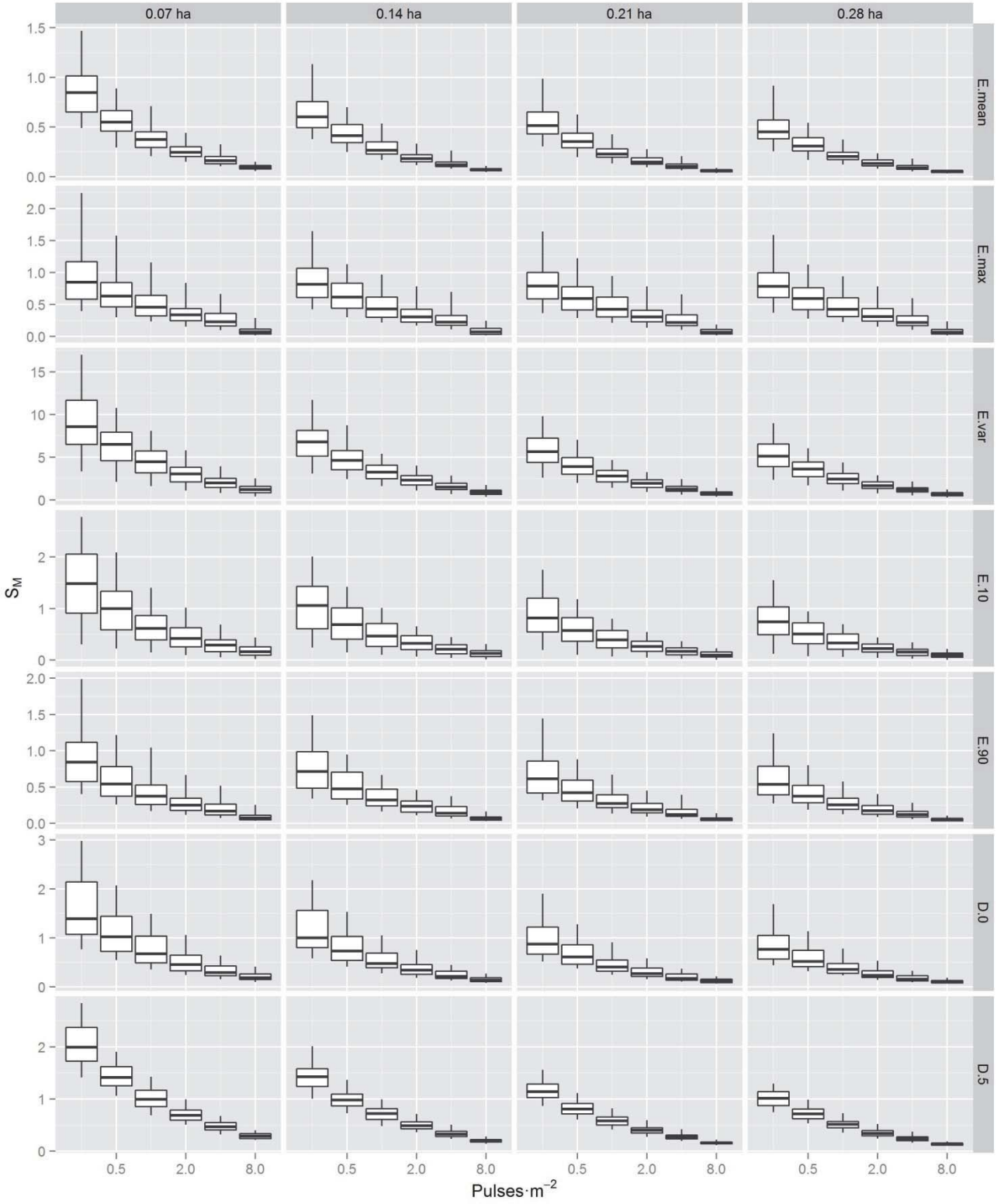

Figure 2. Box and whisker plots of standard deviations (S_M) (whiskers at 5th and 95th percentile) of canopy metrics for plot sizes of 0.07, 0.14, 0.21, and 0.28 ha and pulse densities of 0.25, 0.5, 1, 2, 4, and 8 pulses·m^{-2}. E.mean (mean elevation above ground), E.max (maximum elevation above ground), E.var (variance of the elevation above ground), E.10 and E.90 (10th and 90th height percentile of canopy points), D.0 and D.5 (the proportion of points above the ground and above the mean canopy height).

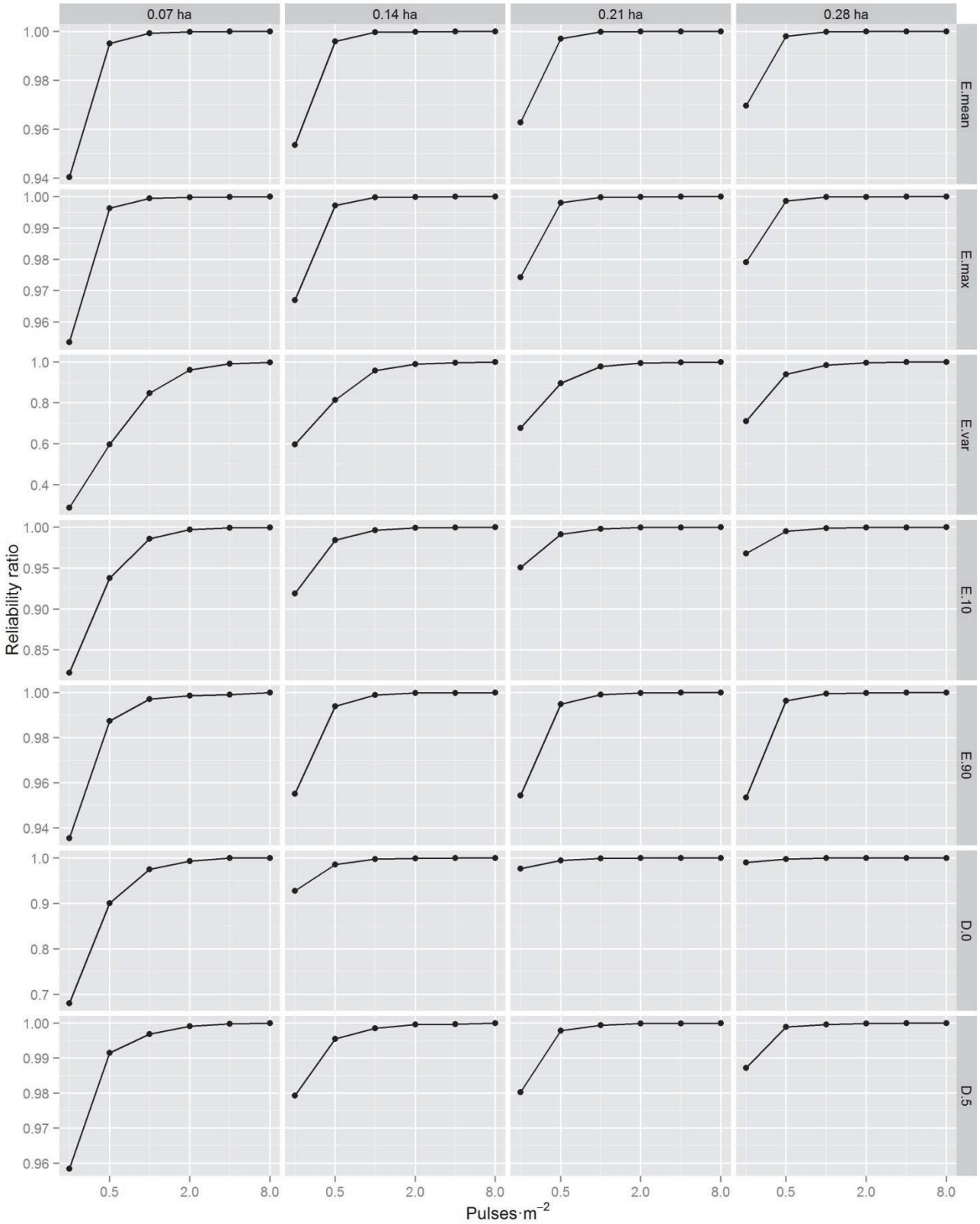

Figure 3. Plots of reliability ratios for canopy metrics at a plot size of 0.07, 0.14, 0.21, and 0.28 ha and pulse densities of 0.25, 0.5, 1, 2, 4, and 8 pulses·m^{-2}. E.mean (mean elevation above ground), E.max (maximum elevation above ground), E.var (variance of the elevation above ground), E.10 and E.90 (10th and 90th height percentile of canopy points), D.0 and D.5 (the proportion of points above the ground and above the mean canopy height).

3.3. Effects of Plot Size on Canopy Metrics

The statistics for the canopy metrics resulting from the Monte Carlo simulations showed that the variation in the metrics was reduced with plot size for all metrics and at all pulse densities (Figure 2). Increasing the plot size means that the probability of including larger trees increase. As a result, we found that the maximum elevation (E.max) and the elevation of the top of the canopy (E.90) increased in value with increased plot size (Table 2). Increasing the plot size also means that the more of the variability in elevation is captured by the plot and that this will result in an increased E.var. Metrics describing the elevation of the lowest part of the canopy (E.10) and the proportion of points above the mean canopy height (D.5), however, decreased in value with increasing plot size. E.mean and D.0 did not show any trend with increased plot size. The reliability ratio increased for all metrics with increasing plot size (Figure 3).

4. Discussion

The present study examined the effects of reduced ALS pulse density on the quality of the derived DTM and selected canopy metrics through Monte Carlo simulation. Pulse density was reduced from 13 pulses·m^{-2} to densities of 8, 4, 2, 1, 0.5, and 0.25 pulses·m^{-2}. Because the accuracy of the dGNSS measurements is unknown (see discussion below), we compared the relative change in elevation of the dGNSS points between pulse densities.

Dense vegetation obstructs the ALS pulses and results in fewer pulses reaching the ground and being available for DTM construction. The effect of vegetation on ALS-derived DTMs has been studied in different conditions and has resulted in both an over-prediction of terrain elevation [54-56] and under-prediction of terrain elevation [24, 28]. Hodgson *et al.* [24] found that ALS-derived elevation was significantly under-predicted in all studied land cover classes. The under-prediction was largest in pine forest areas, by up to 0.24 m. Tinkham *et al.* [28] also found an under-prediction of 0.9–0.16 m in coniferous areas, when comparing two different ground classification algorithms. In their discussion of observed under-predicted terrain elevation in heavily vegetated areas, Hodgson *et al.* [24] suggested that the error was a result of point density, and/or the accuracy of correct classification of points as ground.

Our analysis showed that the mean DTM elevation was unaffected by the reduction in pulse density from 8 to 0.25 pulses·m^{-2}. This was in contradiction with results from other studies on reducing ALS data density [21, 57-58]. In a tropical forest with similar conditions as in the present study, Leitold *et al.* [21] found an increased DTM elevation of 3.02 m at 1 pulse·m^{-2}, compared to a DTM from 20 pulses·m^{-2}. Leitold *et al.* [21] attributed the increased elevation to the morphological filter algorithm [59] used to classify ground points. Hyyppä *et al.* [58], who used data collected in three separate flights, attributed an increased DTM elevation to the beam size and sensitivity of the laser.

Valbuena *et al.* [60] assessed the vertical accuracy of a dGNSS receiver (Topcon Hiperpro), similar to the receiver used in the present study, under pine canopies in Spain. By using true coordinates obtained in a total station traverse, they found the accuracy to be 1.18 m with a standard deviation of 1.55 m. It is therefore expected that our recordings under dense rainforest canopies with the reception of fewer satellite signals and more problems with multipath signals, result in lower accuracy. Thus, the

$\overline{D}$ of 1.8 m in the present study can be explained by the fact that, although the vertical precision of the dGNSS positions was reported to be 0.39 m (section 2.2), the accuracy remains unknown [60].

Recent studies of biomass in tropical forests using ALS have been conducted using different pulse densities and plot sizes. Pulse densities from 25 pulses·m^{-2} [35] down to about 1.5 pulses·m^{-2} [3] have been used. The results from these studies are similar in terms of biomass prediction performance and show that high pulse density is not a requisite for estimation of forest biomass. In biomass studies where the key information is the vegetation height relative to the terrain elevation derived from the same ALS data, a systematic shift in the modelled surface is not a problem in itself. Of greater concern is the random error of the modelled terrain elevation. As expected, the standard deviation of $\overline{D}$ (S_D) increased with reduced pulse density. S_D increased from 2.9 m to 3.2 m when pulse density was reduced from 8 and 0.25 pulses·m^{-2}, respectively. This variation will directly translate into variation in the ALS-derived canopy metrics.

Analysis of commonly applied canopy metrics showed that the metrics were affected differently by pulse density. As previously documented by Gobakken and Næsset [11], E.max, which characterizes the maximum elevation of the canopy, decreases with decreasing pulse density. Mean values of the other metrics assessed in the present study were found to be stable. Reduced pulse density increased the variation in canopy metrics and will result in models with increased residual variance. The estimated reliability of the metrics as predictors, expressed by the reliability ratio, showed that all metrics were reliable (reliability ratio >0.9) at pulse densities of down to 2 pulses·m^{-2}. Further reduction of pulse density resulted in some canopy metrics becoming less reliable although most metrics retain a reliability ratio of >0.9 at 0.5 pulses·m^{-2}. In low pulse density conditions (<1·m^{-2}), and with use of predictors with a reliability ratio <0.9 Magnussen *et al.* [19] proposed the use of a model calibration procedure.

Prediction of forest biomass over large areas using ALS often relies on data collected using different sensors and flying altitudes. Thus, different areas will consequently differ in pulse density. Varying pulse densities within a single ALS mission will also be inevitable as a result of flight line overlap, where the pulse density will be roughly double the density in the rest of the area. In addition, flights covering rugged terrain and steep slopes will result in varying pulse densities depending on the scan angle and distance to the ground. Estimates for parts of the forest area could therefore be over or under-predicted, due to different pulse densities than those in areas used for model development. To prevent such effects, suitable strategies could be to reduce the pulse density down to the smallest density in the project area, to remove points from overlapping flight lines, to weight ALS points by the surrounding number of points [61] or to include pulse density as a predictor in the model [4]. Another strategy could be to let pulse densities be reflected in the sampling design of the field survey, for example by using stratified sampling. That would require access to the ALS data in the design phase of the field survey.

Increasing the field plot size reduces the variation in ALS-derived metrics and could counter the effects in low pulse density missions, concurring with the results of Gobakken and Næsset [11]. However, larger field plots are costly and finding the optimal balance between costs and desired accuracy has for decades been an issue of interest in designing forest inventories. Zeide [62] presented how to optimize the plot size for systematic sampling. The optimal plot size is a function of the

coefficient of variation between plots, plot measurement time, and travelling time between plots, under budgetary restraints or for a desired accuracy.

The present study aimed to simulate the effects caused by various flight elevations and speeds on the DTM and canopy metrics derived from ALS data. Some effects, however, were not simulated and studied. Increased flight elevation will result in increased footprint size. Studies of the effects of footprint size on derived tree heights have shown that increased footprint size reduces the derived tree height estimates [63]. This effect was stronger for trees with a narrow crown and in a tropical forest the effect is likely to be small for the derived canopy metrics. Larger footprint sizes will however also have less energy per area unit and be less able to penetrate through the canopy [58, 64], resulting in a lower proportion of ground points. The influence of footprint size and pulse energy is likely to be of importance and should be investigated in future studies.

4. Conclusions

The present study showed that canopy metrics derived from low pulse density ALS data can be used for biomass estimation in a tropical rainforest. Reducing the pulse density from eight to 0.25 pulses·m^{-2} increased the variation in the DTMs and canopy metrics. However, the replication effects, expressed by the reliability ratio, were not important (reliability ratio >0.9) at pulse densities of >0.5 pulses·m^{-2}. Increased plot size increased the reliability ratio of canopy metrics, and could be used to counter effects of variation in canopy metrics obtained for low pulse densities.

Acknowledgments

The present study is part of the project “Enhancing the measuring, reporting and verification of forests in Tanzania through the application of advanced remote sensing techniques” funded by the Royal Norwegian Embassy in Tanzania as part of the Norwegian International Climate and Forest Initiative. We are grateful to Terratec AS, Norway, for conducting the ALS data acquisition.

Author Contributions

E.H.H. was the main author of the manuscript, planned the study with the co-authors, carried out and supervised the field work, and performed all data processing. T.G planned the acquisition of remotely sensed data, co-authored and revised the manuscript. E.N. designed parts of the study, co-authored and revised the manuscript.

Conflicts of Interest

The authors declare no conflict of interest.

References and Notes

1. Grace, J.; Mitchard, E.; Gloor, E., Perturbations in the carbon budget of the tropics. *Glob. Change Biol.* **2014,** *20* (10), 3238-3255.
2. UNFCCC, Report of the Conference of the Parties on its sixteenth session, held in Cancun from 29 November to 10 December 2010. Addendum. Part two: Action taken by the Conference of the Parties at its sixteenth session. United Nations Office, Geneva, Switzerland: 2011; p 31.
3. Asner, G. P.; Mascaro, J., Mapping tropical forest carbon: Calibrating plot estimates to a simple LiDAR metric. *Remote Sens. Environ.* **2014,** *140*, 614-624.
4. Jubanski, J.; Ballhorn, U.; Kronseder, K.; Franke, J.; Siegert, F., Detection of large above ground biomass variability in lowland forest ecosystems by airborne LiDAR. *Biogeosciences Discuss.* **2012,** *9* (8), 11815-11842.
5. Vincent, G.; Sabatier, D.; Blanc, L.; Chave, J.; Weissenbacher, E.; Pélissier, R.; Fonty, E.; Molino, J. F.; Couteron, P., Accuracy of small footprint airborne LiDAR in its predictions of tropical moist forest stand structure. *Remote Sens. Environ.* **2012,** *125*, 23-33.
6. Hou, Z.; Xu, Q.; Tokola, T., Use of ALS, Airborne CIR and ALOS AVNIR-2 data for estimating tropical forest attributes in Lao PDR. *ISPRS-J. Photogramm. Remote Sens.* **2011,** *66* (6), 776-786.
7. Andersen, H.-E.; Reutebuch, S. E.; McGaughey, R. J.; d'Oliveira, M. V. N.; Keller, M., Monitoring selective logging in western Amazonia with repeat lidar flights. *Remote Sens. Environ.* **2013,** *151*, 157-165.
8. Laurin, G. V.; Chen, Q.; Lindsell, J. A.; Coomes, D. A.; Frate, F. D.; Guerriero, L.; Pirotti, F.; Valentini, R., Above ground biomass estimation in an African tropical forest with lidar and hyperspectral data. *ISPRS-J. Photogramm. Remote Sens.* **2014,** *89*, 49-58.
9. Asner, G. P.; Powell, G. V. N.; Mascaro, J.; Knapp, D. E.; Clark, J. K.; Jacobson, J.; Kennedy-Bowdoin, T.; Balaji, A.; Paez-Acosta, G.; Victoria, E.; Secada, L.; Valqui, M.; Hughes, R. F., High-resolution forest carbon stocks and emissions in the Amazon. *Proc. Natl. Acad. Sci. U. S. A.* **2010,** *107* (38), 16738-16742.
10. Ioki, K.; Tsuyuki, S.; Hirata, Y.; Phua, M.-H.; Wong, W. V. C.; Ling, Z.-Y.; Saito, H.; Takao, G., Estimating above-ground biomass of tropical rainforest of different degradation levels in Northern Borneo using airborne LiDAR. *For. Ecol. Manage.* **2014,** *328*, 335-341.
11. Gobakken, T.; Næsset, E., Assessing effects of laser point density, ground sampling intensity, and field sample plot size on biophysical stand properties derived from airborne laser scanner data. *Can. J. For. Res.* **2008,** *38* (5), 1095-1109.
12. Holmgren, J., Prediction of tree height, basal area and stem volume in forest stands using airborne laser scanning. *Scand. J. Forest Res.* **2004,** *19* (6), 543-553.
13. Maltamo, M.; Eerikainen, K.; Packalen, P.; Hyyppa, J., Estimation of stem volume using laser scanning-based canopy height metrics. *Forestry* **2006,** *79* (2), 217-229.
14. Magnusson, M.; Fransson, J. E. S.; Holmgren, J., Effects on estimation accuracy of forest variables using different pulse density of laser data. *For. Sci.* **2007,** *53* (6), 619-626.

15. Watt, M.; Adams, T.; Gonzalez Aracil, S.; Marshall, H.; Watt, P., The influence of LiDAR pulse density and plot size on the accuracy of New Zealand plantation stand volume equations. *N. Z. J. For. Sci.* **2013,** *43* (1), 15.
16. Vauhkonen, J.; Tokola, T.; Maltamo, M.; Packalen, P., Effects of pulse density on predicting characteristics of individual trees of Scandinavian commercial species using alpha shape metrics based on airborne laser scanning data. *Can. J. Remote Sens.* **2008,** *34*, S441-S459.
17. Strunk, J.; Temesgen, H.; Andersen, H. E.; Flewelling, J. P.; Madsen, L., Effects of lidar pulse density and sample size on a model-assisted approach to estimate forest inventory variables. *Can. J. Remote Sens.* **2012,** *38* (5), 644-654.
18. Jakubowski, M. K.; Guo, Q.; Kelly, M., Tradeoffs between lidar pulse density and forest measurement accuracy. *Remote Sens. Environ.* **2013,** *130*, 245-253.
19. Magnussen, S.; Næsset, E.; Gobakken, T., Reliability of LiDAR derived predictors of forest inventory attributes: A case study with Norway spruce. *Remote Sens. Environ.* **2010,** *114* (4), 700-712.
20. Ruiz, L.; Hermosilla, T.; Mauro, F.; Godino, M., Analysis of the Influence of Plot Size and LiDAR Density on Forest Structure Attribute Estimates. *Forests* **2014,** *5* (5), 936-951.
21. Leitold, V.; Keller, M.; Morton, D. C.; Cook, B. D.; Shimabukuro, Y. E., Airborne lidar-based estimates of tropical forest structure in complex terrain: opportunities and trade-offs for REDD+. *Carbon Balance Manag* **2015,** *10* (1), 3.
22. Treitz, P.; Lim, K.; Woods, M.; Pitt, D.; Nesbitt, D.; Etheridge, D., LiDAR Sampling Density for Forest Resource Inventories in Ontario, Canada. *Remote Sensing* **2012,** *4* (4), 830-848.
23. Anon. National lidar dataset. http://en.wikipedia.org/wiki/National_lidar_dataset (accessed 25.02.2015).
24. Hodgson, M. E.; Jensen, J.; Raber, G.; Tullis, J.; Davis, B. A.; Thompson, G.; Schuckman, K., An evaluation of lidar-derived elevation and terrain slope in leaf-off conditions. *Photogramm. Eng. Remote Sens.* **2005,** *71* (7), 817-823.
25. Bater, C. W.; Coops, N. C., Evaluating error associated with lidar-derived DEM interpolation. *Comput. Geosci.* **2009,** *35* (2), 289-300.
26. Anon. *Testprosjekt laserskanning - Hvordan bestilt punkttetthet og skannetidspunkt påvirker antall bakketreff og nøyaktighet*; Norwegian Mapping Authority (In Norwegian): 2013; p 62.
27. Meng, X. L.; Currit, N.; Zhao, K. G., Ground Filtering Algorithms for Airborne LiDAR Data: A Review of Critical Issues. *Remote Sensing* **2010,** *2* (3), 833-860.
28. Tinkham, W. T.; Huang, H. Y.; Smith, A. M. S.; Shrestha, R.; Falkowski, M. J.; Hudak, A. T.; Link, T. E.; Glenn, N. F.; Marks, D. G., A Comparison of Two Open Source LiDAR Surface Classification Algorithms. *Remote Sensing* **2011,** *3* (3), 638-649.
29. Anon. *Testprosjekt - Klassifisering av laserdata*; Norwegian Mapping Authority (In Norwegian): 2012; p 18.

30. Liu, X.; Zhang, Z.; Peterson, J.; Chandra, S. The effects of LiDAR data density on DEM accuracy, In MODSIM 2007 International Congress on Modeling and Simulation, Christchurch, New Zealand, Christchurch, New Zealand, 2007.
31. Næsset, E., Predicting forest stand characteristics with airborne scanning laser using a practical two-stage procedure and field data. *Remote Sens. Environ.* **2002,** *80* (1), 88-99.
32. Næsset, E.; Bollandsås, O. M.; Gobakken, T., Comparing regression methods in estimation of biophysical properties of forest stands from two different inventories using laser scanner data. *Remote Sens. Environ.* **2005,** *94* (4), 541-553.
33. Li, Y. Z.; Andersen, H. E.; McGaughey, R., A Comparison of Statistical Methods for Estimating Forest Biomass from Light Detection and Ranging Data. *West. J. Appl. For.* **2008,** *23* (4), 223-231.
34. Fassnacht, F. E.; Hartig, F.; Latifi, H.; Berger, C.; Hernández, J.; Corvalán, P.; Koch, B., Importance of sample size, data type and prediction method for remote sensing-based estimations of aboveground forest biomass. *Remote Sens. Environ.* **2014,** *154*, 102-114.
35. d'Oliveira, M. V. N.; Reutebuch, S. E.; McGaughey, R. J.; Andersen, H. E., Estimating forest biomass and identifying low-intensity logging areas using airborne scanning lidar in Antimary State Forest, Acre State, Western Brazilian Amazon. *Remote Sens. Environ.* **2012,** *124*, 479-491.
36. Asner, G. P., Tropical forest carbon assessment: integrating satellite and airborne mapping approaches. *Environ. Res. Lett.* **2009,** *4* (3).
37. Mascaro, J.; Detto, M.; Asner, G. P.; Muller-Landau, H. C., Evaluating uncertainty in mapping forest carbon with airborne LiDAR. *Remote Sens. Environ.* **2011,** *115* (12), 3770-3774.
38. Asner, G. P.; Knapp, D. E.; Martin, R. E.; Tupayachi, R.; Anderson, C. B.; Mascaro, J.; Sinca, F.; Chadwick, K. D.; Higgins, M.; Farfan, W.; Llactayo, W.; Silman, M. R., Targeted carbon conservation at national scales with high-resolution monitoring. *Proc. Natl. Acad. Sci. U. S. A.* **2014,** *111* (47), E5016-E5022.
39. Lim, K.; Hopkinson, C.; Treitz, P., Examining the effects of sampling point densities on laser canopy height and density metrics. *For. Chron.* **2008,** *84* (6), 876-885.
40. Mauya, E.; Hansen, E. H.; Gobakken, T.; Bollandsås, O. M.; Malimbwi, R. E.; Næsset, E., Effects of field plot size on prediction accuracy of aboveground biomass in airborne laser scanning-assisted inventories in tropical rain forests of Tanzania. *Submitted to: Carbon Balance Manage.* **2015**.
41. Hernández-Stefanoni, J.; Dupuy, J.; Johnson, K.; Birdsey, R.; Tun-Dzul, F.; Peduzzi, A.; Caamal-Sosa, J.; Sánchez-Santos, G.; López-Merlín, D., Improving Species Diversity and Biomass Estimates of Tropical Dry Forests Using Airborne LiDAR. *Remote Sensing* **2014,** *6* (6), 4741-4763.
42. Zolkos, S. G.; Goetz, S. J.; Dubayah, R., A meta-analysis of terrestrial aboveground biomass estimation using lidar remote sensing. *Remote Sens. Environ.* **2013,** *128*, 289-298.

43. Tomppo, E.; Malimbwi, R.; Katila, M.; Mäkisara, K.; Henttonen, H. M.; Chamuya, N.; Zahabu, E.; Otieno, J., A sampling design for a large area forest inventory: case Tanzania. *Can. J. For. Res.* **2014,** *44* (8), 931-948.
44. Hamilton, A. C.; Bensted-Smith, R., *Forest conservation in the East Usambara Mountains, Tanzania*. IUCN-The World Conservation Union ; Dar es Salaam, Tanzania : Forest Division, Ministry of Lands, Natural Resources, and Tourism, United Republic of Tanzania: Gland, Switzerland and Cambridge, UK, 1989; p 392.
45. Kouba, J., A guide to using international GNSS service (IGS) products. IGS Central Bureau, Jet Propulsion Laboratory, Pasadena, CA, 2009; p 34.
46. Anon., Pinnacle user's manual. Javad Positioning Systems: San Jose, CA, 1999.
47. Hansen, E.; Gobakken, T.; Bollandsås, O.; Zahabu, E.; Næsset, E., Modeling Aboveground Biomass in Dense Tropical Submontane Rainforest Using Airborne Laser Scanner Data. *Remote Sensing* **2015,** *7* (1), 788-807.
48. McGaughey, R. J. *FUSION/LDV: Software for LIDAR Data Analysis and Visualization*, 3.30; 2013.
49. Kraus, K.; Pfeifer, N., Determination of terrain models in wooded areas with airborne laser scanner data. *ISPRS-J. Photogramm. Remote Sens.* **1998,** *53* (4), 193-203.
50. Holm, S., A simple sequentially rejective multiple test procedure. *Scand. J. Stat.* **1979,** *6* (2), 65-70.
51. Zandbergen, P. A., Positional Accuracy of Spatial Data: Non-Normal Distributions and a Critique of the National Standard for Spatial Data Accuracy. *Trans. GIS* **2008,** *12* (1), 103-130.
52. Höhle, J.; Höhle, M., Accuracy assessment of digital elevation models by means of robust statistical methods. *ISPRS-J. Photogramm. Remote Sens.* **2009,** *64* (4), 398-406.
53. Fuller, W. A., *Measurement error models*. John Wiley and Sons: New York, 1987; p 440.
54. Reutebuch, S. E.; McGaughey, R. J.; Andersen, H. E.; Carson, W. W., Accuracy of a high-resolution lidar terrain model under a conifer forest canopy. *Can. J. Remote Sens.* **2003,** *29* (5), 527-535.
55. Töyrä, J.; Pietroniro, A.; Hopkinson, C.; Kalbfleisch, W., Assessment of airborne scanning laser altimetry (lidar) in a deltaic wetland environment. *Can. J. Remote Sens.* **2003,** *29* (6), 718-728.
56. Bowen, Z. H.; Waltermire, R. G., Evaluation of light detection and ranging (LIDAR) for measuring river corridor topography. *J. Am. Water Resour. Assoc.* **2002,** *38* (1), 33-41.
57. Anderson, E. S.; Thompson, J. A.; Crouse, D. A.; Austin, R. E., Horizontal resolution and data density effects on remotely sensed LIDAR-based DEM. *Geoderma* **2006,** *132* (3–4), 406-415.
58. Hyyppä, J.; Yu, X.; Hyyppä, H.; Kaartinen, H.; Honkavara, E.; Rönnholm, P. In Factors affecting the quality of DTM generation in forested areas, Proceedings of ISPRS Workshop on Laser Scanning 2005, 12–14 September, Enschede, Netherlands, Enschede, Netherlands, 2005; pp 85-90.

59. Zhang, K.; Chen, S.-C.; Whitman, D.; Shyu, M.-L.; Yan, J.; Zhang, C., A progressive morphological filter for removing nonground measurements from airborne LIDAR data. *IEEE Trans. Geosci. Remote Sens.* **2003,** *41* (4), 872-882.
60. Valbuena, R.; Mauro, F.; Rodriguez-Solano, R.; Antonio Manzanera, J., Partial Least Squares for Discriminating Variance Components in Global Navigation Satellite Systems Accuracy Obtained Under Scots Pine Canopies. *For. Sci.* **2012,** *58* (2), 139-153.
61. Nyström, M.; Holmgren, J.; Olsson, H., Prediction of tree biomass in the forest-tundra ecotone using airborne laser scanning. *Remote Sens. Environ.* **2012,** *123*, 271-279.
62. Zeide, B., Plot size optimization. *For. Sci.* **1980,** *26* (2), 251-257.
63. Andersen, H.-E.; Reutebuch, S. E.; McGaughey, R. J., A rigorous assessment of tree height measurements obtained using airborne lidar and conventional field methods. *Can. J. Remote Sens.* **2006,** *32* (5), 355-366.
64. Goodwin, N. R.; Coops, N. C.; Culvenor, D. S., Assessment of forest structure with airborne LiDAR and the effects of platform altitude. *Remote Sens. Environ.* **2006,** *103* (2), 140-152.

PAPER III

Remote Sens. **2015**, *7*, 1-x manuscripts; doi:10.3390/rs70x000x

OPEN ACCESS

remote sensing

ISSN 2072-4292

www.mdpi.com/journal/remotesensing

Article

Impact of Field Plot Size on the Relative Efficiency of Biomass Estimation in a Tanzanian Rainforest using Airborne Laser Scanner and Interferometric Synthetic Aperture Radar as Auxiliary Data

Endre Hofstad Hansen [1,*], Terje Gobakken [1], Svein Solberg [2], Annika Kangas [3] Liviu Ene [1], Ernest Mauya [1] and Erik Næsset [1]

[1] Department of Ecology and Natural Resource Management, Norwegian University of Life Sciences, P.O. Box 5003, NO-1432 Ås, Norway; E-Mails: endre.hansen@nmbu.no (E.H.H.); terje.gobakken@nmbu.no (T.G.); liviu.ene@nmbu.no (L.E.); ernest.mauya@nmbu.no (E.M.); erik.naesset@nmbu.no (E.N.)

[2] Norwegian Forest and Landscape Institute, P.O. Box 115, 1431 Ås, Norway; E-Mail: sos@skogoglandskap.no (S.S.)

[3] Natural Resources Institute Finland (Luke), P.O. Box 68, FI-80101 Joensuu, Finland; E-Mail: annika.kangas@luke.fi (A.K.);

***** Author to whom correspondence should be addressed; E-Mail: endre.hansen@nmbu.no; Tel.: +47-6496-5756;

Academic Editor:

Received: / Accepted: / Published:

Abstract: Forest inventories based on field sample surveys, supported by auxiliary remotely sensed data, have the potential to provide transparent and confident estimates of forest carbon stocks required in climate change mitigation schemes such as the REDD+ mechanism. The field plot size is of importance for the precision of carbon stock estimates, and better information of the relationship between plot size and precision can be useful in designing future inventories. Precision estimates of forest biomass estimates developed from 30 concentric field plots with sizes of 700, 900,…, 1900 m2, sampled in a Tanzanian rainforest, were assessed in a model-based inference framework. Remotely sensed data from airborne laser scanning (ALS) and interferometric synthetic aperture radio detection and ranging (InSAR) were used as auxiliary information. The findings indicate that larger field plots are relatively more efficient for inventories supported by remotely sensed ALS

and InSAR data. A simulation showed that a pure field-based inventory would have to comprise 3.5–6.0 times as many observations for plot sizes of 700–1900 m2 to achieve the same precision as an inventory supported by ALS data.

Keywords: ALS; airborne laser scanning; LiDAR; relative efficiency; tropical rainforest

1. Introduction

Forest inventories provide information for management of forest resources on national, district, and local levels. Precise information about the quantity and quality of forest resources provides a solid basis for forest planning, management, and policies. Over the past decade the role of forests has shifted from a source of timber and non-timber products, to a source of a wide array of ecosystem services. One such service is the forests' role in global climate change mitigation, and the development of a marked-based mechanism to value this service has resulted in what is known as the REDD+ mechanism. REDD+ (reducing emissions from deforestation and forest degradation, conservation and enhancement of forest carbon stocks, and sustainable management of forests in developing countries), described in the 16th session of the Conference of Parties to the United Nations Framework Convention on Climate Change [1], gives developing countries the opportunity to monetize the service of sequestering carbon provided to the global climate. Future payments for performance-based benefits, such as enhanced forest carbon stocks, will require trustworthy systems for measuring, reporting, and verifying (MRV) the carbon stock changes in forests [2]. Forest inventories have the potential to provide transparent and confident estimates of forest carbon stocks needed in such systems.

Forest inventories are usually based on a field sample survey supported by one or several types of remotely sensed data. Information derived from remotely sensed data, in the form of aerial images, has been an important tool in forest inventory since the 1940s [3], and the availability of optical satellite images since the 1970s has resulted in global forest cover statistics [4]. While high costs have prevented the use of aerial images, the use of low-cost optical satellite images have been hampered by low spatial resolution and persistent cloud cover in tropical areas. Furthermore, both technologies have traditionally only provided two-dimensional information, although recent developments have resulted in three-dimensional data from aerial and satellite images with the use of digital photogrammetry and image matching [e.g. 5, 6-8]. Modelling of biomass using image matching requires a high quality digital terrain model (DTM) as reference surface, usually derived from airborne laser scanning (ALS). ALS is itself a remote sensing technology that provides three-dimensional data of the forest vegetation and has been used successfully for biomass estimation, even in tropical areas [9-10]. Another technology that provides three-dimensional data is synthetic aperture radio detection and ranging (SAR). Using a kind of stereo imaging known as interferometry, three-dimensional surface information about the vegetation can be produced from SAR image pairs. Both ALS and SAR sensors are active sensors, emitting pulses of electromagnetic radiation. Being airborne, ALS has the advantage of providing high resolution data and heights of both the terrain and the canopy surface.

Satellite-based SAR has, in comparison, lower spatial resolution, and it can only provide heights of the canopy surface. It has, however, a higher areal capacity and lower costs.

With the ability of providing vegetation height information, data from ALS and SAR sensors have been used as auxiliary information for biomass estimation in all major forest ecosystems [11]. Literature reviews have attempted to assess the impact of different sensors, statistical modelling methods, inventory sample sizes, and inventory plot sizes in different forest types [9, 11]. Results from these studies seem to be conclusive on two issues: 1) Use of ALS-sensors gives the best results compared to all other sensors for modelling biomass in terms of root mean square error (RMSE), and 2) that RMSE, as an expression of model precision, varies with forest type. A discussion on the impact of the size of inventory plots is included in both aforementioned studies but does not draw conclusions on the impact of plot size on model precision, or give practical advice on plot size. Larger plots will inevitably increase the estimated precision of biomass models in sample surveys due to the fact that variance between plots is reduced for larger plot sizes since more of the total variance is captured by the plots, an effect referred to as spatial averaging [9]. In sample surveys, supported by remotely sensed information, additional sources of error have been investigated. Firstly, a mismatch between the remotely sensed data and the field measurements introduce noise into the models [12]. This effect, often referred to as co-registration error, is reduced with increased plot size. Secondly, a discrepancy of measuring trees based on the location of the stem, and the remotely sensed data which are confined by the vertical extent of the field plot boundaries, is a source of model noise [13-14]. This latter source of errors is referred to as boundary effects. Both co-registration errors and boundary effects are reduced with reducing the ratio of field plot periphery to plot area. Accordingly, several studies on modelling of forest biomass using remotely sensed data have documented that increased plot size increased the model precision [13-16].

A common approach to estimation of forest parameters using ALS is known as the area-based approach and was first outlined in Næsset (1997a, 1997b). Following this approach, a relationship between biomass calculated from field measurements on inventory plots and remotely sensed data is modelled using statistical methods such as regression analysis, nearest neighbours, neural-networks or ensemble learning [e.g. 11, 19-20]. The models are subsequently used to predict biomass for population elements of the same size as the inventory plots. Biomass predictions are performed for all population elements covering the study area, given that remotely sensed data are available. The biomass predictions for the population elements are subsequently used to derive an estimate for the population, either as a mean or total biomass estimate. Accompanying the estimate, a variance estimate is calculated to state the precision of the estimate. Two main approaches to variance estimation have been used in forest inventories: design-based and model-based variance estimation. In the design-based approach the population, from which samples are taken, is regarded as fixed. The only source of sampling error is the random selection of elements included in the sample. Thus, the estimated sample error is derived from the inventory sample and the probability of each population element to be included in the sample, referred to as the inclusion probability. This inclusion probability is assumed to be positive and known for all population elements. Such samples are often referred to as probability samples.

It is often the case, however, that the sample has been acquired in a non-probabilistic manner [21], resulting in zero- or unknown inclusion probabilities. The zero- or unknown inclusion probability can

be the result of opportunistic sampling, i.e. sampling close to roads for economic and/or practical reasons. Similarly, purposive sampling, established to investigate a specific subject, often result in samples acquired in a non-probabilistic manner. Furthermore, the inclusion probability can be affected by the accessibility of the area [22, p. 76]. In the case where the sample data does not meet the requirements for a design-based approach to variance estimation, a model-based approach may be a viable alternative. Model-based inference does not, as opposed to design-based inference, rely on a probabilistic sample that represents the population. Instead the statistical inference relies on the model itself as a valid model of the distribution of possible observations for each population element. The population is not viewed as fixed, but rather as a result of a random process, referred to as a "superpopulation" model. This superpopulation model cannot be observed, but the parameters of the model can be estimated from the inventory sample. The inventoried population is viewed as only one random realisation of this superpopulation. An extensive review of design-based and model-based inference for forest survey is given by Gregoire [23].

To examine the effects of co-registration- and boundary-effects on the precision of ALS-supported biomass estimates, Mauya et al. [16] compared the variance of field-based biomass estimates to the corresponding variance of the biomass estimates supported by ALS at different plot sizes. This ratio of variance estimates is referred to as relative efficiency, and has been used to compare different sample designs, estimators, and inferential frameworks, e.g. Payandeh [24], Ene et al. [25]. The objective of calculating the relative efficiencies in Mauya et al. [16] was to assess the effect of plot size on the precision of ALS-derived biomass models. For this purpose the variance was estimated in a design-based framework. Mauya et al. [16] concluded that reduced model noise from co-registration errors and boundary effects meant that larger plot size was preferable for ALS-supported biomass estimates.

In order to plan for cost-effective inventories of forest biomass using sample surveys supported by remotely sensed data, there is a need for better information on how the field plot size impacts the precision of the subsequent biomass estimates [26]. On this basis, the objectives of the present study were to (1) assess the impact of plot size on the relative efficiency of biomass estimation in a Tanzanian rainforest using two different sources of remotely sensed data, and (2) quantify the number of additional field plots needed to compensate, in terms of sampling error, for a lack of remotely sensed data. We made use of a field data set consisting of 30 concentric circular plots of 700 m^2 up to 1900 m^2, and data from ALS and interferometric synthetic aperture radio detection and ranging (InSAR) sensors. Because the field inventory observations had unknown inclusion probabilities a model-based approach to estimation and inference was used.

2. Materials and Methods

2.1. Study Area

The present study was conducted in the Amani Nature Reserve (ANR) (S 5°08', E 38°37', 200–1200 m above sea level). The study area covers around 88 km2 of tropical submontane rainforest and is located in north-eastern Tanzania and is part of the East Usambara Mountains. The area receives around 2000 mm rainfall per year, and most of the rain falls in the two wet seasons, April–May and October–November. Daily mean temperatures vary from about 16 to 25 °C. Before the establishment

of the ANR in 1997, the area was comprised of six forest reserves and about half of the area was classified as logged or covered with non-native species [27]. After the logging was stopped in the late 1980s most of the logged area recovered and is now secondary forest. Due to inaccessibility the other half of the area had a limited human impact and is considered primary forest.

2.2. Field Data

In the present study we utilized field data from a sample survey consisting of 30 circular plots collected during November 2011 in pre-determined locations. The plot locations were chosen to capture the variation in biomass by distributing them in different altitudinal zones [16]. To evaluate the representativeness of the 30 circular plots Mauya *et al.* [16] compared the properties of the sample to a second sample of 153 systematically distributed plots covering the study area. Based on this evaluation Mauya *et al.* [16] concluded that, although being sampled in an opportunistic manner, the distribution in different altitudinal zones resulted in a sample which closely resembled properties of the systematic sample.

The centre coordinates of the plots were established by means of differential global positioning system (GPS) and global navigation satellite system (GLONASS) using survey-grade receivers. All trees with diameter at breast height (DBH) ≥5 cm were callipered, marked, and species identified. The horizontal distance from the plot centre to the front of each tree was measured using a Vertex IV hypsometer [28]. Because the distance was measured to the front of the trees, half of the tree DBH was added during data processing to get the total horizontal distance to the trees from the plot centre. The heights of three trees per plot (the largest, medium, and smallest tree in terms of DBH) were measured using the hypsometer.

Concentric circular plots of 700, 900, …, 1900 m^2 were constructed for each of the 30 field plots centred on the positions determined in field. The plot size of 700 m^2 was chosen because it correspond to the plot size used in the recently established national forest inventory of Tanzania [29]. The maximum plot size on each location was determined by the reach of the hypsometer, and under the most challenging conditions, distance measurement started to fail at 25 m. Thus, the maximum plot size used in the current study was 1900 m^2.

Based on the distance from the plot centre to the centre of the stem, each tree was allocated to their respective concentric plot. Biomass of each tree was computed using an allometric model [30] and a diameter to height model developed from the diameters and the corresponding tree heights, see Mauya *et al.* [16] for further details. The biomass of each tree was then summed at plot level and aggregated biomass was scaled to per-hectare values (Table 1). Although this biomass is referred to as “observed biomass”, the computed values are subject to errors related to the applied allometric model, and the subsampling and measurement of tree DBH and height.

2.3. ALS Data

Collection of ALS data with wall-to-wall coverage was carried out from 19 January to 18 February 2012 using a Leica ALS70 sensor mounted on a fixed wing aircraft. The acquisition parameters are summarized in Table 2. Post flight processing of the ALS data was performed by the contractor (Terratec AS, Norway) using TerraScan software [31]. A terrain model was created by classifying

ALS echoes as ground echoes using a progressive triangulated irregular network (TIN) densification algorithm [32]. The TIN model was used to calculate the elevation above the ground for all echoes. From the TIN model a raster-based digital terrain model (DTM) with a 10 m × 10 m cell size was created for the entire study area.

2.4. InSAR Data

InSAR data were acquired by the Tandem-X satellite mission on 6th August 2011. The incidence angle was 46°, and the polarization was horizontal transmit and horizontal receive. The normal baseline was 210 m, which corresponded to a 2π height of ambiguity of 38 m.

2.5. ALS-derived Explanatory Variables

ALS echoes were extracted for the concentric circular plots of 700, 900, …, 1900 m^2 for each of the 30 locations. From a maximum of five echoes registered per ALS pulse, echoes were categorised as "single", "first of many", and "last of many". "Single" and "first of many" were merged into one dataset and denoted as "first" while "single" and "last of many" were merged into another dataset and denoted as "last". From the ALS echoes in each of the two categories ("first", "last"), variables describing the height and density of the vegetation were derived. The variables were used to construct linear least-square models (section 2.9) for each of the concentric plot sizes. In order to get comparable results between models from different plot sizes we chose to use the same ALS variables in all models. Studies have shown that a model consisting of one canopy height variable and one canopy density variable is often sufficient for modelling forest biomass [33-34]. In a previous study using the same field and ALS data, Mauya *et al.* [16] found that the 60th percentile height from the "first" echo category (H60.F) and the proportion of echoes above a second of ten equally large vertical layers to the total number of echoes from the "last" echo category (D1.L) were the most frequently selected variables in modelling biomass using plot sizes from 700 to 1900 m^2. We therefore a priori selected H60.F and D1.L for construction of biomass models.

2.6. InSAR-derived Explanatory Variable

The Sarscape module of the ENVI 5.0 software was used to process Tandem-X image pairs resulting in a digital surface model (DSM). An interferogram was generated from each image pair, and this was further processed into a differential interferogram by using the ALS DTM as input. Phase noise was removed from the interferogram with a Goldstein filter. Phase offset and phase ramp errors were also removed using 30 ground control points, placed in non-vegetated locations, spread over the study area. Phase unwrapping was carried out using the minimum cost flow method, and the DSM was geocoded to a ground resolution of 10 m × 10 m. Following the construction of the DSM, the DTM derived from the ALS TIN was subtracted from the DSM, resulting in obtained InSAR heights, i.e. heights of the centre of the radar echo above ground. Mean InSAR height was then derived for each field plot by weighting the height of each 10 m × 10 m cell of the normalised InSAR DSM by the area of the cells intersecting the area of the field plot. This mean InSAR height was derived for each concentric field plot area.

2.7. DTM-derived Explanatory Variable

The DTM derived from the ALS TIN was used to calculate the mean terrain elevation (TE) for each concentric plot size, 700, 900, …, 1900 m^2, by weighting the value of each 10 m × 10 m cell of the DTM by the cell area intersected by the plot. The mean TE was subsequently used as an auxiliary variable (See section 2.8).

2.8. Tessellating the Study Area and the Remotely Sensed Data

The study area was tessellated into regular grids with hexagonal tiles of 700, 900, …, 1900 m^2 corresponding to the different plot sizes. To avoid splitting the tiles along the boundary of the study area only tiles with the centroid falling inside of the study area were retained. Remotely sensed variables from ALS and InSAR, along with the TE information were calculated for all hexagonal tiles in the study area.

2.9. Model Construction

For each plot size, separate linear least-square models were constructed with the biomass estimated on the ground plots as response variable and the corresponding remotely sensed variables, from either ALS or InSAR, as explanatory variables. In a study of forest biomass in two mountain locations in Tanzania, including ANR, Marshall *et al.* [35] found TE to be positively related to biomass. Therefore, to compare variance estimates obtained using ALS and InSAR, a model with TE as explanatory variable was also constructed for each plot size. This resulted in a model for each of the three sources of auxiliary data: 1) ALS, 2) InSAR, and 3) TE for each plot size. To improve the linear relationship between the explanatory variables and the response, a natural-log transformation of both response and explanatory variable was performed for all models. Such log-log models have been found to be suitable for estimating forest properties using remotely sensed data [33, 36-38]. This transformation will introduce a bias by back-transformed to arithmetic scale, and a ratio of the mean observed biomass to the mean of the back-transformed estimated biomass proposed by Snowdon [39] was therefore used as a correction factor for the model predictions.

Unlike design-based estimators, which often are unbiased or nearly unbiased, the unbiasedness of model-based estimators depends on the model being correctly specified. It was therefore paramount to assess how well the model fitted the field plot observations. Assessment of the fit of the models followed the approach used by McRoberts *et al.* [40]. Scatterplots of observed vs. predicted biomass were produced for each plot size. Correctly specified models should result in points falling closely along a 1:1 line with intercept 0 and slope 1. Further, pairs of observations and predictions were ordered with respect to the predicted values and grouped into three classes of 10 pairs. The mean of the observed versus predicted biomass was plotted for each group. A correctly specified model should again result in points falling along a 1:1 line.

2.10. Model-based Inference

Model-based inference does not, as opposed to design-based inference, rely on a probabilistic sample that represents the population. Instead, as stated above, the inference relies on the model itself

as a valid model of a superpopulation. Following the notation in Ståhl *et al.* [41] an element of the superpopulation was expressed as

$$y_i = g(x_i, \alpha, \varepsilon_i), \quad (1)$$

where y is a vector of the observed plot biomass on plot i, x is a vector of variables derived from the auxiliary data, α is a vector of model parameters and ε is a vector of errors, and g is a function describing the superpopulation. It is assumed that the errors are independent, normally distributed, with a constant variance, and without spatial auto-correlation. The parameters α were estimated with $\hat{\alpha}$ using least square regression, and used to estimate the population mean by

$$\hat{\mu} = \frac{1}{N}\sum_{i=1}^{N} g(x_i, \hat{\alpha}), \quad (2)$$

where i indexes the population elements and N is the number of elements, i.e., i=1, 2, …, N. Assuming that the estimated $\hat{\alpha}$ is accurate, the g function was linearized in the neighbourhood of the true function using first order Taylor series expansion:

$$g(x, \hat{\alpha}) \approx g(x, \alpha) + (\hat{\alpha}_1 - \alpha_1) * g'_1(x, \alpha) + (\hat{\alpha}_2 - \alpha_2) * g'_2(x, \alpha) + \ldots + (\hat{\alpha}_p - \alpha_p) * g'_p(x, \alpha), \quad (3)$$

where $g'_j(x, \alpha) = \partial g(x, \alpha)/\partial \alpha_j$, j indexes the parameters and p is the number of parameters, i.e., j=1, 2, …, k, …, p. The variance of the population mean was then estimated by

$$\widehat{var}(\hat{\mu}) = \sum_{j=1}^{p}\sum_{k=1}^{p} \widehat{Cov}(\hat{\alpha}_j, \hat{\alpha}_k)\hat{\bar{g}}'_j\hat{\bar{g}}'_k, \quad (4)$$

where $\hat{\bar{g}}'_j$ and $\hat{\bar{g}}'_k$ are the estimated mean values of the first order derivatives of the g function for parameters j and k, respectively [cf. 41].

Standard errors (SE) of the mean estimates, i.e., the square root of the variance estimate, were reported along with SE relative to the mean estimates.

2.11. Relative Efficiency

To assess the gain in precision of using remotely sensed data to enhance the estimates, relative efficiency was calculated for both ALS ($RE_{TE:ALS}$) and InSAR ($RE_{TE:InSAR}$). The relative efficiencies were calculated as ratios of the estimated variance for the mean biomass estimate ($\hat{\mu}$) for each plot size using the TE models divided by the variance estimates for each plot size using the ALS models:

$$RE_{TE:ALS_s} = \widehat{var}(\hat{\mu}_{TE})_s / \widehat{var}(\hat{\mu}_{ALS})_s, \quad (5)$$

where s is an indicator of the plot sizes 700, 900, …, 1900 m^2. Similarly, relative efficiency for InSAR was computed as:

$$RE_{TE:InSAR_s} = \widehat{var}(\hat{\mu}_{TE})_s / \widehat{var}(\hat{\mu}_{InSAR})_s. \quad (6)$$

Efficiency of ALS was also calculated relative to InSAR ($RE_{InSAR:ALS}$) in the same way by dividing the variance estimates for each plot size using the InSAR models by the variance estimates for each plot size using the ALS models:

$$RE_{InSAR:ALS_s} = \widehat{var}(\hat{\mu}_{InSAR})_s / \widehat{var}(\hat{\mu}_{ALS})_s. \quad (7)$$

Together with information about inventory costs and the costs of the auxiliary data, the relative efficiency can be used to compare costs of attaining a certain level of precision of the estimation. In a design-based framework, applying simple random sampling (SRS), the relative efficiency can be used directly to calculate the additional number of field observations needed to compensate for the contribution of the remotely sensed data, which is a fundamental quantity in cost comparisons. This is because the SE of the mean estimate under SRS is proportional to the square root of the sample size minus the number of explanatory variables minus one [42, p. 181]. In practice, a relative efficiency of two would mean that the gain of the remotely sensed data could be compensated by twice as many field plots, assuming that the sample variance remain constant. In the model-based framework we also assume that the SE of the mean estimate is reduced with increased number of observations. However, we are not able to derive the number of observations needed to reach the same SE for the different models by analytical means. Instead we applied a basic Pólya-urn resampling scheme described in Köhl *et al.* [22, pp. 195–196] to simulate the variance of the TE models. The Pólya-urn resampling scheme generates a design-consistent posterior predictive distribution of the property in interest, given that the sample is reasonably large and representative of the population [43, p. 44–46]. We consider our field sample of u=30 observations as representative of the population, and the Pólya-urn resampling generated posterior predictive distributions of biomass for U=60, 120, and 180 observations based on the sample. From a virtual urn, containing the 30 observations, one observation was randomly drawn, duplicated, and returned to the urn together with the duplicate. The urn thus contained u+1=31 observations. The selection scheme was repeated until the desired number U of observations in the urn was reached. The simulations were repeated 200 times and the mean variance of observed biomass reported.

2. Results and Discussion

Use of remotely sensed data to support field-based sample surveys will be part of any REDD+ MRV system. Better information on how the relative efficiency of using remotely sensed data is affected by plot size would benefit future MRV designs. The findings in the present study demonstrate the impact of the size of the field plots on the precision of biomass estimates using two types of three dimensional remotely sensed data.

Separate log-log models were constructed for each plot size of 700, 900, …, 1900 m^2 using auxiliary data from 1) ALS, 2) InSAR, and 3) TE. TE models showed a positive correlation between biomass and elevation, and the explanatory variable was increasingly significant from $p = 0.044$ at 700 m^2 to $p = 0.002$ at 1900 m^2. Biomass was also positively correlated to the two explanatory variables in the ALS models and the variable in the InSAR models. All variables were significant at a 95% level except one of the ALS variables (D1.L) at plot sizes of 1100-1700 m^2.

Inspection of the scatterplots of observed versus predicted biomass (Figures 1–3) showed that the models had a lack of fit resulting in over-prediction of biomass in areas of low biomass and under-prediction in areas of high biomass. Similar lack of fit has been reported in studies from areas with high forest density [e.g. 44, 45]. The plots of the grouped means of observations versus predictions (Figures 4–6), however, showed small differences.

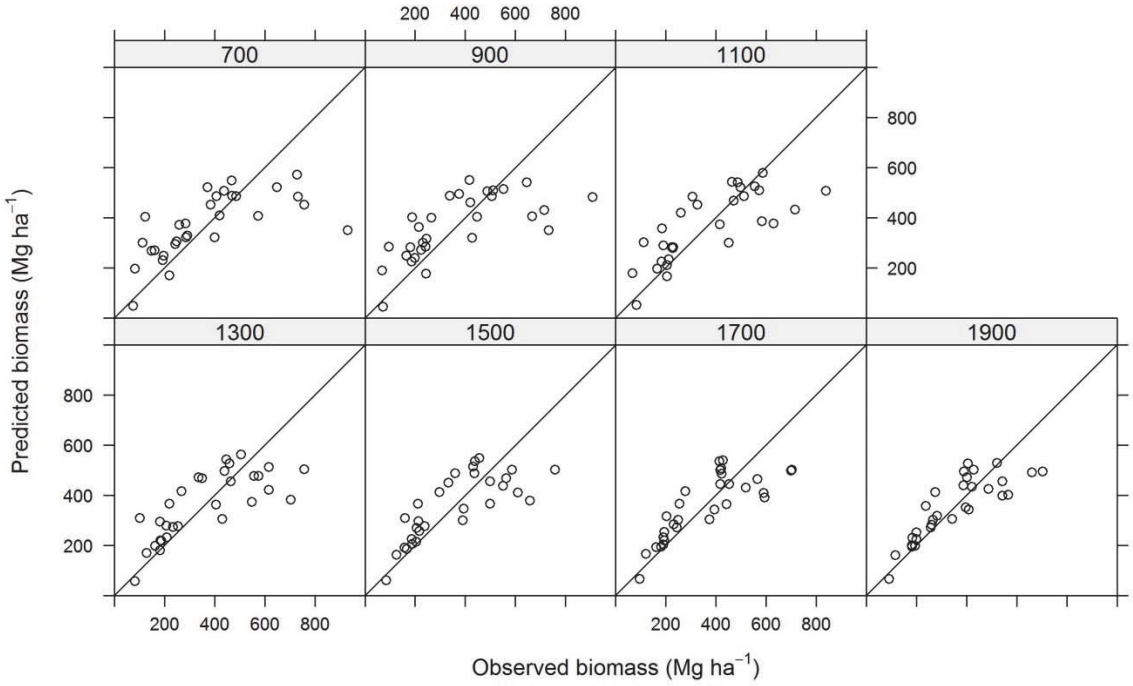

Figure 1. Observed versus predicted biomass values using ALS for plot sizes of 700, 900,…, 1900 m^2.

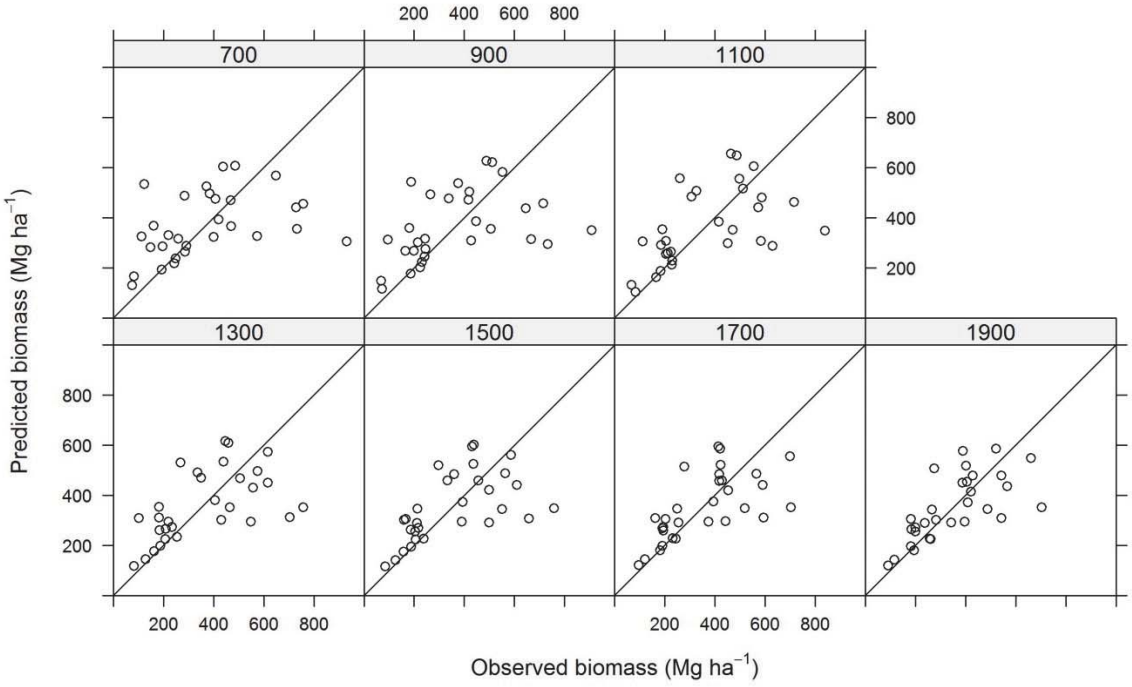

Figure 2. Observed versus predicted biomass values using InSAR for plot sizes of 700, 900,…, 1900 m^2.

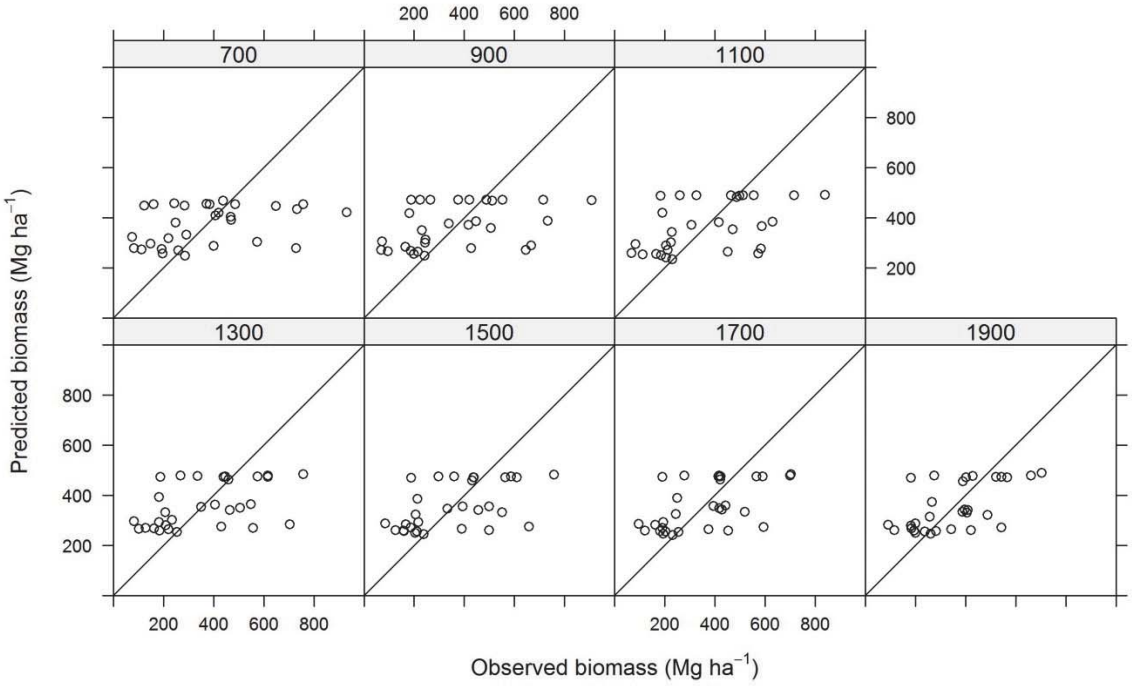

Figure 3. Observed versus predicted biomass values using TE for plot sizes of 700, 900,…, 1900 m^2.

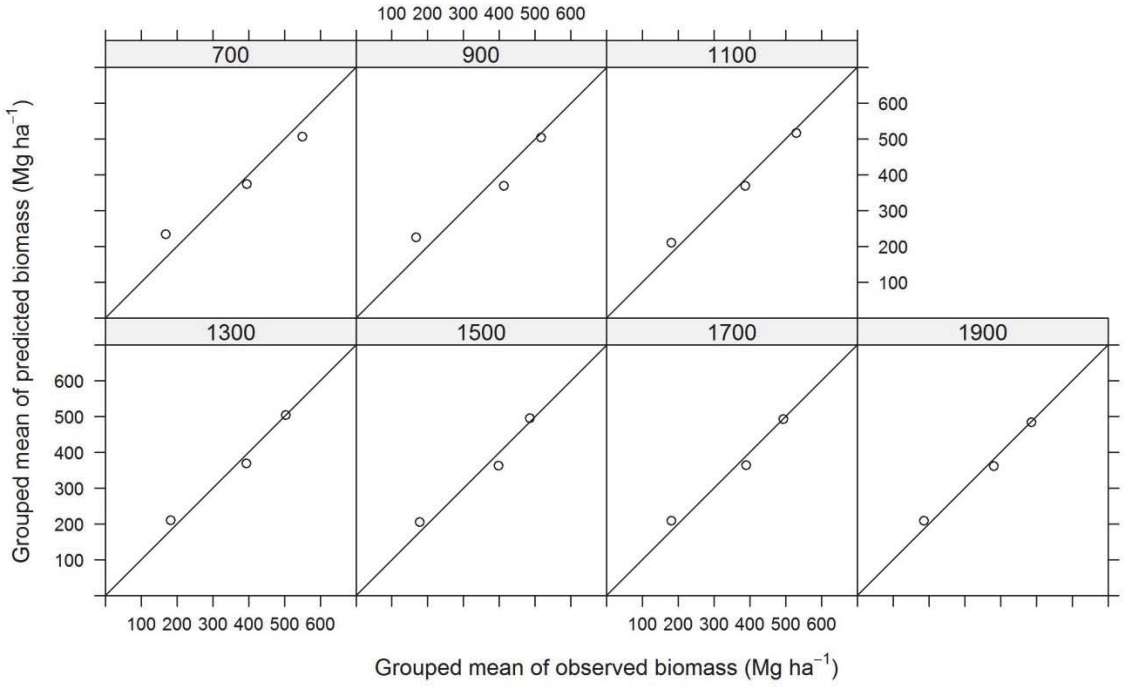

Figure 4. Grouped means of observed versus predicted biomass values using ALS for plot sizes of 700, 900,…, 1900 m^2.

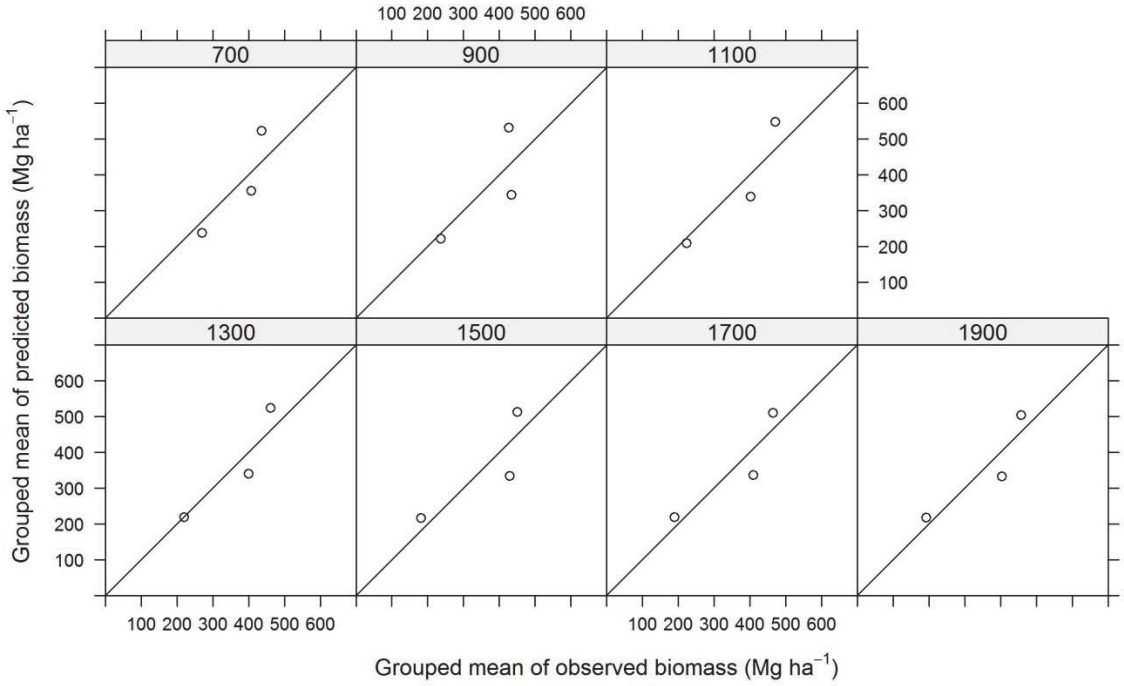

Figure 5. Grouped means of observed versus predicted biomass values using InSAR for plot sizes of 700, 900,…, 1900 m^2.

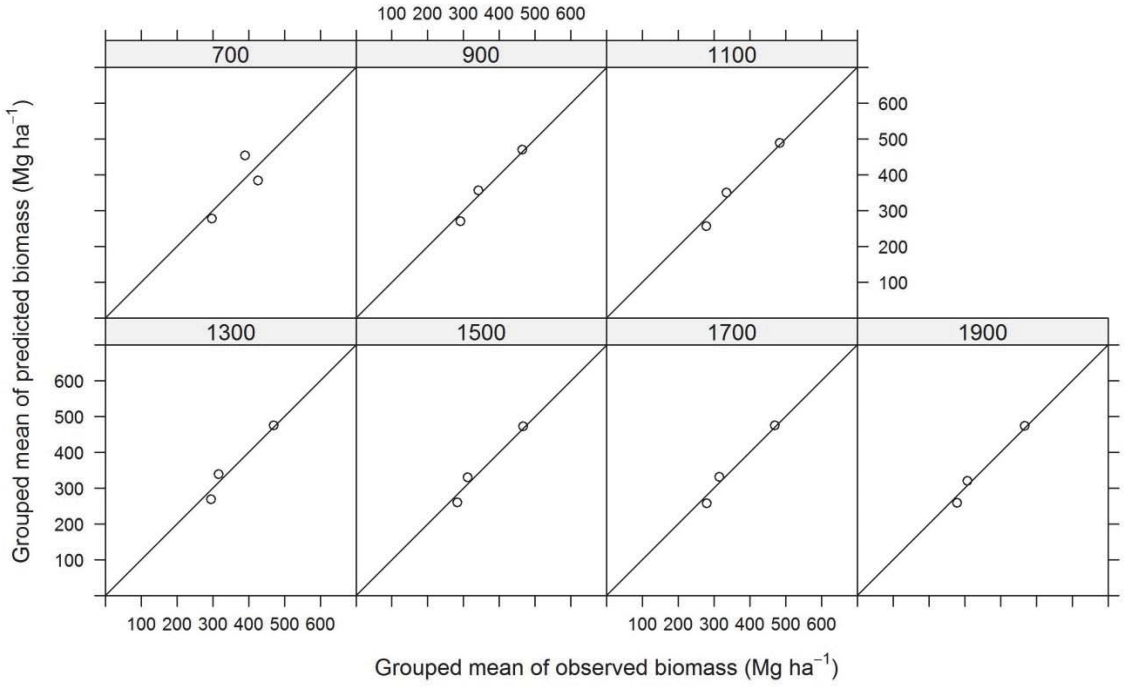

Figure 6. Grouped means of observed versus predicted biomass values using TE for plot sizes of 700, 900,…, 1900 m^2.

As pointed out in section 2.2, the observed biomass is subject to uncertainty not accounted for in the present study, related to the allometric models and field measurements of DBH and tree height. Thus, errors related to the biomass observations are not accounted for. Overlooking these errors lead to overoptimistic precision of the variance estimates. In a study conducted in a tropical forest in Ghana, in which the forest conditions and the plot size of 1600 m^2 resembled the conditions in the present study, Chen *et al.* [46] found that the impact of allometric error contributed about 11% to the total relative prediction error.

Mean biomass estimates of the ANR from both ALS and InSAR were lower than the mean estimate from the model with TE (Table 3). The differences were however not statistically significant at the 5% level.

Increasing the plot size from 700 to 1900 m^2 reduced the SE of the mean estimates from 15.3 to 10.6% using TE, from 10.1 to 5.1% using ALS, and from 11.3 to 6.4% using InSAR (Figure 7). Both ALS and InSAR performed well compared to TE in terms of SE. ALS and InSAR estimates had an SE of about 5 and 4 percentage points lower than TE, respectively. Further, InSAR performed well compared to the ALS with only 0.4–1.3 percentage points higher SE depending on plot size. The differences in SE translated into relative efficiencies of 3.6–6.7 using ALS and 2.6–4.0 using InSAR, compared to TE (Figure 8). The relative efficiency of the ALS data also increased with increased plot size relative also to the InSAR data (Figure 8). At a plot size of 1900 m^2 the ALS was 6.7 times as efficient as using TE and 1.7 times as efficient as InSAR. The fact that the relative efficiency of ALS and InSAR increased with increased plot size may partly be due to reduced relative influence of boundary effects and co-registration errors. The slight increase in relative efficiency of ALS compared to InSAR may also indicate that the relative influence of boundary effects and co-registration errors is stronger for ALS than for InSAR. The relative efficiency of ALS compared to InSAR is modest compared to studies in Norway that have found the relative efficiency of ALS to be about twice to that of InSAR [34, 47].

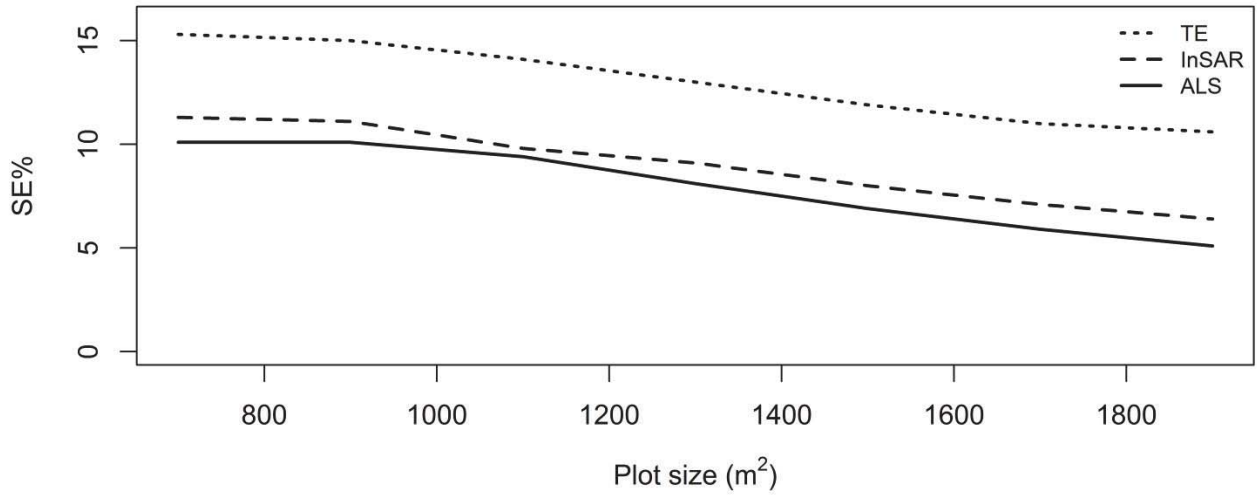

Figure 7. Relative standard error of biomass estimates (SE%) using models with auxiliary data of terrain elevation (TE) derived from a digital terrain model (dotted line), InSAR (dashed line), and ALS (solid line).

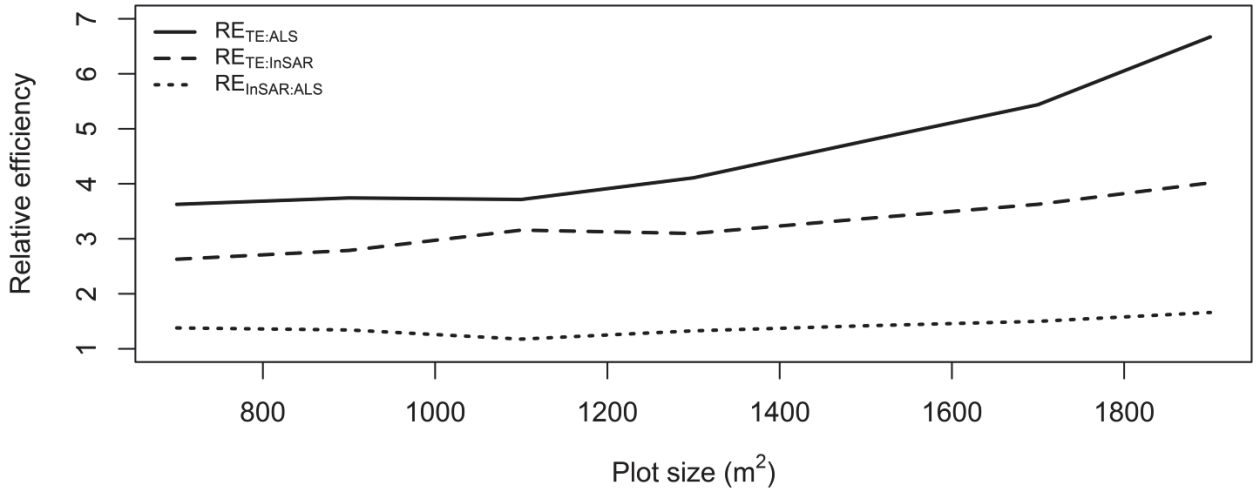

Figure 8. Relative efficiency of using InSAR ($RE_{TE:InSAR}$, dashed line) and ALS ($RE_{TE:ALS}$, solid line) relative to TE for biomass estimation, and ALS relative to InSAR ($RE_{InSAR:ALS}$, dotted line).

As stated by Gregoire *et al.* [48], information about the approach to statistical inference, design- or model-based, is essential in assessing the estimated variance. Taking the design-based approach to variance estimation d'Oliveira *et al.* [49], reported a relative efficiency of 3.4 in a study utilising 50 plots of ~0.25 ha in the Brazilian Amazon. We can similarly compute the relative efficiency from the variance estimates reported by Hansen *et al.* [10]. For a plot size of ~0.1 ha the relative efficiency was 2.1. The latter study discusses large negative boundary-effects in the ALS-derived variables, which would contribute to a low relative efficiency.

The DTM used directly to derive the TE variable in the TE-models, and to derive the InSAR elevation above the terrain, was derived from the ALS data. DTMs constructed from ALS data have generally high accuracy [50]. In the absence of an ALS-derived DTM, a DTM derived from other sources would have influenced the results. A DTM derived from sources like P-band SAR [e.g. 51] or the topographic map series of Tanzania, would most likely have resulted in substantially increased SE of the InSAR and TE estimates. In a study using InSAR height to estimate forest biomass in Norway Næsset *et al.* [34] it was found that relative RMSE was approximately seven percentage points higher using a DTM from topographic maps with a contour interval of 20 m, compared to using an ALS-derived DTM. P-band SAR, used with good results in Neeff *et al.* [51], is currently only available from airborne platforms, and was not collected in ANR.

The analysis in the present study showed that use of remotely sensed data from ALS and InSAR was able to increase the precision of the estimates. However, ALS data are expensive compared to the cost of establishing additional inventory plots (100–150 USD per plot, E. Mauya 2015, pers. comm. 19 Jan.). The effect of increased number of field plots on the sampling error of the TE models was simulated using a Pólya-urn resampling scheme. To reach similar levels of sampling error as for the ALS models, the number of field plots would have to be increased by a factor of 3.5–6 depending on plot size (Figure 9).

With the relatively low cost of increasing the intensity of the field inventory (180 plots × a cost of 125 USD = 22 500 USD), the increased precision of using ALS is not solely enough to defend the investment of about 100 000 USD for the ALS mission. However, ALS does provide a good quality DTM which can be used for future surveys supported by other sources of remotely sensed data requiring such a DTM. The cost of ALS is largely governed by the flight time. By flying higher, covering a larger area with a single flight strip, the cost of acquiring ALS can be reduced. Findings from studies of reduced pulse density either by means of simulations [e.g. 52], or acquisitions from different altitudes [e.g. 53], have shown that satisfactory results can be attained at lower pulse densities. A simulation study conducted in ANR [54], confirmed that explanatory variables derived from low pulse density is reliable down to about 0.5 pulses m^{-2}, even in dense tropical forests.

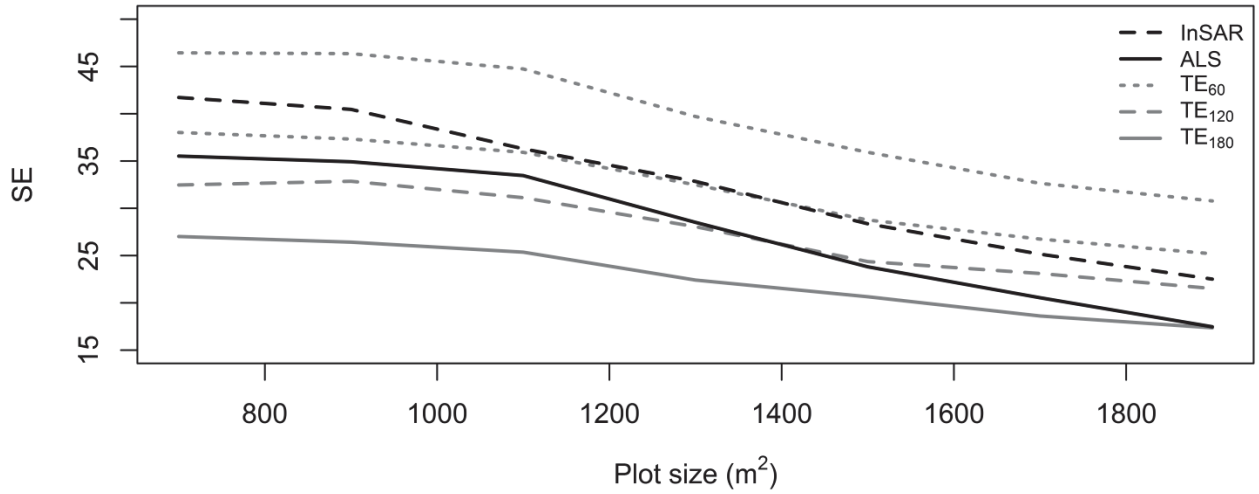

Figure 9. Standard error of biomass estimates (SE) using models with auxiliary data of InSAR (dashed line), ALS (solid line), and TE. TE model SE is derived from 60 (dotted grey line), 120 (dashed grey line), and 180 (solid grey line) simulated observations.

Table 1. Mean biomass and standard deviation (SD) of the 30 field plots with plot sizes of 700, 900,…, 1900 m^2.

Plot size (m^2)	Mean biomass (Mg ha^{-1})	SD (Mg ha^{-1})
700	371.8	221.5
900	366.1	216.3
1100	365.6	203.0
1300	361.0	190.5
1500	354.2	180.4
1700	355.0	170.2
1900	351.1	159.6

Table 2. ALS acquisition parameters.

Flight speed (m s^{-1})	70
Flying altitude (m a.g.l.)	800
Scanner frequency (kHz)	339
Footprint size (cm)	22
Beam divergence (mrad)	0.28
Half scan angle (deg.)	16

Table 3. Estimated mean biomass ($\hat{\mu}$) in Mg ha^{-1} and standard error of the estimate (SE) in Mg ha^{-1} and in % of the mean estimate for three different sources of auxiliary data (terrain elevation (TE), ALS, and InSAR).

		TE			ALS			InSAR		
Plot size	N	$\hat{\mu}$ (Mg ha^{-1})	SE (Mg ha^{-1})	SE (%)	$\hat{\mu}$ (Mg ha^{-1})	SE (Mg ha^{-1})	SE (%)	$\hat{\mu}$ (Mg ha^{-1})	SE (Mg ha^{-1})	SE (%)
700	126772	442.2	67.6	15.3	352.9	35.5	10.1	368.0	41.7	11.3
900	98635	449.1	67.6	15.0	346.1	34.9	10.1	365.7	40.5	11.1
1100	80667	458.6	64.5	14.1	356.3	33.5	9.4	369.1	36.3	9.8
1300	68279	443.6	57.8	13.0	350.5	28.5	8.1	361.0	32.8	9.1
1500	59154	435.7	52.1	11.9	345.5	23.8	6.9	354.2	28.4	8.0
1700	52214	435.0	47.9	11.0	346.4	20.5	5.9	354.2	25.2	7.1
1900	46727	427.2	45.1	10.6	341.4	17.5	5.1	350.3	22.5	6.4

4. Conclusions

The results from the present study showed that the relative efficiency of using remotely sensed data from both ALS and InSAR sensors increased with increased field plot size. Thus, biomass estimation assisted by remotely sensed data from ALS and InSAR will profit relatively more in terms of increased precision by increasing plot size than estimation without ALS and InSAR data. To compensate for a lack of ALS data a pure field-based inventory would have to contain 3.5–6.0 times as many observations for plot sizes of 700–1900 m^2 to achieve the same precision as an inventory supported by ALS data.

Acknowledgments

This work has been funded by the Royal Norwegian Embassy in Tanzania as part of the Norwegian International Climate and Forest Initiative. We wish to thank Terratec AS, Norway, for acquiring and processing the ALS data and Deutsches Zentrum für Luft und Raumfahrt for providing the InSAR data.

Author Contributions

E.H.H. was the main author of the manuscript, planned the study with the co-authors, and performed data processing. T.G, S.S., and E.N. planned the acquisition of remotely sensed data. A.K. and L.E. contributed in statistical analysis. E.M. collected the field data. All co-authors contributed in writing and critically revising the manuscript.

Conflicts of Interest

The authors declare no conflict of interest.

References

1. UNFCCC, Report of the Conference of the Parties on its sixteenth session, held in Cancun from 29 November to 10 December 2010. Addendum. Part two: Action taken by the Conference of the Parties at its sixteenth session. United Nations Office, Geneva, Switzerland: 2011; p 31.
2. UNFCCC, Report of the Conference of the Parties on its fifteenth session, held in Copenhagen from 7 to 19 December 2009. Addendum. Part Two: Action taken by the Conference of the Parties at its fifteenth session. United Nations Office, Geneva, Switzerland: 2010; p 43.
3. FAO, Forest resources of the world. In *Unasylva* [Online] Fortunescu, R. C., Ed. 1948. http://www.fao.org/docrep/x5345e/x5345e00.htm (accessed 16.01.2015).
4. Boyd, D. S.; Danson, F. M., Satellite remote sensing of forest resources: three decades of research development. *Progress in Physical Geography* **2005,** *29* (1), 1-26.
5. Bohlin, J.; Wallerman, J.; Fransson, J. E. S., Forest variable estimation using photogrammetric matching of digital aerial images in combination with a high-resolution DEM. *Scand. J. Forest Res.* **2012,** *27* (7), 692-699.

6. Persson, H.; Wallerman, J.; Olsson, H.; Fransson, J. E. S., Estimating forest biomass and height using optical stereo satellite data and a DTM from laser scanning data. *Can. J. Remote Sens.* **2013,** *39* (3), 251-262.
7. Gobakken, T.; Bollandsås, O. M.; Næsset, E., Comparing biophysical forest characteristics estimated from photogrammetric matching of aerial images and airborne laser scanning data. *Scand. J. Forest Res.* **2014**, 1-14.
8. Næsset, E., Determination of Mean Tree Height of Forest Stands by Digital Photogrammetry. *Scand. J. Forest Res.* **2002,** *17* (5), 446-459.
9. Zolkos, S. G.; Goetz, S. J.; Dubayah, R., A meta-analysis of terrestrial aboveground biomass estimation using lidar remote sensing. *Remote Sens. Environ.* **2013,** *128*, 289-298.
10. Hansen, E.; Gobakken, T.; Bollandsås, O.; Zahabu, E.; Næsset, E., Modeling Aboveground Biomass in Dense Tropical Submontane Rainforest Using Airborne Laser Scanner Data. *Remote Sensing* **2015,** *7* (1), 788-807.
11. Fassnacht, F. E.; Hartig, F.; Latifi, H.; Berger, C.; Hernández, J.; Corvalán, P.; Koch, B., Importance of sample size, data type and prediction method for remote sensing-based estimations of aboveground forest biomass. *Remote Sens. Environ.* **2014,** *154*, 102-114.
12. Gobakken, T.; Næsset, E., Assessing effects of positioning errors and sample plot size on biophysical stand properties derived from airborne laser scanner data. *Can. J. For. Res.* **2009,** *39* (5), 1036-1052.
13. Mascaro, J.; Detto, M.; Asner, G. P.; Muller-Landau, H. C., Evaluating uncertainty in mapping forest carbon with airborne LiDAR. *Remote Sens. Environ.* **2011,** *115* (12), 3770-3774.
14. Frazer, G. W.; Magnussen, S.; Wulder, M. A.; Niemann, K. O., Simulated impact of sample plot size and co-registration error on the accuracy and uncertainty of LiDAR-derived estimates of forest stand biomass. *Remote Sens. Environ.* **2011,** *115* (2), 636-649.
15. Hernández-Stefanoni, J.; Dupuy, J.; Johnson, K.; Birdsey, R.; Tun-Dzul, F.; Peduzzi, A.; Caamal-Sosa, J.; Sánchez-Santos, G.; López-Merlín, D., Improving Species Diversity and Biomass Estimates of Tropical Dry Forests Using Airborne LiDAR. *Remote Sensing* **2014,** *6* (6), 4741-4763.
16. Mauya, E.; Hansen, E. H.; Gobakken, T.; Bollandsås, O. M.; Malimbwi, R. E.; Næsset, E., Effects of field plot size on prediction accuracy of aboveground biomass in airborne laser scanning-assisted inventories in tropical rain forests of Tanzania. *Submitted to: Carbon Balance Manage.* **2015**.
17. Næsset, E., Determination of mean tree height of forest stands using airborne laser scanner data. *ISPRS-J. Photogramm. Remote Sens.* **1997,** *52* (2), 49-56.
18. Næsset, E., Estimating timber volume of forest stands using airborne laser scanner data. *Remote Sens. Environ.* **1997,** *61* (2), 246-253.
19. Næsset, E.; Bollandsås, O. M.; Gobakken, T., Comparing regression methods in estimation of biophysical properties of forest stands from two different inventories using laser scanner data. *Remote Sens. Environ.* **2005,** *94* (4), 541-553.

20. Li, Y. Z.; Andersen, H. E.; McGaughey, R., A Comparison of Statistical Methods for Estimating Forest Biomass from Light Detection and Ranging Data. *West. J. Appl. For.* **2008,** *23* (4), 223-231.
21. Clark, D. B.; Kellner, J. R., Tropical forest biomass estimation and the fallacy of misplaced concreteness. *Journal of Vegetation Science* **2012,** *23* (6), 1191-1196.
22. Köhl, M.; Magnussen, S.; Marchetti, M., *Sampling methods, remote sensing and GIS multiresource forest inventory*. Springer: Berlin, 2006; p 365.
23. Gregoire, T. G., Design-based and model-based inference in survey sampling: appreciating the difference. *Can. J. For. Res.* **1998,** *28* (10), 1429-1447.
24. Payandeh, B., Relative Efficiency of Two-Dimensional Systematic Sampling. *For. Sci.* **1970,** *16* (3), 271-276.
25. Ene, L. T.; Næsset, E.; Gobakken, T.; Gregoire, T. G.; Stahl, G.; Nelson, R., Assessing the accuracy of regional LiDAR-based biomass estimation using a simulation approach. *Remote Sens. Environ.* **2012,** *123*, 579-592.
26. Næsset, E., Area-Based Inventory in Norway – From Innovation to an Operational Reality. In *Forestry Applications of Airborne Laser Scanning*, Maltamo, M.; Næsset, E.; Vauhkonen, J., Eds. Springer Netherlands: 2014; Vol. 27, pp 215-240.
27. Hamilton, A. C.; Bensted-Smith, R., *Forest conservation in the East Usambara Mountains, Tanzania*. IUCN-The World Conservation Union ; Dar es Salaam, Tanzania : Forest Division, Ministry of Lands, Natural Resources, and Tourism, United Republic of Tanzania: Gland, Switzerland and Cambridge, UK, 1989; p 392.
28. Anon., Users Guide Vertex III V1.5 and Transponder T3. Haglöf Sweden AB: Långsele,Sweden, 2007; p 24.
29. Tomppo, E.; Malimbwi, R.; Katila, M.; Mäkisara, K.; Henttonen, H. M.; Chamuya, N.; Zahabu, E.; Otieno, J., A sampling design for a large area forest inventory: case Tanzania. *Can. J. For. Res.* **2014,** *44* (8), 931-948.
30. Masota, A. M.; Zahabu, E.; Malimbwi, R.; Bollandsås, O. M.; Eid, T., Tree Allometric Models for Above- and Belowground Biomass of Tropical Rainforests in Tanzania. *Submitted to: Southern Forests: a Journal of Forest Science* **2015**.
31. Anon., TerraScan user's guide. Terrasolid Oy: Jyvaskyla, Finland, 2012; p 311.
32. Axelsson, P., DEM generation from laser scanner data using adaptive TIN models. *International Archives of the Photogrammetry and Remote Sensing* **2000,** *33*, 110-117.
33. Ioki, K.; Tsuyuki, S.; Hirata, Y.; Phua, M.-H.; Wong, W. V. C.; Ling, Z.-Y.; Saito, H.; Takao, G., Estimating above-ground biomass of tropical rainforest of different degradation levels in Northern Borneo using airborne LiDAR. *For. Ecol. Manage.* **2014,** *328*, 335-341.
34. Næsset, E.; Gobakken, T.; Solberg, S.; Gregoire, T. G.; Nelson, R.; Stahl, G.; Weydahl, D., Model-assisted regional forest biomass estimation using LiDAR and InSAR as auxiliary data: A case study from a boreal forest area. *Remote Sens. Environ.* **2011,** *115* (12), 3599-3614.

35. Marshall, A. R.; Willcock, S.; Platts, P. J.; Lovett, J. C.; Balmford, A.; Burgess, N. D.; Latham, J. E.; Munishi, P. K. T.; Salter, R.; Shirima, D. D.; Lewis, S. L., Measuring and modelling above-ground carbon and tree allometry along a tropical elevation gradient. *Biol. Conserv.* **2012,** *154*, 20-33.
36. Means, J. E.; Acker, S. A.; Harding, D. J.; Blair, J. B.; Lefsky, M. A.; Cohen, W. B.; Harmon, M. E.; McKee, W. A., Use of large-footprint scanning airborne lidar to estimate forest stand characteristics in the Western Cascades of Oregon. *Remote Sens. Environ.* **1999,** *67* (3), 298-308.
37. Lim, K.; Treitz, P.; Baldwin, K.; Morrison, I.; Green, J., Lidar remote sensing of biophysical properties of tolerant northern hardwood forests. *Can. J. Remote Sens.* **2003,** *29* (5), 658-678.
38. Næsset, E., Predicting forest stand characteristics with airborne scanning laser using a practical two-stage procedure and field data. *Remote Sens. Environ.* **2002,** *80* (1), 88-99.
39. Snowdon, P., A ratio estimator for bias correction in logarithmic regressions. *Can. J. For. Res.* **1991,** *21* (5), 720-724.
40. McRoberts, R. E.; Næsset, E.; Gobakken, T., Inference for lidar-assisted estimation of forest growing stock volume. *Remote Sens. Environ.* **2013,** *128*, 268-275.
41. Ståhl, G.; Holm, S.; Gregoire, T. G.; Gobakken, T.; Næsset, E.; Nelson, R., Model-based inference for biomass estimation in a LiDAR sample survey in Hedmark County, Norway. *Can. J. For. Res.* **2011,** *41* (1), 96-107.
42. Stoltzenberg, R. M., Multiple Regression Analysis. In *Handbook of Data Analysis*, Hardy, M. A.; Bryman, A., Eds. SAGE Publications Ltd: London, 2009; pp 165-207.
43. Ghosh, M.; Meeden, G., *Bayesian methods for finite population sampling*. Chapman & Hall: London, UK, 1997.
44. Vincent, G.; Sabatier, D.; Blanc, L.; Chave, J.; Weissenbacher, E.; Pélissier, R.; Fonty, E.; Molino, J. F.; Couteron, P., Accuracy of small footprint airborne LiDAR in its predictions of tropical moist forest stand structure. *Remote Sens. Environ.* **2012,** *125*, 23-33.
45. Nord-Larsen, T.; Schumacher, J., Estimation of forest resources from a country wide laser scanning survey and national forest inventory data. *Remote Sens. Environ.* **2012,** *119*, 148-157.
46. Chen, Q.; Vaglio Laurin, G.; Valentini, R., Uncertainty of remotely sensed aboveground biomass over an African tropical forest: Propagating errors from trees to plots to pixels. *Remote Sens. Environ.* **2015,** *160* (0), 134-143.
47. Rahlf, J.; Breidenbach, J.; Solberg, S.; Næsset, E.; Astrup, R., Comparison of four types of 3D data for timber volume estimation. *Remote Sens. Environ.* **2014,** *155*, 325-333.
48. Gregoire, T. G.; Næsset, E.; Ståhl, G.; Andersen, H.-E.; Gobakken, T.; Ene, L.; Nelson, R. F.; McRoberts, R. E., Statistical rigor in LiDAR-assisted estimation of aboveground forest biomass. *Remote Sens. Environ.* **2015,** *under review*.
49. d'Oliveira, M. V. N.; Reutebuch, S. E.; McGaughey, R. J.; Andersen, H. E., Estimating forest biomass and identifying low-intensity logging areas using airborne scanning lidar in Antimary State Forest, Acre State, Western Brazilian Amazon. *Remote Sens. Environ.* **2012,** *124*, 479-491.

50. Meng, X. L.; Currit, N.; Zhao, K. G., Ground Filtering Algorithms for Airborne LiDAR Data: A Review of Critical Issues. *Remote Sensing* **2010,** *2* (3), 833-860.
51. Neeff, T.; Dutra, L. V.; dos Santos, J. R.; Freitas, C. d. C.; Araujo, L. S., Tropical Forest Measurement by Interferometric Height Modeling and P-Band Radar Backscatter. *For. Sci.* **2005,** *51* (6), 585-594.
52. Gobakken, T.; Næsset, E., Assessing effects of laser point density, ground sampling intensity, and field sample plot size on biophysical stand properties derived from airborne laser scanner data. *Can. J. For. Res.* **2008,** *38* (5), 1095-1109.
53. Næsset, E., Effects of different sensors, flying altitudes, and pulse repetition frequencies on forest canopy metrics and biophysical stand properties derived from small-footprint airborne laser data. *Remote Sens. Environ.* **2009,** *113* (1), 148-159.
54. Hansen, E.; Gobakken, T.; Næsset, E., Effects of Pulse Density on Digital Terrain Models and Canopy Metrics using Airborne Laser Scanning in a Tropical Rainforest. *Submitted to: Remote Sensing* **2015**.

ISBN: 978-82-575-1269-9
ISSN: 1894-6402

Norwegian University
of Life Sciences

Postboks 5003
NO-1432 Ås, Norway
+47 67 23 00 00
www.nmbu.no